UNIVERSIDAD POLITECNICA DE VALENCIA

motores térmicos

TRABAJO DE FIN DE MASTER

Aplicación y evaluación de un modelo euleriano-lagrangiano de atomización de chorros en simulaciones CFD de chorros Diesel

Realizado por: **KHUONG Anh Dung**
Dirigido por: **Hoyas Calvo Sergio**

Valencia, Septiembre de 2011

Master en
Motores de Combustión Interna Alternativos

DEPARTAMENTO DE MÁQUINAS Y MOTORES TÉRMICOS

Contenidos:

1. INTRODUCCION 3

1.1. Antecedentes 3

1.2. Memoria 4
1.2.1. Objetivos y metodología 4
1.2.2. Revisión bibliográfica 4
1.2.3. Modelo numérico y configuración física 5
1.2.4. Modelo de evaluación en los experimentos básicos de spray 5
1.2.5. Resultados 5

2. ANEXOS 6

2.1. DISEÑO DE EXPERIMENTOS 6

2.1.1. Design and analysis of various factors which affect the Diesel spray simulation using Fractional Factorial design 2k and 2k-p 6

2.2. PUBLICACIONES 7

2.2.1. On the boundary condition setup of Large Eddy Simulation of Diesel sprays. Modelling for Addictive Behaviour, Medicine and Engineering 2010. pp. 87-99. I.S.B.N.: 978-84-693-9537-0. 7

2.2.2. A Large-Eddy Simulation of Diesel-like gas jets. International Conference on Mechanical, Automotive and Aerospace Engineering 2011 (Published in International Journal of Vehicle Systems Modelling and Testing – IJVSMT) 8

2.2.3. Evaluation of the Eulerian-Lagrangian Spray Atomization (ELSA) in spray simulations. International Conference on Mechanical, Automotive and Aerospace Engineering 2011 (Published in International Journal of Vehicle Systems Modelling and Testing – IJVSMT) 9

2.2.4. Application and evaluation of the Eulerian-Lagrangian Spray Atomization (ELSA) model on CFD Diesel spray simulations. SAE Paper 2011-37-0029 10

2.2.5. ELSA model of Diesel sprays. Mathematical Modelling in Engineering & Human Behaviour 2011 (oral presentation at IMM 2011, will submit final paper in Oct 2011) 11

2.3. INFORMES 12

2.3.1. D11: Intermediate report on Multi-attribute Balancing and Optimization in the Concept Design Phase, Balancing of injection/combustion efficiency and NVH: Optimal design approach for spray penetration of Diesel engine 12

2.3.2. Deliverable D8: Intermediate Report on Techniques for Powertrain Concept and Simulation. Representative approaches for powertrain concept modelling and simulation: Thermo-dynamic processes: injection/combustion, subjective noise, air management and turbo charging 13

2.4. PRESENTACIONES Y CONFERENCIAS: 14

1. INTRODUCCION

1.1. Antecedentes

El mundo de automóviles ha cambiado rápidamente en la última década. Los nuevos estándares de eficiencia requieren una reducción del consumo de combustible. Los vehículos del futuro cercano serán los coches más eficientes en combustible, vehículos eléctricos e híbridos. A pesar de que se han obtenido grandes avances durante la última década en la eficiencia de la gasolina y diesel, los fabricantes insisten en que todavía hay mucho que mejorar en el motor de combustión, y que planean llevar a cabo la búsqueda de todas las mejoras que puedan conseguir. Dentro de este objetivo, los fabricantes han prestado más atención a fomentar la mejora de los recursos de I + D en la industria automotriz. Hay una gran variedad de campos de investigación, e incluyen: el combustible, el motor, ruido, vibraciones y asperezas (NVH - Noise, Vibration and Harshness), la simulación del rendimiento del vehículo, dinámica, seguridad, durabilidad, etc.

En el campo de la simulación numérica, la mecánica de Fluidos Computacional (CFD - Computational Fluid Dynamics) ha establecido su papel en la industria del automóvil. Sobre todo, CFD ha sido ampliamente utilizado en el modelado del motor de combustión interna. En el marco de la investigación, los diferentes modelos y técnicas disponibles para la simulación CFD de chorros, así como la comparación con los datos experimentales, son de gran importancia en múltiples aplicaciones industriales. En especial, los modelos de chorro juegan un papel importante en la simulación de motores diesel. Más específicamente, la comprensión de las características de la evolución del chorro y los parámetros que influyen en un suministro de combustible eficiente, son aspectos clave en el proceso de desarrollo de nuevos motores. El objetivo es por tanto aumentar la eficiencia del combustible, la eficiencia energética, reducir la emisión de contaminantes de los aerosoles de combustión con el fin de generar un motor altamente eficiente.

El proceso de inyección de combustible y la posterior formación de la mezcla aire-combustible desempeña un papel significativo en la combustión y en la formación de contaminantes en los motores de combustión interna. De esta forma, se hace necesaria la predicción exacta de estos procesos para llevar a cabo el modelado la combustión de motores fiables y las subsecuentes simulaciones de la formación de contaminantes. Sin embargo, es necesario destacar que el modelado de los procesos de inyección de combustible diesel y de formación del chorro sigue siendo una tarea difícil debido a los complejos fenómenos relacionados entre sí, algunos de ellos, tales como la atomización primaria o cavitación de la tobera del inyector que no se entienden completamente a día de hoy.

Las simulaciones tradicionales CFD de chorros se basan en la física de partículas discretas (DDM - Discrete Droplet Method), que aplica un enfoque de Lagrange para el modelado de spray líquido. Este enfoque presenta algunos inconvenientes, por lo general requiere de una calibración intensa con el fin de poder ser empleado en las simulaciones del motor. Los principales problemas provienen de las limitaciones físicas y numéricas en la tobera del inyector, cerca de la región densa del chorro.

Con el fin de mejorar las simulaciones CFD de chorro, el modelo ELSA (modelo euleriano-lagrangiano de atomización de chorros) ha sido desarrollado por Renault en los últimos años e integrado en el código de cálculo Star-CD. Este modelo se basa en un enfoque de Euler para la descripción de la región densa, donde el método estándar de DDM no es adecuado. En la región de

diluida del modelo ELSA podría pasar a la descripción tradicional de Lagrange de la fase líquida, aprovechando los submodelos existentes desarrollados con anterioridad.

El modelo de chorros ELSA permite resolver la geometría de la sección de salida de la tobera con suficiente resolución espacial, con lo que podría aprovecharse de los resultados de la simulación del flujo interno del inyector, para la obtención de las condiciones de salida en la tobera. Por lo tanto, también es posible utilizar este tipo de simulaciones para investigar sobre la vinculación entre el flujo interno en el inyector y la formación de chorro.

1.2. Memoria

1.2.1. Objetivos y metodología

El modelo ELSA se ha implementado en Star-CD, el cual es el código utilizado para todos los cálculos presentados en este informe. De acuerdo con lo comentado anteriormente en el tema general de la tesis, el propósito del presente estudio es la mejora de las simulaciones CFD de chorros Diesel en el marco del modelo ELSA. El objetivo general de la tesis es desarrollar, evaluar y validar una nueva herramienta computacional de chorro, con aplicación práctica en los cálculos CFD del motor. Dentro de este objetivo general, se incluye evaluar y validar los submodelos diferentes que representan los fenómenos involucrados en la formación del chorro Diesel y en el desarrollo del mismo desde la sección de la tobera hasta la evaporación completa del combustible.

El objetivo es centrarse en el acoplamiento y la coherencia entre los diferentes submodelos en lugar de en los procesos del chorro de forma aislada. Se propone hacer hincapié en la transición del flujo de la tobera interna para los cálculos iniciales del desarrollo del chorro. El trabajo también se centrará en la integración adecuada de los submodelos utilizados para la descripción de la región densa y diluida, en términos de ruptura de la vena líquida, la coalescencia, vaporización y evolución de las gotas.

El objetivo en este trabajo es desarrollar y validar una técnica híbrida euleriana-lagrangiana para simular la atomización del chorro Diesel en motores de combustión. El modelo se define implícitamente, y está implementado en Star-CD. La transición de la zona de atomización primaria (Euleriana) a la secundaria (Lagrangiana) juega un papel importante en estos modelos. Por tanto, en el punto donde se diluye el chorro suficientemente, se inicia una transición a la formulación de las partículas de Lagrange con el fin de beneficiarse de las ventajas de este enfoque en las últimas etapas de la atomización. El autor aplica la metodología desarrollada para la serie de casos de atomización de complejidad creciente. El punto principal de la obra que aquí se presenta se basa en el estudio de diversos factores y parámetros que se efectuarán para el modelado de spray de euleriano-lagrangiano. En la actual contribución se presentan algunas simulaciones preliminares spray, así como submodelos spray.

1.2.2. Revisión bibliográfica

La revisión de la literatura se centró principalmente en los siguientes temas:

- Los fenómenos de flujo interno en tobera.
- Atomización principal de chorros.
- Atomización secundaria, dinámica y termodinámica de gotas.

1.2.3. Modelo numérico y configuración física

Basándose en los datos obtenidos de la revisión bibliográfica se llevará a cabo la configuración del modelo CFD. En este paso los aspectos numéricos y físicos que se consideran son:

- Estudio de tamaño y topología de malla, tanto para el flujo interno de la tobera como para el modelado chorro.
- Influencia de los esquemas de discretización numérica.
- La evaluación del modelo de turbulencia.
- Submodelos de chorros para la región densa y diluida.

1.2.4. Modelo de evaluación en los experimentos básicos de spray

Spray model set-up will be evaluated and compared with experimental results from CMT present or further studies on this topic or other well established results from literature. It is planed to employ data from isolated free diesel spray experiments performed under engine-like ambient conditions.

La configuración del modelo de chorro se evaluará y se comparará con resultados experimentales realizados en el instituto CMT, u otros resultados provenientes de la literatura. La intención es utilizar datos de chorro libre obtenidos en experimentos realizados bajo condiciones ambientales similares a las condiciones motor.

Se proponen inicialmente los siguientes resultados experimentales de la CMT:

- Gasto másico y cantidad de movimiento en la tobera
    - Validación de los cálculos del flujo en toberas y obtención de las condiciones de contorno para el cálculo de chorros.
- Instalación experimental para la visualización de la zona cercana a la tobera: Estructura del flujo de salida y ángulo del chorro cerca de la tobera
    - Estos datos podrían ser utilizados con el fin de evaluar la dispersión incial de la fase líquida en la zona densa del chorro.
- El tamaño de gotas: PDA (SMD y velocidad)
    - A pesar de que no se puede aplicar a la zona densa del chorro, esta técnica proporciona información útil para la evaluación del modelo entre la zona densa y la zona diluida del spray.
- Parámetros macroscópicos del chorro: Longitud líquida y de vapor y el ángulo de dispersión de spray.
    - Con el fin de evaluar el comportamiento global del proceso de mezcla en el chorro.

1.2.5. Resultados

Todos los resultados han sido publicados y presentados en los diferentes informes, conferencias, talleres, reuniones y artículos que se especifica en la sección 2: anexos.

2. ANEXOS

2.1. DISEÑO DE EXPERIMENTOS

2.1.1. Design and analysis of various factors which affect the Diesel spray simulation using Fractional Factorial design 2k and 2k-p

Diseño De Experimentos

FINAL PROJECT

Project title:

Design and analysis of various factors which affect the Diesel spray simulation using Fractional Factorial design 2^k and 2^{k-p}

Students: Khuong Anh Dung &

Juan Manuel Mompó Laborda

Lecturer: Prof. Jose Miguel Carot Sierra

Date: 22th Jun 2010

1. DEFINE THE PROBLEM AND OBJECTIVES OF THE STUDY

1.1 Model used for the study

To realize a further optimization of the engine design, this requires a good understanding of the combustion process and how these processes are influenced by engine design and settings.

The spray behavior itself comprises a range of complex physical and chemical processes which are difficult to incorporate in the engine design or computer models. Therefore empirical relations have been developed for the spray behavior which are essential for the engine designer and the developers of multi-dimensional computational models.

For engine designers insight in the behavior of an evaporating fuel spray is of great importance. Improvements in injection equipment reduce emissions and increase power by a more effective combustion process. The major objective of this work is to numerically investigate the interacting physical and chemical phenomena that characterize the flow in a diesel fuel spray evaporation system.

Within this limited topic, the Numerical Simulation of Diesel Spray with the isothermal, non-vaporizing conditions is examed.

- **Isothermal**: indicating equal or constant temperatures.
- A **non-evaporating** fuel spray is defined as the spray produced under variable chamber pressure condition by maintaining the chamber temperature equal to the ambient temperature.

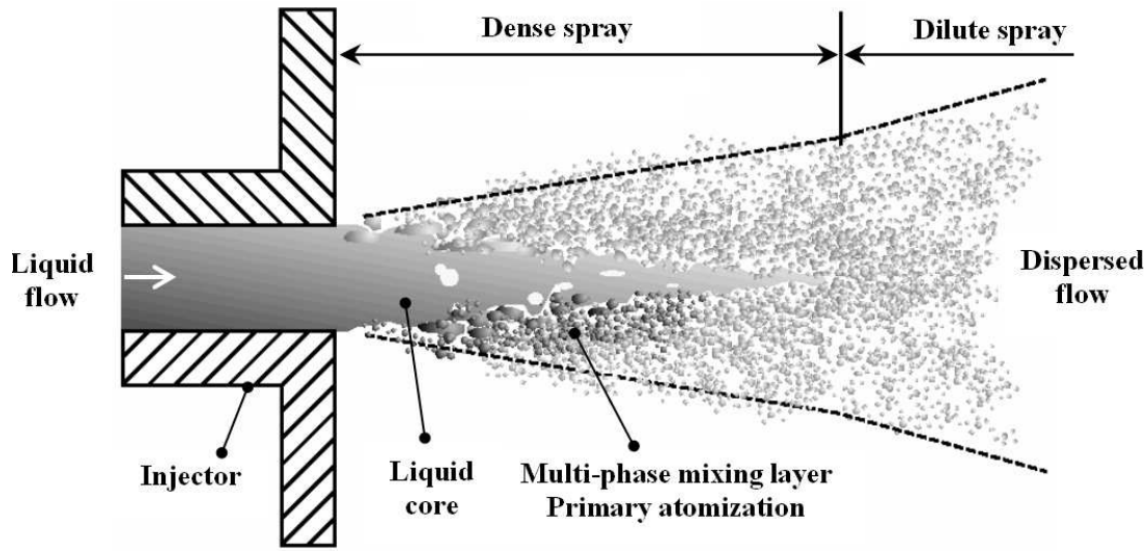

Figure 1: Spray structure

We used OpenFOAM with Computational fluid dynamics tool for the calculation, some detail techniques and methods are described shortly hereafter.

1.2 Computational fluid dynamics

Computational fluid dynamics (CFD) [1] is one of the branches of fluid mechanics that uses numerical methods and algorithms to solve and analyze problems that involve fluid flows. Computers are used to perform the millions of calculations required to simulate the interaction of liquids and gases with surfaces defined by boundary conditions. Even with high-speed supercomputers only approximate solutions can be achieved in many cases.

1.3 Overview of OpenFOAM

The OpenFOAM® [2] (Open Field Operation and Manipulation) CFD Toolbox is a free, open source CFD software package produced by a commercial company, OpenCFD Ltd. It has a large user base across most areas of engineering and science, from both commercial and academic organisations. OpenFOAM has an extensive range of features to solve anything from complex fluid flows involving chemical reactions, turbulence and heat transfer, to solid dynamics and electromagnetics.

The core technology of OpenFOAM is a flexible set of efficient C++ modules. These are used to build a wealth of: solvers, to simulate specific problems in engineering mechanics; utilities, to perform pre- and post-processing tasks ranging from simple data manipulations to visualisation and mesh processing; libraries, to create toolboxes that are accessible to the solvers/utilities, such as libraries of physical models.

OpenFOAM is supplied with numerous pre-configured solvers, utilities and libraries and so can be used like any typical simulation package. However, it is open, not only in terms of source code, but also in its structure and hierarchical design, so that its solvers, utilities and libraries are fully extensible.

OpenFOAM uses finite volume numerics to solve systems of partial differential equations ascribed on any 3D unstructured mesh of polyhedral cells. The fluid flow solvers are developed within a robust, implicit, pressure-velocity, iterative solution framework, although alternative techniques are applied to other continuum mechanics solvers. Domain decomposition parallelism is fundamental to the design of OpenFOAM and integrated at a low level so that solvers can generally be developed without the need for any 'parallel-specific' coding.

1.4 Parallel computing

The availability of parallel computing provides an opportunity for solving increasingly complex problems.

OpenFOAM employs domain decomposition to run cases on more than one processor. The domain is automatically decomposed into a number of sub-domains, each of which is solved on a separate processor. The communication between processors uses the MPI communications protocol (or shmem on Cray platforms).

OpenFOAM has been used for calculations with 10 million cells and has run on a 256 processor Cray T3E.

OpenFOAM displays excellent scaling performance, i.e. reduction in computing time with increase in number of processors. The table below presents timing data for a 3-D linear stress analysis problem on a Diesel injector valve seat with 360,000 cells. The calculation was performed on a 24 CPU Silicon Graphics Origin 2000 in non-dedicated mode, i.e. other jobs were running on the machine during the test.

No of CPUs	CPU time to convergence	Speedup
1	35620.4 s	1.00
2	22398.8 s	1.60
4	11406.6 s	3.10
8	4247.32 s	8.88
16	2872.58 s	12.4

Table 1: CPU time consuming

1.5 Fractional Factorial Designs:

A factorial design is one in which every possible combination of treatment levels for different factors appears.

Why do we need the factorial designs? For example, if there are , say, a levels of factor A, b levels of factor B, c levels of factors C, then a factorial design requires at least abc observations, and more if one wants to estimate the three way interaction among the factors. This can get expensive when experiments have many different factors.

To keep experimental costs in line, one approach is to use fractional factorial designs. In these, one does not take measurements upon every possible combination of factor levels, but only upon a very carefully chosen few.

These few are selected to ensure that the main effects and low-order interactions can be estimated and tested, at the expense of high-order interactions.

The scientific intuition is that it is unlikely for there to be complex interactions among many different factors; instead, there are probably only main effects and a few low-order interactions.

Thus one might design the collection in a fractional factorial so that all main effects and two-way interactions can be tested, but not three-way or higher interactions.

In this report, the experimental data will be analyzed using Statgraphics software.

A step-by-step analysis of a fractional factorial experiment for the case will be shown in this report.

1.6 Purposes of the study

- Reduced the calculation time by optimizing the calculation from 1 node into parallel computation.
- To determine the significant factors that affect the behaviour of the modelling.
- From the obtained results, an optimal reference will be used for future study.

2. Define the response variable

- The Speed of the spray.
- The magnitude directly calculates by the computer programming. The speed range is located from 0 – 300 m/s.

3. Selection of the factors and definition of the levels

Some numbers, controlling the numerical behaviour of the calculation, have been selected as the factors that affect the difference founded between the 1 node calculation and the parallelization. The tolerance for the residuals of the variables directly calculated by the code, the Courant–Friedrichs–Lewy condition (CFL) and the correctors present inside the PISO loop, are the factors studied.

The residual is ostensibly a measure of the error in the solution so that the smaller it is, the more accurate the solution. Besides, it is normalised in to make

it independent of the scale of problem being analysed. The solver **tolerance** should represents the level at which the residual is small enough that the solution can be deemed sufficiently accurate.

In mathematics, the **CFL** condition is a necessary condition for convergence while solving certain partial differential equations numerically. For example, if a wave is crossing a discrete grid, then the time step must be less than the time for the wave to travel adjacent grid points. As a corollary, when the CFL is reduced, the upper limit for the time step also decreases. At the OpenFOAM's use guide there are some suggested values for a given solver.

The number *v* is called the Courant number, and is set as a constant number in the current case, thus the time step changes to fulfill this factor of study in the cell with the highest ratio speed-time vs cell distance.

$$\nu = \frac{u \cdot \Delta t}{\Delta x}$$

Fluid dynamics solver applications in OpenFOAM use the pressure-implicit split-operator (**PISO**) algorithm for transient problems. This algorithm is an iterative procedure for solving equations for velocity and pressure, based on evaluating some initial solutions and then correcting them. Other algorithms only make 1 correction whereas PISO requires more than 1, but typically not more than 4. Therefore **nCorrectors** must be specified by the user between 2 and 4 (OF's recommendation) but , after some bibliography review, for the solver used for diesel sprays under chemical reactions, authors have set this number up to 8. Although no reactive conditions have been used in the current problem the students wanted to know its influence for a wider range since it may be used in future works.

nNonOrthogonalCorrectors stands for an additional correction to account mesh non-orthogonality. **nOuterCorrectors** specifies the number of outer loops around the complete system of equations.

The values for each of the factors are presented in the Table 1.

Factor	CFL	nCorrectors	nNonOrth	nOuterCor	p,rho,U,Yi,h,k,epsilon
Value	0,5; 0,1	2; 8	1; 5	1; 5	1e-6; 1e-10

Table 1: Factors value

4. Setup the test

The case is calculated up to 0.0003s, when the spray reaches the halve of the domain. By this time 8400 time steps have been calculated under a CFL=0.5. The U file calculated at 0.0003s with the domain splitted is compared with the

one calculated in one node. Specifically, the maximum absolute value of the difference of the speed axial component in the domain was identified to get the outcome variable analyzed in this study.

5. Number of observations

We use a factorial experimental design of 2 levels and 32 tries as presented in the Table 2.

6. Organize the experiments

In order to minimize the human error and save time, the run of the cases was automatized following a binary code that identifies the level of each of the factors of study. In the following script, the case pointer is taken from the case folder (i.e. reactingFoam_01111011001_2par) to change the value of the factors

```
setReactingFoam ()

{

# get the case pointer

   caseID=`pwd | grep reactingFoam | cut -d'_' -f2`

# ascribe the value to the factor
   CFL=`expr substr $caseID 1 1`

   nCorrectors=`expr substr $caseID 2 1`
   nNonOrth=`expr substr $caseID 3 1`
   nOuterCor=`expr substr $caseID 4 1`
   p=`expr substr $caseID 5 1`
   rho=`expr substr $caseID 6 1`
   U=`expr substr $caseID 7 1`
   Yi=`expr substr $caseID 8 1`
   h=`expr substr $caseID 9 1`
   k=`expr substr $caseID 10 1`
   epsilon=`expr substr $caseID 11 1`
```

```
# change the level when required

if [ $CFL = 1 ]

then

   sed\
   -e s/"\(maxCo[ \t]*\) 0.5;"/"\1 0.1;"/g \
   $controlDict > temp.$$
   mv temp.$$ $controlDict
fi


if [ $nCorrectors = 1 ]

then

   sed\
   -e s/"\(nCorrectors *\) 2;"/"\1 8;"/g \
   $fvSolution > temp.$$
   mv temp.$$ $fvSolution
fi
```

7. Conduct the experiment

caso	CFL	nCorrectors	nNonOrth	nOuterCor	p	rho	U	Yi	h	k	epsilon	caso	
1	0	0	0	0	0	0	0	0	0	0	0	reactingFoamCase_	0 0 0 0 0 0 0 0 0 0 0 0
2	1	0	0	0	0	1	0	0	1	1	0	reactingFoamCase_	1 0 0 0 0 1 0 0 1 1 0
3	0	1	0	0	0	1	1	0	0	0	1	reactingFoamCase_	0 1 0 0 0 1 1 0 0 0 1
4	1	1	0	0	0	0	1	0	1	1	1	reactingFoamCase_	1 1 0 0 0 0 1 0 1 1 1
5	0	0	1	0	0	1	1	1	1	0	0	reactingFoamCase_	0 0 1 0 0 1 1 1 1 0 0
6	1	0	1	0	0	0	1	1	0	1	0	reactingFoamCase_	1 0 1 0 0 0 1 1 0 1 0
7	0	1	1	0	0	0	0	1	1	0	1	reactingFoamCase_	0 1 1 0 0 0 0 1 1 0 1
8	1	1	1	0	0	1	0	1	0	1	1	reactingFoamCase_	1 1 1 0 0 1 0 1 0 1 1
9	0	0	0	1	0	0	1	1	1	1	1	reactingFoamCase_	0 0 0 1 0 0 1 1 1 1 1
10	1	0	0	1	0	1	1	1	0	0	1	reactingFoamCase_	1 0 0 1 0 1 1 1 0 0 1
11	0	1	0	1	0	1	0	1	1	1	0	reactingFoamCase_	0 1 0 1 0 1 0 1 1 1 0
12	1	1	0	1	0	0	0	1	0	0	0	reactingFoamCase_	1 1 0 1 0 0 0 1 0 0 0
13	0	0	1	1	0	1	0	0	0	1	1	reactingFoamCase_	0 0 1 1 0 1 0 0 0 1 1
14	1	0	1	1	0	0	0	0	1	0	1	reactingFoamCase_	1 0 1 1 0 0 0 0 1 0 1
15	0	1	1	1	0	0	1	0	0	1	0	reactingFoamCase_	0 1 1 1 0 0 1 0 0 1 0
16	1	1	1	1	0	1	1	0	1	0	0	reactingFoamCase_	1 1 1 1 0 1 1 0 1 0 0
17	0	0	0	0	1	0	0	1	0	1	1	reactingFoamCase_	0 0 0 0 1 0 0 1 0 1 1
18	1	0	0	0	1	1	0	1	1	0	1	reactingFoamCase_	1 0 0 0 1 1 0 1 1 0 1
19	0	1	0	0	1	1	1	1	0	1	0	reactingFoamCase_	0 1 0 0 1 1 1 1 0 1 0
20	1	1	0	0	1	0	1	1	1	0	0	reactingFoamCase_	1 1 0 0 1 0 1 1 1 0 0
21	0	0	1	0	1	1	1	0	1	1	1	reactingFoamCase_	0 0 1 0 1 1 1 0 1 1 1
22	1	0	1	0	1	0	1	0	0	0	1	reactingFoamCase_	1 0 1 0 1 0 1 0 0 0 1
23	0	1	1	0	1	0	0	0	1	1	0	reactingFoamCase_	0 1 1 0 1 0 0 0 1 1 0
24	1	1	1	0	1	1	0	0	0	0	0	reactingFoamCase_	1 1 1 0 1 1 0 0 0 0 0
25	0	0	0	1	1	0	1	0	1	0	0	reactingFoamCase_	0 0 0 1 1 0 1 0 1 0 0
26	1	0	0	1	1	1	1	0	0	1	0	reactingFoamCase_	1 0 0 1 1 1 1 0 0 1 0
27	0	1	0	1	1	1	0	0	1	0	1	reactingFoamCase_	0 1 0 1 1 1 0 0 1 0 1
28	1	1	0	1	1	0	0	0	0	1	1	reactingFoamCase_	1 1 0 1 1 0 0 0 0 1 1
29	0	0	1	1	1	1	0	1	0	0	0	reactingFoamCase_	0 0 1 1 1 1 0 1 0 0 0
30	1	0	1	1	1	0	0	1	1	1	0	reactingFoamCase_	1 0 1 1 1 0 0 1 1 1 0
31	0	1	1	1	1	0	1	1	0	0	1	reactingFoamCase_	0 1 1 1 1 0 1 1 0 0 1
32	1	1	1	1	1	1	1	1	1	1	1	reactingFoamCase_	1 1 1 1 1 1 1 1 1 1 1

Table 2: The value 0 sets the first level of the factors, and 1 the second level

After running all the cases the students realized that most of the cases with the lower CFL didn't progress. As it had been said above “when the CFL is reduced, the upper limit for the time step also decreases”, therefore, the residuals at the beginning of their calculation loops are sometimes lower than the tolerance set. These generate some instabilities leading to the calculation diverged.

Consequently, the experiment was re-design, taking in account only the higher CFL (CFL=0,5) and swapping the first factor (CFL) by a new one in order to take advantage of the cases which were already calculated. The new factor substituting CFL is number of processors (**nproc**). Thus, the cases were run in 2 and 4 nodes. Level 0 = 4 processors; level 1 = 2 processors.

case	nproc	nCorrectors	nNonOrth	nOuterCor	p	rho	U	Yi	h	k	epsilon	max speed diff
1	0	0	0	0	0	0	0	0	0	0	0	1,651
2	1	0	0	0	0	1	0	0	1	1	0	1,4514
3	0	1	0	0	0	1	1	0	0	0	1	0,1779
4	1	1	0	0	0	0	1	0	1	1	1	0,0155
5	0	0	1	0	0	1	1	1	1	0	0	1,6699
6	1	0	1	0	0	0	1	1	0	1	0	1,533
7	0	1	1	0	0	0	0	1	1	0	1	2,322
8	1	1	1	0	0	1	0	1	0	1	1	0,0511
9	0	0	0	1	0	0	1	1	1	1	1	0,0934
10	1	0	0	1	0	1	1	1	0	0	1	0,0342
11	0	1	0	1	0	1	0	1	1	1	0	5,8886
12	1	1	0	1	0	0	0	1	0	0	0	1,175
13	0	0	1	1	0	1	0	0	0	1	1	0,4616
14	1	0	1	1	0	0	0	0	1	0	1	4,936
15	0	1	1	1	0	0	1	0	0	1	0	1,4933
16	1	1	1	1	0	1	1	0	1	0	0	1,0986
17	0	0	0	0	1	0	0	1	0	1	1	0,0409
18	1	0	0	0	1	1	0	1	1	0	1	0,0339
19	0	1	0	0	1	1	1	1	0	1	0	1,9963
20	1	1	0	0	1	0	1	1	1	0	0	0,9997
21	0	0	1	0	1	1	1	0	1	1	1	0,0282
22	1	0	1	0	1	0	1	0	0	0	1	0,0336
23	0	1	1	0	1	0	0	0	1	1	0	1,1333
24	1	1	1	0	1	1	0	0	0	0	0	0,4792
25	0	0	0	1	1	0	1	0	1	0	0	1,1397
26	1	0	0	1	1	1	1	0	0	1	0	0,8998
27	0	1	0	1	1	1	0	0	1	0	1	0,0621
28	1	1	0	1	1	0	0	0	0	1	1	0,0173
29	0	0	1	1	1	1	0	1	0	0	0	1,8359
30	1	0	1	1	1	0	0	1	1	1	0	1,884
31	0	1	1	1	1	0	1	1	0	0	1	0,0676
32	1	1	1	1	1	1	1	1	1	1	1	0,0165

Table 3: Observation factors and results.

8. Data analysis

Table 4: Initial data

Source	*Sum of Squares*	*Df*	*Mean Square*	*F-Ratio*	*P-Value*
A:nproc	0,912229	1	0,912229	0,73	0,4316
B:nCorrectors	0,0167674	1	0,0167674	0,01	0,9122
C:nNonOrth	0,354293	1	0,354293	0,28	0,6170
D:nOuterCor	1,75158	1	1,75158	1,40	0,2894
E:p	5,59828	1	5,59828	4,49	0,0877
F:rho	0,172593	1	0,172593	0,14	0,7252
G:U	4,59507	1	4,59507	3,68	0,1131
H:Yi	0,650798	1	0,650798	0,52	0,5026
I:h	3,66196	1	3,66196	2,93	0,1474
J:k	0,0158465	1	0,0158465	0,01	0,9147
K:epsilon	10,0541	1	10,0541	8,06	0,0363
AB+CF+GI+JK	5,42316	1	5,42316	4,35	0,0915
AC+BF+DI+HJ	1,73133	1	1,73133	1,39	0,2919
AD+CI+EJ+FG	0,37008	1	0,37008	0,30	0,6094
AE+DJ+HI	0,0724758	1	0,0724758	0,06	0,8191
AF+BC+DG+HK	3,58363	1	3,58363	2,87	0,1509
AG+BI+DF	0,0554528	1	0,0554528	0,04	0,8414
AH+CJ+EI+FK	3,76168	1	3,76168	3,01	0,1430
AI+BG+CD+EH	0,07997	1	0,07997	0,06	0,8102
AJ+BK+CH+DE	0,822756	1	0,822756	0,66	0,4537
AK+BJ+FH	2,62875	1	2,62875	2,11	0,2064
BD+CG+EK+FI	0,151071	1	0,151071	0,12	0,7421
BE+DK+GH	0,0717731	1	0,0717731	0,06	0,8200
BH+CK+EG+FJ	4,1441	1	4,1441	3,32	0,1280
CE+DH+GK+IJ	0,243236	1	0,243236	0,19	0,6773
EF+GJ+IK	0,18327	1	0,18327	0,15	0,7173
Total error	6,23968	5	1,24794		
Total (corr.)	57,346	31			

Table 5: Final data

Source	Sum of Squares	Df	Mean Square	F-Ratio	P-Value
A:nproc	0,912229	1	0,912229	1,26	0,2762
D:nOuterCor	1,75158	1	1,75158	2,42	0,1371
E:p	5,59828	1	5,59828	7,74	0,0123
F:rho	0,172593	1	0,172593	0,24	0,6311
G:U	4,59507	1	4,59507	6,35	0,0214
H:Yi	0,650798	1	0,650798	0,90	0,3554
I:h	3,66196	1	3,66196	5,06	0,0372
J:k	0,0158465	1	0,0158465	0,02	0,8840
K:epsilon	10,0541	1	10,0541	13,90	0,0015
AF+DG+HK	3,58363	1	3,58363	4,95	0,0390
AH+EI+FK	3,76168	1	3,76168	5,20	0,0350
EG+FJ	4,1441	1	4,1441	5,73	0,0278
GI+JK	5,42316	1	5,42316	7,50	0,0135
Total error	13,0209	18	0,723384		
Total (corr.)	57,346	31			

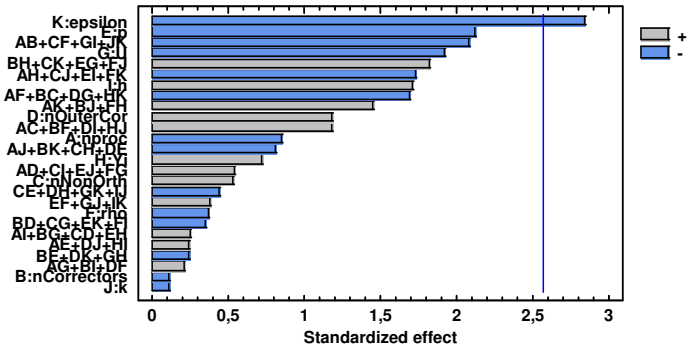

Figure 2: Standardized pareto chart of maximum speed difference

In the initial data, standard errors are based on total error with 5 d.f, whereas the final selection of the factors, standard errors are based on total error with 18 d.f .

The estimation in decreasing order of significance is plotted by Pareto Chart in Figure 2. Using this graph and the values of P-Value shown in Table 4, the non-significant cross factors were taken out in the downward order, one by one, because the elimination of each factor imply the modification of the values of Table 4, specifically the P-Value. The reduction processes started with the combined factors, then following by each individual factors respectively. The Factors were erased in the following order:

	Factors	Reasons
1	AG+BI+DF	P-Value higher than 0.05
2	BE+DK+GH	P-Value higher than 0.05
3	AE+DJ+HI	P-Value higher than 0.05
4	AI+BG+CD+EH	P-Value higher than 0.05
5	BD+CG+EK+FI	P-Value higher than 0.05
6	AF+BC+DG+HK	P-Value higher than 0.05
7	CE+DH+GK+IJ	P-Value higher than 0.05
8	AD+CI+EJ+FG	P-Value higher than 0.05
9	AJ+BK+CH+DE	P-Value higher than 0.05
10	AC+BF+DI+HJ	P-Value higher than 0.05
11	AK+BJ+FH	P-Value higher than 0.05

At this stage all the p-values of the cross interactions were lower than 0.05. A closed observation on the residual log file (the program file which used for setting up the calculation) show that the variables under **nNonOrthogonal** loop were no calculated because the initial residual value was already lower than the tolerance imposed because the calculation performed in the outer loops. Thus, the C factor call nNonOrth and its correlations were taken out of the analysis list

	Old factor	New factor	Reasons
12	AF+BC+DG+HK	AF +DG+HK	C factor no contribution
13	AH+CJ+EI+FK	AH +EI+FK	C factor no contribution
14	BH+CK+EG+FJ	BH +EG+FJ	C factor no contribution
15	AB+CF+GI+JK	AB +GI+JK	C factor no contribution

Then the lower contribution of cross factors due to higher P-Value was removed.

	Old factor	New factor	Reasons
16	AB +GI+JK	GI+JK	AB factor lower contribution compare with G, I, K
17	BH +EG+FJ	EG+FJ	BH factor lower contribution compare with E, G

As B (nCorrectors) does not appear anymore crossed with any other factors and the simply effect has a P-Value higher than 0.05, it was removed from the analysis.

Regarding the rest of factors, no further reason is found in which needs to eliminate their cross effect. Although some of the P-Values for the single effect are higher than 0.05, this factors can not be deleted because their presence in the cross effect. The

Table 5 show the final parameters remain for our investigation.

The final configuration gave us the following results:

- **R-squared = 77,2941 percent**
- **R-squared (adjusted for d.f.) = 60,8954 percent**
- **Standard Error of Est. = 0,85052**

The R-square is slightly low but acceptable in our case. This parameter indicates how linear is the behaviour of the factors studied, suggesting future studies of 3 levels for some of the factors must be performed in order to take in account non-linearity.

The optimization approach is to minimize the speed difference, given that the ideal minimum for a difference between results is zero [Table 6]. In this case the optimum value has a negative sign, which has no mathematical sense. However, the values of the factors to minimize the difference are reasonable. The tolerances should be set to level 1, which means a lower tolerance. Also, lower number of processors will reduce the difference with the solution calculated in one processor. Although this is unlikely expectation, the factor “number of processors” is insignificant, and it is not the main target in this exercise.

9. Conclusion

From our analysis we can use the results as a reference for future calculations to reduce the time and the effect of insignificant factors.

Appendix A

INITIAL DATA

Estimated effects for SpeedDiff

Effect	*Estimate*	*Stnd. Error*	*V.I.F.*
average	1,08502	0,197479	
A:nproc	-0,337681	0,394958	1,0
B:nCorrectors	-0,0457812	0,394958	1,0
C:nNonOrth	0,210444	0,394958	1,0
D:nOuterCor	0,467919	0,394958	1,0
E:p	-0,836531	0,394958	1,0
F:rho	-0,146881	0,394958	1,0
G:U	-0,757881	0,394958	1,0
H:Yi	0,285219	0,394958	1,0
I:h	0,676569	0,394958	1,0
J:k	-0,0445063	0,394958	1,0
K:epsilon	-1,12106	0,394958	1,0
AB+CF+GI+JK	-0,823344	0,394958	1,0
AC+BF+DI+HJ	0,465206	0,394958	1,0
AD+CI+EJ+FG	0,215081	0,394958	1,0
AE+DJ+HI	0,0951813	0,394958	1,0
AF+BC+DG+HK	-0,669294	0,394958	1,0
AG+BI+DF	0,0832563	0,394958	1,0
AH+CJ+EI+FK	-0,685719	0,394958	1,0
AI+BG+CD+EH	0,0999812	0,394958	1,0
AJ+BK+CH+DE	-0,320694	0,394958	1,0
AK+BJ+FH	0,573231	0,394958	1,0
BD+CG+EK+FI	-0,137419	0,394958	1,0
BE+DK+GH	-0,0947188	0,394958	1,0
BH+CK+EG+FJ	0,719731	0,394958	1,0
CE+DH+GK+IJ	-0,174369	0,394958	1,0
EF+GJ+IK	0,151356	0,394958	1,0

Standard errors are based on total error with 5 d.f

The StatAdvisor

This table shows each of the estimated effects and interactions. Also shown is the standard error of each of the effects, which measures their sampling error. Note also that the largest variance inflation factor (V.I.F.) equals 1,0. For a perfectly orthogonal design, all of the factors would equal 1. Factors of 10 or larger are usually interpreted as indicating serious confounding amongst the effects.

To plot the estimates in decreasing order of importance, select Pareto Charts from the list of Graphical Options. To test the statistical significance of the effects, select ANOVA Table from the list of Tabular Options. You can then remove insignificant effects by pressing the alternate mouse button, selecting Analysis Options, and pressing the Exclude button.

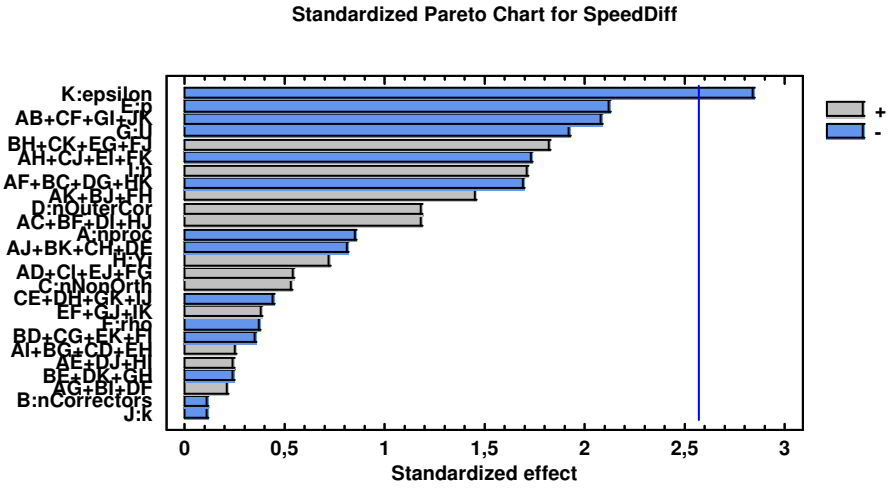

Analysis of Variance for SpeedDiff

Source	*Sum of Squares*	*Df*	*Mean Square*	*F-Ratio*	*P-Value*
A:nproc	0,912229	1	0,912229	0,73	0,4316
B:nCorrectors	0,0167674	1	0,0167674	0,01	0,9122
C:nNonOrth	0,354293	1	0,354293	0,28	0,6170
D:nOuterCor	1,75158	1	1,75158	1,40	0,2894
E:p	5,59828	1	5,59828	4,49	0,0877
F:rho	0,172593	1	0,172593	0,14	0,7252
G:U	4,59507	1	4,59507	3,68	0,1131
H:Yi	0,650798	1	0,650798	0,52	0,5026
I:h	3,66196	1	3,66196	2,93	0,1474
J:k	0,0158465	1	0,0158465	0,01	0,9147
K:epsilon	10,0541	1	10,0541	8,06	0,0363
AB+CF+GI+JK	5,42316	1	5,42316	4,35	0,0915
AC+BF+DI+HJ	1,73133	1	1,73133	1,39	0,2919
AD+CI+EJ+FG	0,37008	1	0,37008	0,30	0,6094
AE+DJ+HI	0,0724758	1	0,0724758	0,06	0,8191
AF+BC+DG+HK	3,58363	1	3,58363	2,87	0,1509
AG+BI+DF	0,0554528	1	0,0554528	0,04	0,8414
AH+CJ+EI+FK	3,76168	1	3,76168	3,01	0,1430
AI+BG+CD+EH	0,07997	1	0,07997	0,06	0,8102
AJ+BK+CH+DE	0,822756	1	0,822756	0,66	0,4537
AK+BJ+FH	2,62875	1	2,62875	2,11	0,2064
BD+CG+EK+FI	0,151071	1	0,151071	0,12	0,7421
BE+DK+GH	0,0717731	1	0,0717731	0,06	0,8200
BH+CK+EG+FJ	4,1441	1	4,1441	3,32	0,1280
CE+DH+GK+IJ	0,243236	1	0,243236	0,19	0,6773
EF+GJ+IK	0,18327	1	0,18327	0,15	0,7173
Total error	6,23968	5	1,24794		
Total (corr.)	57,346	31			

R-squared = 89,1192 percent

R-squared (adjusted for d.f.) = 32,5393 percent

Standard Error of Est. = 1,11711

Mean absolute error = 0,364605

Durbin-Watson statistic = 2,51078 (P=0,6752)

Lag 1 residual autocorrelation = -0,255401

The StatAdvisor

The ANOVA table partitions the variability in SpeedDiff into separate pieces for each of the effects. It then tests the statistical significance of each effect by comparing the mean square against an estimate of the experimental error. In this case, 1 effects have P-values less than 0,05, indicating that they are significantly different from zero at the 95,0% confidence level.

The R-Squared statistic indicates that the model as fitted explains 89,1192% of the variability in SpeedDiff. The adjusted R-squared statistic, which is more suitable for comparing models with different numbers of independent variables, is 32,5393%. The standard error of the estimate shows the standard deviation of the residuals to be 1,11711. The mean absolute error (MAE) of 0,364605 is the average value of the residuals. The Durbin-Watson (DW) statistic tests the residuals to determine if there is any significant correlation based on the order in which they occur in your data file. Since the P-value is greater than 5,0%, there is no indication of serial autocorrelation in the residuals at the 5,0% significance level.

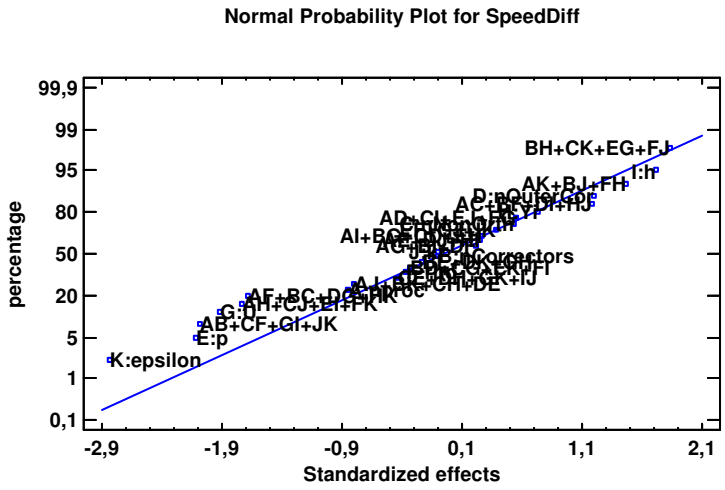

Appendix B

SELECTION OF FINAL PARAMETERS

Analyze Experiment - SpeedDiff

Estimated effects for SpeedDiff

Effect	*Estimate*	*Stnd. Error*	*V.I.F.*
average	1,08502	0,150352	
A:nproc	-0,337681	0,300704	1,0
D:nOuterCor	0,467919	0,300704	1,0
E:p	-0,836531	0,300704	1,0
F:rho	-0,146881	0,300704	1,0
G:U	-0,757881	0,300704	1,0
H:Yi	0,285219	0,300704	1,0
I:h	0,676569	0,300704	1,0
J:k	-0,0445063	0,300704	1,0
K:epsilon	-1,12106	0,300704	1,0
AF+DG+HK	-0,669294	0,300704	1,0
AH+EI+FK	-0,685719	0,300704	1,0
EG+FJ	0,719731	0,300704	1,0
GI+JK	-0,823344	0,300704	1,0

Standard errors are based on total error with 18 d.f.

The StatAdvisor

This table shows each of the estimated effects and interactions. Also shown is the standard error of each of the effects, which measures their sampling error. Note also that the largest variance inflation factor (V.I.F.) equals 1,0. For a perfectly orthogonal design, all of the factors would equal 1. Factors of 10 or larger are usually interpreted as indicating serious confounding amongst the effects.

To plot the estimates in decreasing order of importance, select Pareto Charts from the list of Graphical Options. To test the statistical significance of the effects, select ANOVA Table from the list of Tabular Options. You can then remove insignificant effects by pressing the alternate mouse button, selecting Analysis Options, and pressing the Exclude button.

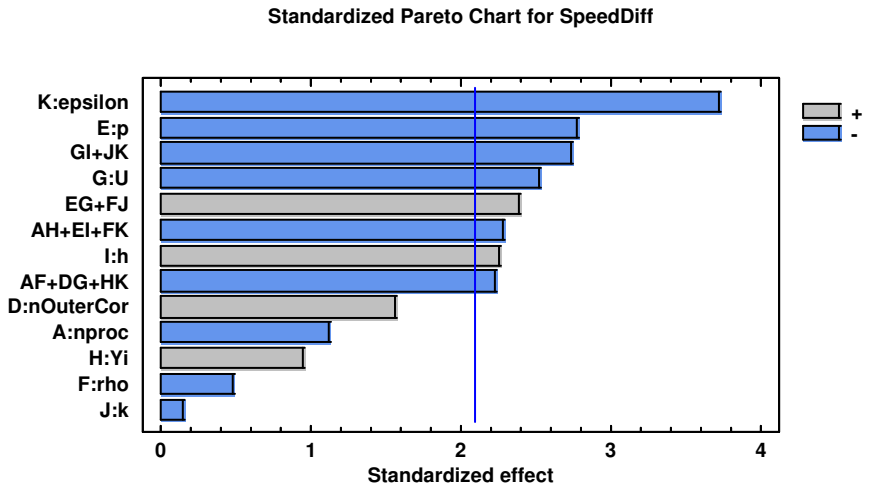

Analysis of Variance for SpeedDiff

Source	*Sum of Squares*	*Df*	*Mean Square*	*F-Ratio*	*P-Value*
A:nproc	0,912229	1	0,912229	1,26	0,2762
D:nOuterCor	1,75158	1	1,75158	2,42	0,1371
E:p	5,59828	1	5,59828	7,74	0,0123
F:rho	0,172593	1	0,172593	0,24	0,6311
G:U	4,59507	1	4,59507	6,35	0,0214
H:Yi	0,650798	1	0,650798	0,90	0,3554
I:h	3,66196	1	3,66196	5,06	0,0372
J:k	0,0158465	1	0,0158465	0,02	0,8840
K:epsilon	10,0541	1	10,0541	13,90	0,0015
AF+DG+HK	3,58363	1	3,58363	4,95	0,0390
AH+EI+FK	3,76168	1	3,76168	5,20	0,0350
EG+FJ	4,1441	1	4,1441	5,73	0,0278
GI+JK	5,42316	1	5,42316	7,50	0,0135
Total error	13,0209	18	0,723384		
Total (corr.)	57,346	31			

R-squared = 77,2941 percent

R-squared (adjusted for d.f.) = 60,8954 percent

Standard Error of Est. = 0,85052

Mean absolute error = 0,471606

Durbin-Watson statistic = 2,25152 (P=0,7096)

Lag 1 residual autocorrelation = -0,143933

The StatAdvisor

The ANOVA table partitions the variability in SpeedDiff into separate pieces for each of the effects. It then tests the statistical significance of each effect by comparing the mean square against an estimate of the experimental error. In this case, 8 effects have P-values less than 0,05, indicating that they are

significantly different from zero at the 95,0% confidence level.

The R-Squared statistic indicates that the model as fitted explains 77,2941% of the variability in SpeedDiff. The adjusted R-squared statistic, which is more suitable for comparing models with different numbers of independent variables, is 60,8954%. The standard error of the estimate shows the standard deviation of the residuals to be 0,85052. The mean absolute error (MAE) of 0,471606 is the average value of the residuals. The Durbin-Watson (DW) statistic tests the residuals to determine if there is any significant correlation based on the order in which they occur in your data file. Since the P-value is greater than 5,0%, there is no indication of serial autocorrelation in the residuals at the 5,0% significance level.

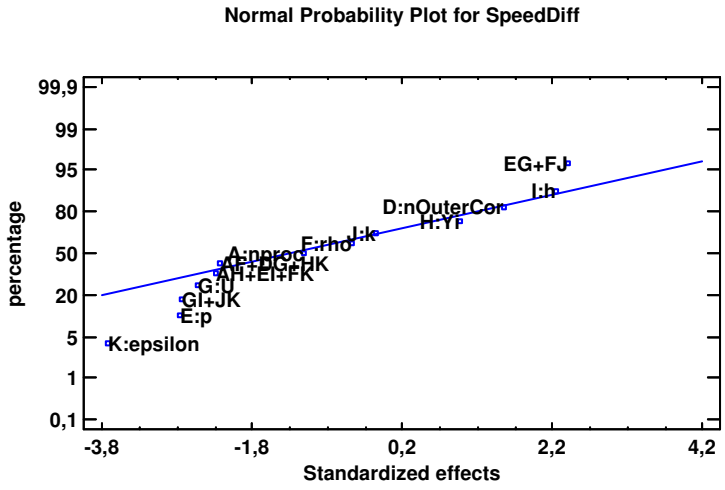

Optimize Response

Goal: minimize SpeedDiff

Optimum value = -0,976133

Factor	*Low*	*High*	*Optimum*
nproc	-1,0	1,0	0,999627
nCorrectors	-1,0	1,0	0,339439
nNonOrth	-1,0	1,0	0,999152
nOuterCor	-1,0	1,0	-1,0
p	-1,0	1,0	0,731128
rho	-1,0	1,0	0,984508
U	-1,0	1,0	0,999058
Yi	-1,0	1,0	0,990301
h	-1,0	1,0	0,977513
k	-1,0	1,0	0,232391
epsilon	-1,0	1,0	1,0

Table 6: Factor levels

The StatAdvisor

This table shows the combination of factor levels which minimizes SpeedDiff over the indicated region. Use the Analysis Options dialog box to indicate the region over which the optimization is to be performed. You may set the value of one or more factors to a constant by setting the low and high limits to that value.

10. REFERENCES

1. Computational Fluid Dynamics:
   http://en.wikipedia.org/wiki/Computational_fluid_dynamics
2. OpenFOAM
   http://www.openfoam.com

2.2. PUBLICACIONES

2.2.1. On the boundary condition setup of Large Eddy Simulation of Diesel sprays. Modelling for Addictive Behaviour, Medicine and Engineering 2010. pp. 87-99. I.S.B.N.: 978-84-693-9537-0.

On the boundary condition setup of Large Eddy Simulation of Diesel sprays.*

S. Hoyas† A. Gil, J. M. Mompó-Laborda, D. Khuong-Anh

CMT - Motores Térmicos,

Universidad Politécnica de Valencia,

Edificio 6D,46022, Valencia, Spain.

October 10, 2010

1 Introduction

For engine designers insight in the behaviour of an evaporating fuel spray is of great importance. Improvements in injection equipment reduce emissions and increase power by a more effective combustion process. Therefore, a deep understanding of the physics of Diesel spray will provide some fundamental knowledge for the design of more efficient, less consuming and cleaner engines.

During the last years great advances on the comprehension of several physical phenomena in liquid jets and sprays have been achieved, both by means of diagnosis experimental tests and CFD techniques mainly based on RANS (Reynolds Averaged Navier-Stokes) to simulate turbulence. These computational methods are very useful to study the averaged flow, but they do not provide any information neither about the turbulent fluctuations nor about the flow on the jet boundary. In this paper we present an implementation of a LES (Large Eddy Simulations) method in an non-reactive sprays. LES methods are computationally more expensive than RANS, but modelling required by RANS is reduced, and therefore they are more accurate. Furthermore, a detailed study of the flow characteristics in zones where turbulent fluctuations are significant is allowed by means of LES, while RANS, by definition, cannot model these features. For a comprehensive description of both methods, the book of Pope [1] is an excellent starting point.

Regarding Diesel spray injection, the most commonly used codes in the automotive industry, until very recently, are based on the RANS approach because of their reasonably accurate results and relatively lower computational cost. However as the RANS approach

*This research was funded by the Spanish Government (ENE2010-18542), the Universidad Politécnica de Valencia (PAID-2759) and the Generalitat Valenciana (GV/2010/039)

†Correspondig author.

has the highest level of modelling it can be seen as a successful interpolation between experimental data sets. On the contrary, direct numerical simulation (DNS) methods solve all the significative scales of the flow, so no modelling is require and it provides the highest level of description of the flow. Since the smallest structures of the flow have to be solved, the computational cost increases as $Re^{9/4}$ and the resources required for most practical cases are above current computer hardware limitations (and will probably be in the next 20 years). While the use of LES increases the computational cost, these methods are able to consistently simulate the complex structures related with turbulent mixing, which is decisive in the injection and combustion processes and invisible for RANS solvers ([2], and [3]).

The main goal of this work is to numerically investigate the influence of the inlet boundary conditions on a LES of the flow in a Diesel fuel spray evaporation system. This is the first part of a research project where the idea is to obtain a LES solver able to reproduce the different turbulent patterns that appear in the free shear flow of Diesel sprays, as well as the velocities profiles. In this paper we limited ourselves to the numerical simulation of Diesel spray with the isothermal, isodense and non-vaporizing conditions. Following the characteristic features of this congress, the paper concentrates on the mathematical aspects of the simulation. Thus, the chemical and physical analysis have also not discussed in this article and will be published elsewhere. The results are compared with the classical numerical RANS method with both Eulerian-Eulerian and Lagrangian-Eulerian approaches and are simultaneously validated with experimental data. Our algorithm has been implemented in the free all-purposes CFD code OpenFOAM © 2004-2010 OpenSource Ltd.

2 Numerical Technique

As mentioned above, the RANS approach has been traditionally used in order to model Diesel spray injections[4]. The RNG (Renormalization Group Theory) k-epsilon turbulence model with the default coefficients for the turbulent dissipation rate equation and turbulent viscosity is used for both Euler – Euler and Lagrangian – Euler spray calculations. Previous works [5] showed that RANS accurately predicts average velocity profiles and average spray's shape (i.e. dispersion rate, penetration), since the mean velocity profile and the spreading rate are independent of Re. Nevertheless, RANS is not valid if higher level of turbulence structure description is required during the calculations [3]. Table 1 resume the main characteristics of RANS models compared to LES formulation. Differences are based on the statistical treatment of the turbulence (RANS) and the use of the self-similarity theory of Kolmogorov (LES). Also differences can be found on the time-averaging of the Navier-Stokes equations and the spatial filtering for the RANS and LES respectively, see Table 2.

Application of the filtering operation to the continuity and momentum equations [1] yields:

Table 1: Comparison between RANS and LES.

RANS Reynolds-averaged Navier-Stokes	LES Large Eddy Simulation
Statistical phenomena	Kolmogorov theory of self similarity [1]
Time-averaged NS [2]	Spatial filtered NS
k - ϵ model (Jones and Launder, 1972) RNG k - ϵ model (Yakhot, 1992)	Smagorinsky (Smagorinsky, 1963) One Equation model (Yoshizawa,1985)
Less computationally demanding	Predict transient flows better

[1]Large eddies of the flow are dependent on the flow geometry, while smaller eddies are self similar and have a universal character.

[2]NS: Navier-Stokes Equations

$$\nabla \cdot \overline{u} = 0 \tag{1}$$

$$\frac{\partial \overline{u}}{\partial t} + \nabla \cdot \overline{uu} = -\frac{1}{\rho}\nabla \overline{p} + \nu \nabla^2 \overline{u} - \nabla \tau \tag{2}$$

where $\overline{u}$ is the filtered velocity field, t is the time, $\overline{p}$ is the filtered pressure, ρ is the fuel density, ν is the uniform kinematic viscosity and τ is the stress-like tensor ($\tau = \overline{uu} - \overline{uu}$). Eqs. (1) and (2) govern the evolution of the large (energy-carrying) scales of motion and the modelled stress term is τ . Also, this SGS stress tensor provides the communication between the resolved scales and the dissipation scales [6].

Closure is obtained by modelling the residual-stress tensor. The Smagorinsky [7] model is used for the sub-grid scale tensor:

$$\tau_{ij}^d = -2\mu_{SGS} S_{ij} \tag{3}$$

where τ_{ij}^d is the deviatoric SGS stress with $\mu_{SGS} = \overline{\rho}\,(C_S \Delta^2) \left\| \widetilde{S_{ij}} \right\|$. C_S is the Smagorinsky constant, a theoretical value (0.065–0.2) and $\left\| \widetilde{S_{ij}} \right\|$ is the Frobenious norm $\left\| \widetilde{S_{ij}} \right\| = \sqrt{2\widetilde{S_{ij}}\widetilde{S_{ij}}}$ of the filtered strain tensor, $\widetilde{S_{ij}} = \frac{1}{2}\left(\frac{\partial \overline{u_i}}{\partial \overline{x_j}} + \frac{\partial \overline{u_j}}{\partial \overline{x_i}}\right)$. Δ is the filter width, here assigned to be the cube root of the local cell volume.

3 Boundary conditions

Experimental results have confirmed the hypothesis that spray evolution is controlled by fuel-air mixing rates and thus they can be analysed in the same way as a gas jets [5]. Besides

Table 2: Time Averaging vs. Spatial Filtering.

Instantaneous = Average + Fluctuations ($u = \overline{u} + u'$) Averaging or filtering of NS equations gives identical equations for the averaged/filtered variables plus averaged fluctuation terms.	
Time Averaging	Spatial Filtering
$u_i(x) = \frac{1}{T}\int_t^{t+T} \overline{u_j}(x,s)\,ds.$	$u(x_0) = \int_\Omega u(x,t)\,G(x_0,x,\Delta)\ \llcorner^3 dx.$
$\overline{u_i'} = 0$, and $\overline{\overline{u_i}} = \overline{u_i}.$	$\overline{u_i'} \neq 0$, and $\overline{\overline{u_i}} \neq \overline{u_i}.$
Reynolds Stress Tensor $\tau_{ij}^R = \overline{u_j' u_i'}$	SGS[4] Stress Tensor $\tau_{ij}^S = -\left(\overline{\overline{u_i}u_j'} + \overline{u_i'\overline{u_j}} + \overline{u_i'u_j'}\right) = \overline{u_i u_j} - \overline{u_i}\,\overline{u_j}$

[3]Spatial filter $G(x_0, x, \Delta)$ with filter size Δ

[4]Subgrid Scale

the simplifications brought by the experimental researches, CFD still remains limitations in term of the modelling of the atomisation process of the nearby zone which is not the goal of the present study. In addition, the present work can be seen as a previous approach to the inclusion of droplets (Lagrangian term) as a source of mass and momentum. Hence, to keep the same computational domain will provide a better application of present conclusions to future Lagrangian-Eulerian LES calculation and a more suitable framework for further comparison between them. Consequently, the simplification of the computational domain presented by Vuorinen [8] is also assumed. In his work the inlet boundary condition is set far enough from the nozzle avoiding the problems of the void fraction limits which grid resolution required by LES makes it more restrictive. As presented below, turbulent gas jet theory will be applied to set the fields in the inlet boundary conditions of the domain.

Studies show how under certain conditions, for any section perpendicular to the spray axis in the steady region of the gas jet or diesel spray, momentum flux is conservative, and thus equal to that existing at the nozzle exit ([9], [10]). Therefore, a proper implementation of the inlet boundary condition would perform the same spray development independent of where it would be placed. Consequently, the inlet boundary condition must be perpendicular to the spray axis, contain the whole spray and the same momentum flux as at the nozzle exit and in order to ensure a more realistic development of the flow the boundary inlet has to reproduce the same profile of the fields as in a steady spray.

Since momentum flux can be obtained from experimental data, the unknown factors to set up the BC. can be identified by integrating momentum over the whole spray section:

$$\begin{aligned}\dot{M}_0 &= \frac{\pi}{2\alpha}\cdot\rho_a\cdot\tan^2\left(\frac{\theta_u}{2}\right)\\ &\cdot x^2\cdot U_{axis}^2\cdot\sum_{i=0}^{\infty}\frac{1}{\left(1+i\frac{S_C}{2}\right)}\\ &\cdot\left[\left(\frac{U_{axis}}{U_0}\right)\left(\frac{1+S_C}{2}\right)\left(\frac{\rho_f-\rho_a}{\rho_f}\right)\right]^i\end{aligned} \tag{4}$$

Desantes et al. obtain the previous expression for the spray momentum [11] assuming a Gaussian radial profile [12] for fuel concentration and axial velocity. Here the Schmidt number (S_C) represents the relative rate of momentum and mass transport and θ_u is the spray cone angle. The point of interest for the present work can be seen in Figure 1 where the axis velocity equals the injected velocity ($U_{axis} = U_0$) and a Gaussian radial profile can be assumed. The spray injected under the physical conditions shown in Table 3 has been simulated [13]. In these conditions the end of the non-perturbed zone for the isodense case is located at 4.073mm, approximately $8d_{eq}$ from the nozzle exit (with $d_{eq} = d_0\sqrt{\rho_f/\rho_a}$) and the spray diameter is 2.07mm which is set as the inlet boundary condition diameter. Since LES calculation requires perturbed inlet boundary conditions, the velocity and concentration reference profiles at the inlet boundary condition are Gaussian profiles randomly perturbed a 10% as a first simplify approximation. The discussion of the convenience of this hypothesis will be discussed in the followings sections.

Table 3: Definition of experimental and gas jet CFD simulation $\dot{M} = 1.11N$.

	reference[13]	simulation
Fuel	$C_{13}H_{28}$(l)	fuel (N_2)
Air	N_2	N_2
P_{inj} (MPa)	73.995	-
$P_{a,\infty}$ (MPa)	3.5	3.55
$T_{f,0}$ (K)	307.58	307.58
$T_{a,\infty}$	307.58	307.58
$\rho_{f,0}/\rho_{a,\infty}$	21.26	1
U_0 m/s	373.27	373.27
d_{inlet} μm	112	2070
d_{eq} μm	516	516

The computational domain is a cylindrical volume (d = 40mm, L = 70mm) that represents the shape of the injection test rig chamber. The meshing methodology is fairly the same for the RANS and LES calculations, with different grid densities depending on

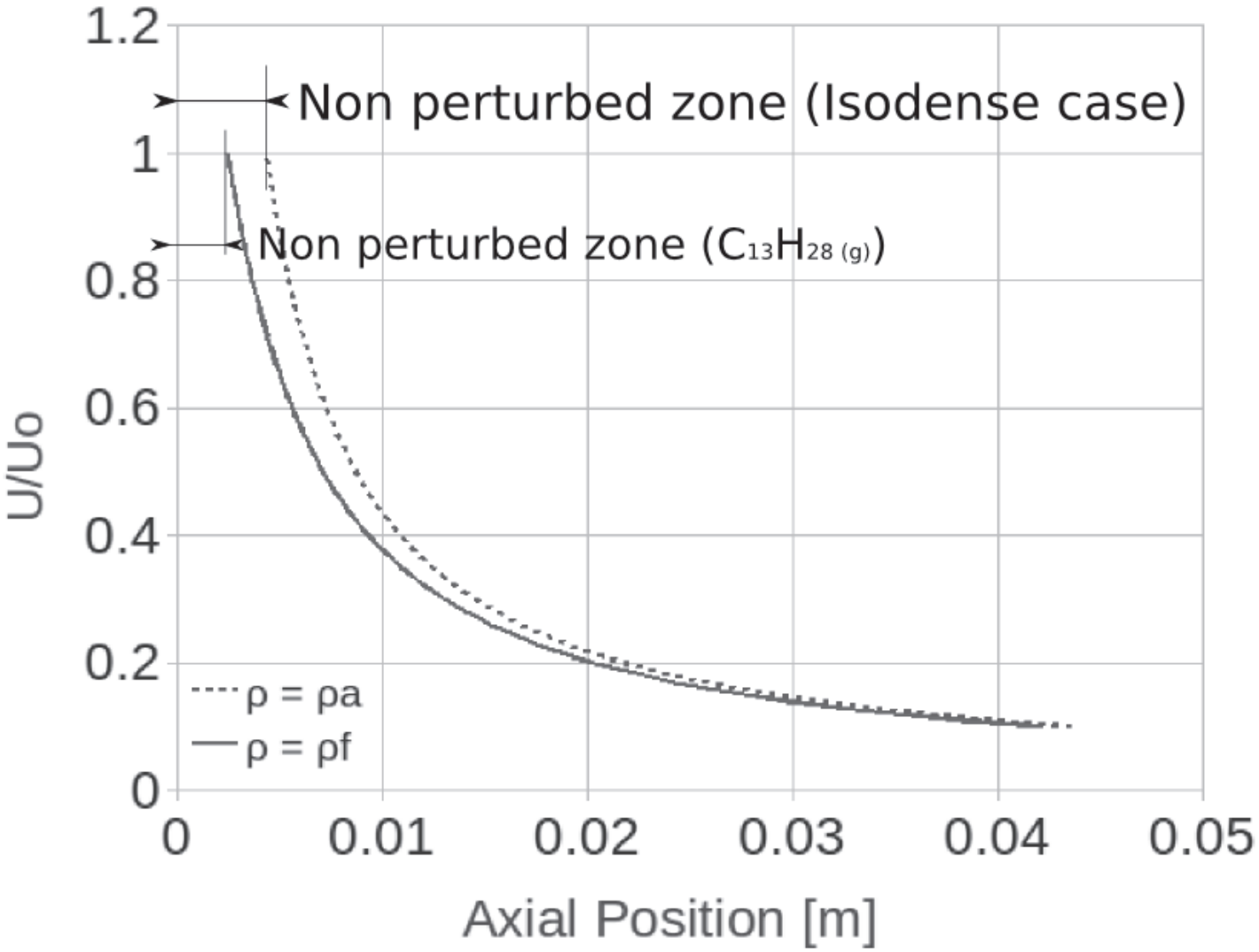

Figure 1: Axis velocity. Red line: Isodense case, Blue line: $C_{13}H_{28}$(g) case

Table 4: Definition of gas jet CFD boundary conditions.

Surface	Boundary type	Defining variables
Spray inlet diameter	Velocity turbulent inlet	$U_0(r)\&C(r)$, T_f
Wall	rigid wall, non-slip condition	–
outlet	constant pressure,	$P_{a,\infty}$;
	wave Transmissive boundary	$T_{a,\infty}$

the turbulence formulation. Hexahedral cells have been preferred for the grid generation, since they provide better accuracy and stability than tetrahedral cells. The computational domain has been decomposed into hexahedral subparts in order to get a semi-structured topology mesh, as shown in Figure 2(a). Cells are concentrated around the spray diameter (d = 2.07mm) to get a cell size of 60 μm and 20 μm for the RANS and LES meshes respectively. Downstream the nozzle the mesh is progressively adapted to the shape of the computational domain in order to obtain a homogeneous cell size at sections located downstream the inlet boundary condition, see circular sections on the right of Figure 2(a) &(b). The number of cells is around $4\text{x}10^5$ and $5.5\text{x}10^6$ for the RANS and LES formulation respectively. Also, an evolution on the LES mesh has been performed in order to optimize skewness, uniformity and number of cells (reduced to $4.9\text{x}10^6$ elements) of the mesh along the fluid zone occupied by the spray. Previous studies performed on RANS Euler – Euler [14] in similar spray conditions show that the structure of the mesh and cell size are enough to get a grid independent solution. Also, the meshes used for the LES formulation have comparable and also smaller cell sizes than recent LES studies [8] for sprays characterization where the grid independence is proved. Finally, three boundary conditions are assigned in the computational domain as depicted in Table 4.

4 Numerical results

The obtained numerical results are contrasted with those predicted by classical RANS models and compared with experimental data. Experimental results have been obtained from previously published data from the authors' research group [10], [15], [13].

Temporal evolution of the axial velocity at 25mm of the virtual nozzle has been used to justify the beginning for the statistical measurements. In Figure 3 (first of temp ev.) the criteria of a constant spray angle was used to set the radial position range of the probes. It is also shown the velocity value imposed in the center of the inlet boundary condition (4.073mm from the virtual nozzle under the isodense conditions). The difference in both the frequency content and the width of the velocity signals in the inlet boundary condition and the axis velocity at 25mm show a lack of precision of the spray fields simulated at the inlet boundary condition and justify the transient period needed for the turbulent

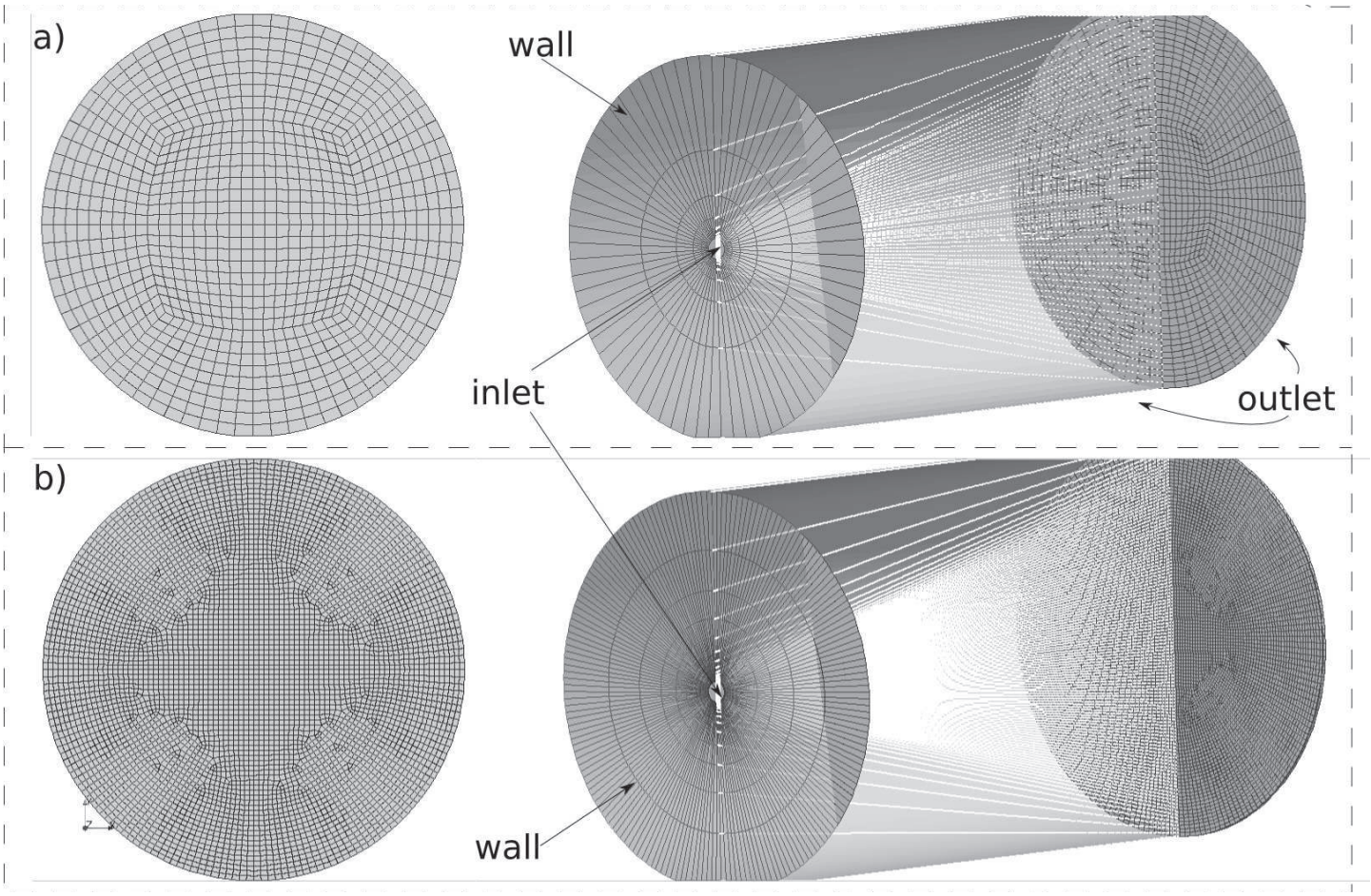

Figure 2: Calculation domain and boundary conditions. a) RANS case, b) LES case

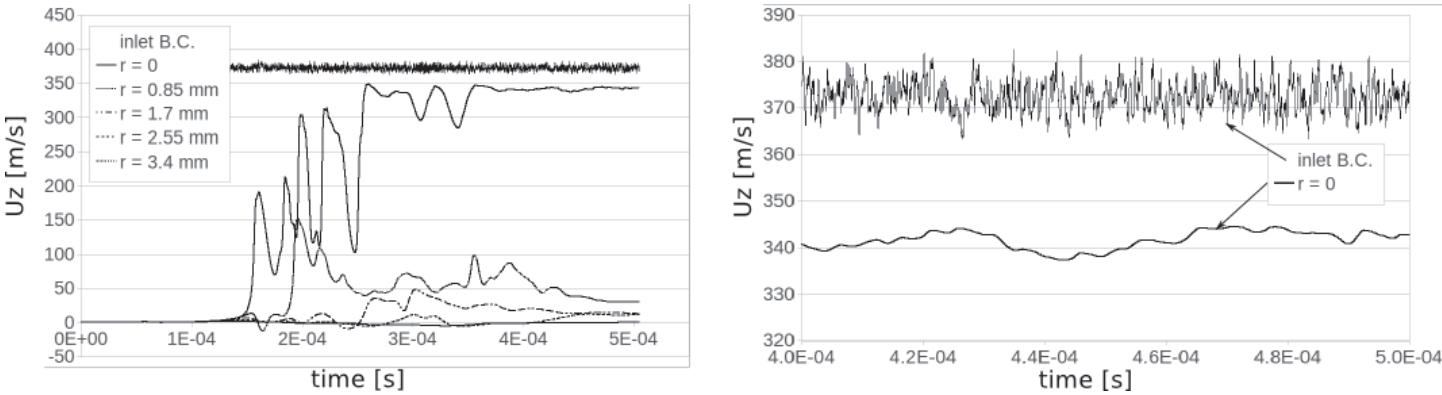

Figure 3: Measurements of radial probes (x=25mm)

evolution. Its effect in LES in terms of the classical parameters to characterize the spray is decisive as shown in Figures 4 and 5

The maximum axial distance for a 1% fuel concentration is the criteria used to define the penetration at Figures 4. Notice that this distance is located at the edge of the spray for theoretical and RANS calculations but not necessarily for LES simulations as shown in Figures 5. RANS and LES (E-E) calculations correspond to isodense cases detailed in previous sections and to obtain the RANS (L-E) penetration a Lagrangian formulation is coupled with an Eulerian one to track the particle dispersion and solve the gas phase variables.

The over prediction of both the RANS and LES Eulerian-Eulerian penetration at is affected by: the different injection mass flow rate shape, the fact that spray is more effective in transferring injection momentum to the ambient than the gas jet [16] and the non-fulfilment of the isodense hypothesis up to $30d_{eq}$. Furthermore, for the LES calculation, the first 5mm can be seen as a length required to develop turbulence Figure 5. Thus, the first assumption of a 1% of velocity fluctuation at the inlet boundary condition is not a good enough turbulent initialization of the flow. Although the inlet is placed at the end of an not well-known zone, authors think a more realistic turbulent conditions can be achieved by applying more realistic measured or calculated profiles of velocity variation [17], [18]. The Figure 5 show iso-surfaces of fuel concentration for the LES simulation at 0.3ms. The red line and the green line mark the stoichiometric iso-surface for LES and RANS (E-E) simulations respectively. These areas have a relevant importance in combustion processes. The upper part of the figure plots the radial distance of these surfaces where detached surfaces far from the jet can be found.

A comparison with the Gaussian radial profiles is shown in Figure 6. In both the axial velocity has been normalized with the axis velocity. In Figure 6(left) the radial distance is normalized with the jet's half-width as defined by Pope [1] where in Figure 6(right) is normalized with the axial distance. A spatial average at 25mm of the nozzle of the axial velocity (t= 0.5ms) shows a good agreement with the theoretical Gaussian profile from the edge to the 30% of the axis speed Figure 6(left). Differences in simulated profiles at 20

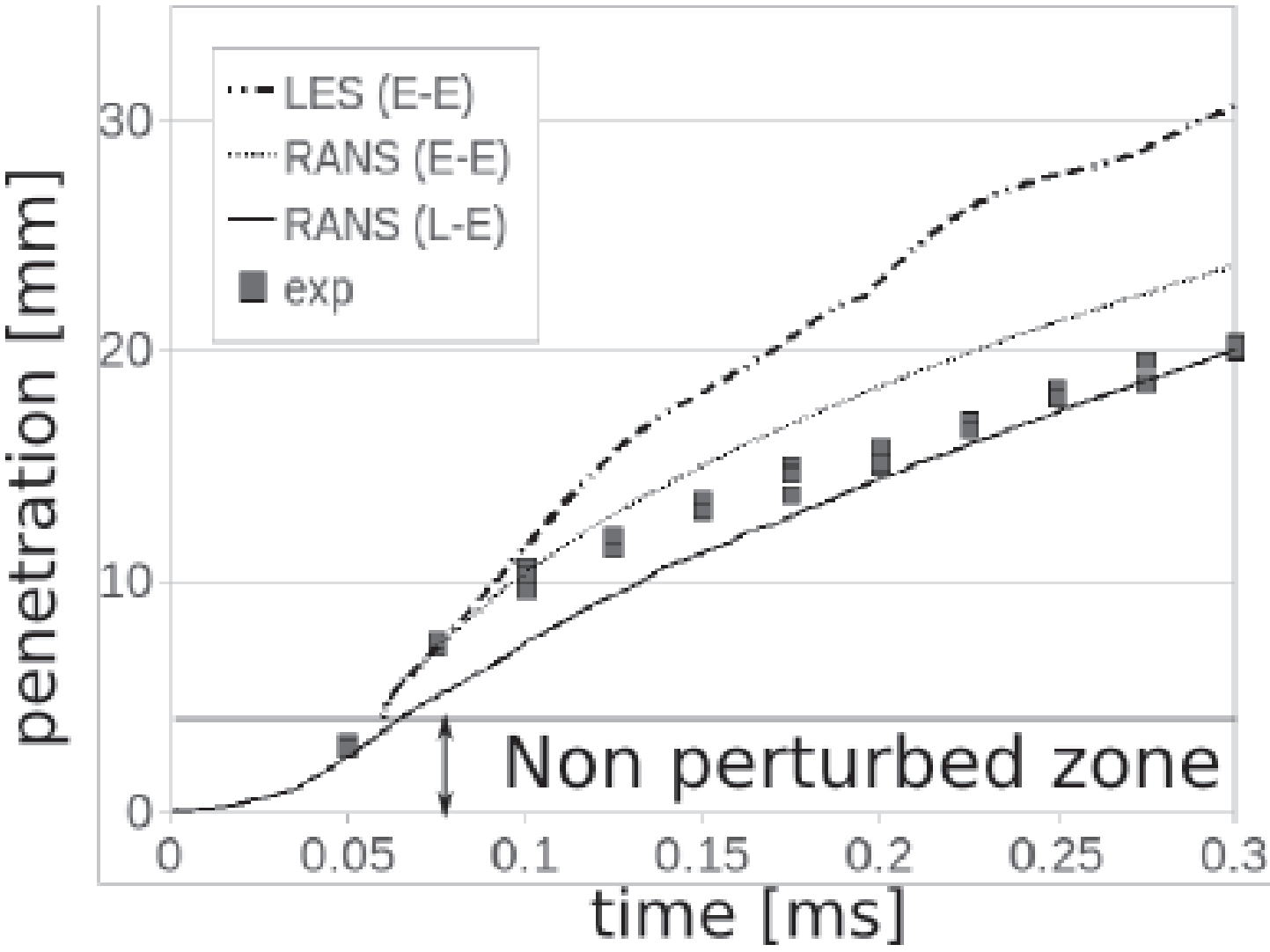

Figure 4: Comparison between experimental spray tip penetration (symbols) and CFD simulations (lines). The time axis is referred to the start of injection.

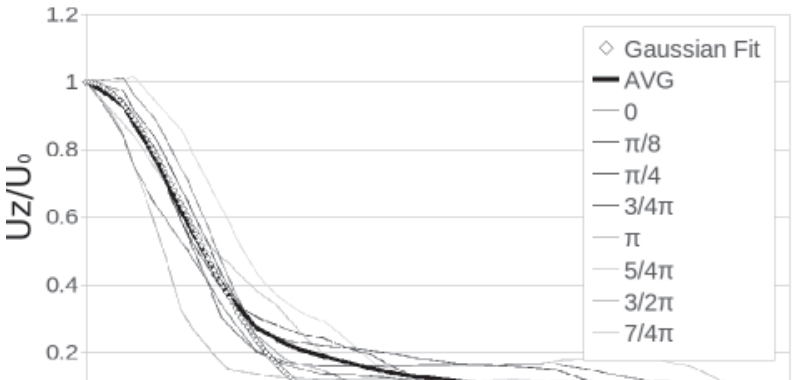

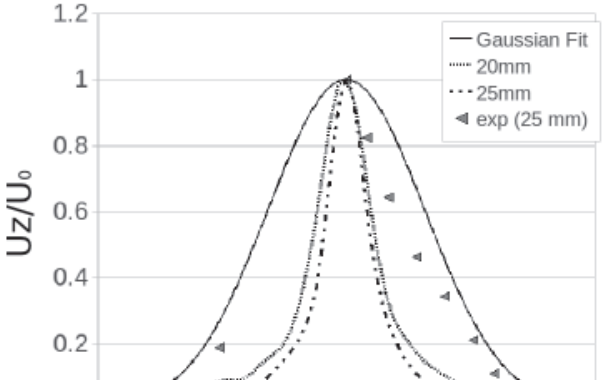

Figure 6: Radial velocity profiles (t=0.5ms). Left: Spatial average of eight different angles, Right: Time-averaged.

and 25 mm in Figure 6(right) can be affected by the amount of statistics for each location (around 0.05ms of data less at 25mm). Experimental data is close to LES simulated profile near the edge of the spray but moves to the Gaussian one as r increases.

5 Conclusions

Using the OpenFOAM code, the authors have performed a completed simulation of diesel spray in LES. Even the results do not match completely with the experimental results and RANS simulation, however; it performs a correct trend of spray simulation. These depict the complicate of modelling of spray processes with many direct or indirect parameters involved. Some specific needs are presented in our paper as challenges to overcome. The future research is now focusing on identifying the important parameters that affect the model and on improving the stability and accuracy of algorithms within OpenFOAM code. By so doing, the better spray simulation will be performed and a reliable tool will be used in modelling the spray simulation in the near future. Hence, LES modelling can become the practical tool in both industry and academic in the design process of combustion systems.

References

[1] Pope S. B., Turbulent Flows, Cambridge University Press, 2000. 771 pp.

[2] J.J. Riley, Review of large-eddy simulation of non-premixed turbulent combustion, J Fluids Eng 128 (2006), pp. 209-215.

[3] Pitsch, H., Large-Eddy Simulation of Turbulent Combustion, Annual Review of Fluid Mechanics, Vol. 38, No. 1, 2006, pp. 453-482.

[4] Fabian Peng-Krrholm, Numerical modelling of diesel spray injection, turbulence and combustion, Ph.D. Thesis, Chalmers Uni. of Technology, 2008.

[5] J.M. Desantes and J.V. Pastor and J.M. García-Oliver and J.M. Pastor, A 1D model for the description of mixing-controlled reacting diesel spray, Combustion and Flame, 2009, 156, pp 234 - 249.

[6] R. Payri and B. Tormos and J. Gimeno and G. Bracho, The potential of Large Eddy Simulation (LES) code for the modeling of flow in diesel injectors, Mathematical and Computer Modelling, Volume 52, Issues 7-8, 2010, Pages 1151-1160.

[7] J.S. Smagorinsky, General circulation experiments with the primitive equations. I. The basic experiment, Mon. Weather Rev. 91 (1963), pp. 99–164.

[8] Ville Vuorinen, LES of Certain Droplet Size Effects in Fuel Sprays, PhD Thesis, the Aalto University School of Science and Technology, 2010.

[9] Desantes JM, Payri R, Salvador FJ, Gimeno J. Measurements of spray momentum for the study of cavitation in diesel injection nozzles. SAE Paper 2003-01-0703; 2003.

[10] R. Payri, J.M. García, F.J. Salvador and J. Gimeno, Using spray momentum flux measurements to understand the influence of Diesel nozzle geometry on spray characteristics, Fuel 84 (2005), pp. 551–561.

[11] J.M. Desantes, R. Payri, J.M. Garcí

a and F.J. Salvador, A contribution to the understanding of isothermal diesel spray dynamics, Fuel 86 (2007), pp. 1093–1101.

[12] Correas D. Theoretical and experimental study of isothermal Diesel free sprays (In Spanish), PhD Thesis, Universidad Politcnica de Valencia; 1998.

[13] D. Jaime Gimeno Garca, Desarrollo y aplicacin de la medida del flujo de cantidad de movimiento de un chorro diesel, PhD thesis, Universidad Politécnica de Valencia, 2008.

[14] Abraham J, What is Adequate Resolution in the Numerical Computations of Transient Jets? SAE 970051 pp 81-95

[15] L. Araneo, V. Soare, R. Payri, J. Shakal, Setting up PDPA system for measurement in a diesel spray, Journal of Physics, 45, 2006, 85-93.

[16] Abraham J, Magi V, Macinnes J, Bracco FV. Gas versus Spray Injection: Which Mixes Faster? SAE paper 940895; 1994, pp163-177

[17] Hussein HJ, Capp and George WK. Velocity measurements in a high-Reynolds-number, momentum-conserving, axisymetric, turbulent jet, J Fluid Mech (1994). 258, 31-75.

[18] Levy Y, Lockwood FC, Combust. Flame 40, 333 (1981)

2.2.2. A Large-Eddy Simulation of Diesel-like gas jets. International Conference on Mechanical, Automotive and Aerospace Engineering 2011 (Published in International Journal of Vehicle Systems Modelling and Testing – IJVSMT)

A large-eddy simulation of diesel-like gas jets

Sergio Hoyas*, Antonio Gil,
Juan Manuel Mompó-Laborda and
Dung Khuong-Anh

CMT – Motores Térmicos,
Universidad Politécnica de Valencia,
Camino de Vera S/N, 46022 Valencia, Spain
E-mail: serhocal@mot.upv.es
E-mail: angime@mot.upv.es
E-mail: juamomla@mot.upv.es
E-mail: ankh2@mot.upv.es
*Corresponding author

Abstract: Some aspects of the transient evolution of diesel-liked gas jets by means of large-eddy simulation (LES) are discussed in this work. In order to understand the relationship between the inlet boundary condition and the development of the turbulent motions of the diesel sprays, a 3D injection chamber is simulated. The main assumption of the setup is the turbulent gas jet theory hypothesis applied to the inlet boundary conditions. Validation of the results is achieved by comparing with both experimental diesel spray measurements and trusted Reynolds-averaged Navier-Stokes (RANS) simulations. Results show that reasonable simulation of turbulent patterns from one diameter far away of the inlet boundary condition is achieved.

Keywords: LES methods; diesel sprays; biphasic flows.

Reference to this paper should be made as follows: Hoyas, S., Gil, A., Mompó-Laborda, J.M. and Khuong-Anh, D. (xxxx) 'A large-eddy simulation of diesel-like gas jets', *Int. J. Vehicle Systems Modelling and Testing*, Vol. X, No. Y, pp.000–000.

Biographical notes: Sergio Hoyas is an Associate Professor of Aerospace Engineering at the Universidad Politécnica de Valencia, where is also serving as a CFD Coordinator of the CMT-Motores Térmicos Research Institute. He holds a PhD in Applied Mathematics, and his expertise includes supercomputation and wall turbulence.

Antonio Gil is a Senior Lecturer of Civil Engineering at the Universidad Politécnica de Valencia, where is also a researcher at the CMT-Motores Térmicos Research Institute. He holds a PhD in Civil Engineering and has been working also in the industry for several years.

Juan Manuel Mompó Laborda finished his degree in Engineering (2009) with a six-month stay at the Yacht Research Unit (University of Auckland) and with the first Promoe scholarship to New Zealand that has been managed by the Polytechnic University of Valencia (Spain). In November 2009, he joined the CMT-Motores Térmicos for his doctoral thesis on LES of diesel sprays with OpenFOAM. Previously, he has participated in three R&D projects in his institute as a Research Fellow.

Dung Khuong-Anh graduated with a degree in Mechanical Engineering in 2005. He obtained his dual Master in Computational Mechanics from the Universitat Politècnica de Catalunya (2008) and École centrale de Nantes (2009), and his Master in Internal Combustion Engine from the Universidad Politécnica de Valencia (2011). His research interests are computational mechanics, FE, CFD and CAx. Currently, he works as a researcher for European Commission Marie Curie FP7 ITN 'VECOM' at UPV. His research activities include CFD simulation of direct injection diesel sprays within the framework of the Eulerian Lagrangian spray atomisation model in order to develop and validate a numerical tool for spray modelling in engine simulation and calculation.

1 Introduction

For engine designers, insight in the behaviour of an evaporating fuel spray is of great importance. Improvements in injection equipment reduce emissions and increase power by a more effective combustion process. Therefore, a deep understanding of the physics of diesel spray will provide some fundamental knowledge for the design of more efficient, less consuming and cleaner engines.

During the last years great advances on the comprehension of several physical phenomena in liquid jets and sprays have been achieved, both by means of diagnosis experimental tests and computational fluid dynamics (CFD) techniques. Simulation of turbulence is still one of the most challenging problems in physics and there is a general agreement that this simulation can be done within three levels of accuracy. The most used approaches to simulate turbulence are based on Reynolds-averaged Navier-Stokes (RANS). These computational methods are very useful to study the averaged flow, but they do not provide any information neither about the turbulent fluctuations nor about the flow on the jet boundary. Regarding diesel spray injection, the most commonly used codes in the automotive industry, until very recently, are based on this approach because of their reasonably accurate results and relatively lower computational cost. However, as the RANS approach has the highest level of modelling it can be seen as a successful interpolation between experimental datasets, and without a careful check of the results against experiments, little can be said. On the contrary, direct numerical simulation (DNS) methods solve all the significative scales of the flow, so no modelling is required and it provides the highest level of description of the flow. Since the smallest structures of the flow have to be solved, the computational cost increases as $Re^{9/4}$ and the resources required for most practical cases are above current computer hardware limitations (and will probably be in the next 20 years) (Jiménez, 2003; Hoyas and Jiménez, 2006). In this paper, we present an implementation of the third method: LES. It is computationally more expensive than RANS, but modelling required by RANS is reduced, and therefore it is more accurate. Furthermore, a detailed study of the flow characteristics in zones where turbulent fluctuations are significant is allowed by means of large-eddy simulation (LES), while RANS, by definition, cannot model these features. For a comprehensive description of these methods, the book of Pope (2000) is an excellent starting point.

As it has been said, LES increases the computational cost, but these methods are able to consistently simulate the complex structures related with turbulent mixing, which is decisive in the injection and combustion processes and invisible for RANS solvers

(Riley, 2006; Pitsch, 2006). A good knowledge of this part of the spray is crucial in order to reduce the diesel emissions. Apart from the turbulence modelling, the spray behaviour itself comprises a range of complex physical and chemical processes which are difficult to incorporate in the engine design or computer models. The nozzle internal flow greatly affects the fuel atomisation characteristics and so the subsequent engine combustion and exhaust emissions (Desantes et al., 2010; Payri et al., 2009b). The transient nature of the flow is greatly affected by the needle movement which associated with cavitation has dominated recent studies as the key phenomenon connecting internal flow and spray behaviour (Payri et al., 2009a; Margot et al., 2010). Thus, simulating the transient behaviour inside the nozzle (Payri et al., 2010) and predicting the real spray characteristics is of great importance.

Experimental information [refereed by Pastor et al. (2008)] shows that diesel sprays under both non-evaporising and vaporising conditions can be properly described with a mixing-controlled approach, and thus they can be analysed in the same way as a gas jets. However, since fuel-air mixing process is significantly influenced by fuel atomisation, breakup and collision, the idea to approximate the spray evolution using gas injection cannot be completely acceptable for LES due to its degree of physical description. LES was originally developed to deal with turbulence in single phase flows. Therefore, different approaches have been recently implemented in LES, in order to deal with this a priori complicated two-phase problem. The Eulerian-Eulerian (E-E) approach for two-phase flow has based models like the mesoscopic (Fevrier et al., 2005) or the volume of fluid (VOF) (Befrui et al., 2008). Regarding the Lagrangian-Eulerian (L-E) approach, a direct use in LES can be performed by taking into account the models needed for the sub-grid two-phase interaction (viscous work, dissipation rate, turbulent viscosity, heat flux, and species flux) (Bharadwaj and Rutland, 2010). Each of them has both advantages and disadvantages in the various regions of spray consisting of the dense zone and the downstream dilute zone. Hence, the Eulerian-Lagrangian spray atomisation (ELSA) is an integrated model for capturing the whole spray evolution in RANS calculations (Deportes et al., 2010). Consequently, LES of atomisation seems to be a necessarily step forward as depicted by Chesnel et al. (2010).

The main goal of this work is to numerically investigate the influence of the inlet boundary conditions on a LES of the flow in a diesel fuel spray evaporation system. Therefore, in this paper, we limited ourselves to the numerical simulation of diesel-liked gas jet in a combustion chamber. By including in future works those phenomena and conditions omitted here, the effect of more complex/realistic hypothesis on the physical behaviour of the spray will be noticed and its contribution on the fuel-air mixing process could be quantified. The results are compared with the classical numerical RANS method with both E-E and L-E approaches and are simultaneously validated with experimental data. Our algorithm has been implemented in the free all-purposes CFD code OpenFOAM.

The paper is structured as follows: after the introduction, the basis of the LES methodology and the main differences with RANS provide the needed mathematical background. In a subsequent section, the detailed description of the assumptions to set the boundary conditions together with the computational domain is presented. Finally, the numerical results with the main conclusions are exposed.

2 Numerical technique

As we said in the introduction, there are basically three types of methods to solve a CFD problem depending on the modelling and the description of turbulence: RANS, LES and DNS. DNS was the first developed method, but it is inapplicable in most practical cases. Both RANS and LES methods where developed more or less at the same time in the sixties. LES methods where first described by Smagorinsky in 1963 (Launder and Spalding, 1974) but, due to the computational resources required, it has not been wide applied in engineering until very recently.

Pope (2000), in his book gives an excellent introduction to LES that we are going to follow here. There are three conceptual steps in LES. First, define a filtering operation to decompose the velocity field as:

$$u(x,t) = \overline{u}(x,t) + u'(x,t). \tag{1}$$

Here, the filtered component $\bar{u}$ represents the motion of the large scales while the small scale motions that occur on length scales smaller than the mesh spacing are included in the residual component u'. The motion of these sub-grid scales (SGSs) cannot be captured and therefore their effect on the large scales is modelled in a subsequent step.

In a second stage, the Navier-Stokes equations are spatially filtered assuming that the filtering operator is commutative with the differential operator. The filtering operation is defined as:

$$\overline{f}(x,t) = \int_{\Omega} G\left(x - x'; \Delta(x)\right) f\left(x', t\right) dx', \tag{2}$$

where G is the filter function and Δ is the filter width, here assigned to be the cube root of the local cell volume. As the isodense condition was set, the introduction of density filter quantities $\tilde{f} = \overline{\rho f}/\overline{\rho}$ is negligible. A deep explanation can be found in Payri et al. (2010). In this study, the conservation equations governing the filtered velocity field $\bar{u}(x', t)$ are obtained by applying the filtering operation to the Navier-Stokes equation, for an incompressible flow of a Newtonian fluid. Thus, the filtered continuity equation and the filtered momentum equation become:

$$\nabla \cdot \overline{u} = 0, \tag{3}$$

$$\frac{\partial \overline{u}}{\partial t} + \nabla \cdot \overline{uu} = -\frac{1}{\rho}\nabla \overline{p} + \nu \nabla^2 \overline{u} - \nabla \tau, \tag{4}$$

where $\bar{u}$ is the filtered velocity field, t is the time, is the filtered pressure, ρ is the fuel density, ν is the uniform kinematic viscosity and τ is the stress-like tensor ($\tau = \overline{uu} - \overline{u}\overline{u}$). Notice that the filtered product $\overline{uu}$ differs from the product of the filtered velocities $\bar{u}\bar{u}$. Equations (3) and (4) govern the evolution of the large (energy-carrying) scales of motion and the modelled stress term is τ. Also, this SGS stress tensor provides the communication between the resolved scales and the dissipation scales (Payri et al., 2010).

In the last step, closure is obtained by modelling the residual-stress tensor. The Smagorinsky (1963) model is used for the SGS tensor:

$$\tau_{ij}^{d} = -2\mu_{SGS}S_{ij}, \tag{5}$$

where τ_{ij}^{d} is the deviatoric SGS stress with:

$$\mu_{SGS} = \bar{\rho}\left(C_S\Delta^2\right)\left\|\widetilde{S_{ij}}\right\|$$

CS is the Smagorinsky constant, with a theoretical value in the interval (0.065–0.2) and $\| \widetilde{S_{ij}} \|$ is the Frobenious norm $\| \widetilde{S_{ij}} \|= \sqrt{2\widetilde{S_{ij}}\widetilde{S_{ij}}}$ of the filtered strain tensor, $\widetilde{S_{ij}} = \frac{1}{2}\left(\frac{\partial\overline{u_i}}{\partial\overline{x_j}} + \frac{\partial\overline{u_j}}{\partial\overline{x_i}}\right)$.

The Smagorinsky constant varies with both grid mesh aspect ratio as pointed out by Scotti et al. (1993) and the mean shear (Horiuti, 1993; Yakhot et al., 1989). Although some dynamic implementations of the Smagorinsky model allow to determine CS as a function of time and position (Piomelli and Liu, 1995; Germano, 1992), there is little to be gained by the use of more complex SGS models in the case of high Reynolds number free flows of the type considered. As it was shown clearly in the previous results (Jones et al., 2010), the standard Smagorinsky model and even more simple models (Vuorinen, 2010) give good results for free flows.

The time derivative terms in equations (3) and (4) are discretised using a first order Euler scheme. The discretisation scheme for the diffusive term in equation (4) is a second order Gaussian integration interpolated linearly by a centred scheme. The convection term in equations (3) and (4) is discretised implicitly using a second order Gaussian limited linear differencing scheme. The PISO (Barton, 1998) method is used to solve the pressure correction equation.

As mentioned above, the RANS approach has been traditionally used in order to model diesel spray injections (Peng-Krrholm, 2008). The renormalisation group theory (RNG) k-epsilon turbulence model with the default coefficients for the turbulent dissipation rate equation and turbulent viscosity is used for both Euler-Euler and Lagrangian-Euler spray calculations. Previous works (Pastor et al., 2008) showed that RANS accurately predicts average velocity profiles and average spray's shape (dispersion rate, penetration), since the mean velocity profile and the spreading rate are independent of Reynolds number. Nevertheless, RANS is not valid if higher level of turbulence structure description is required during the calculations (Pitsch, 2006).

Table 1 resumes the main characteristics of RANS models compared to LES formulation. Differences are based on the statistical treatment of the turbulence (RANS) and the use of the self-similarity theory of Kolmogorov (LES). Consequently, differences can be found on the time-averaging of the Navier-Stokes equations and the spatial filtering for the RANS and LES respectively, see Table 2.

Solutions schemes for the E-E spray simulations with the RANS formulation are exactly the same to those used and described in the previous section for the LES E-E spray calculations.

Table 1 Comparison between RANS and LES

RANS	*LES*
Statistical phenomena	Kolmogorov theory of self similarity[a]
Time-averaged NS[b]	Spatial filtered NS
k – ε model RNG k – ε model	Smagorinsky (1963) One equation model
Less computationally demanding	Predict transient flows better

Notes: [a]Large eddies of the flow are dependent on the flow geometry, while smaller eddies are self similar and have a universal character.
[b]NS: Navier-Stokes equations

Table 2 Time averaging vs. spatial filtering

Instantaneous = Average + Fluctuations ($u = \bar{u} + u'$)

Averaging or filtering of NS equations gives identical equations for the averaged/filtered variables plus averaged fluctuation terms.

Time averaging	*Spatial filtering*
$u_i(x) = \frac{1}{T}\int_t^{t+T} \overline{u_j}(x, s)ds.$	$u(x_0) = \int_\Omega u(x, t)G(x_0, x, \Delta)\ ^3 dx.$
$\overline{u_i'} = 0$, and $\overline{\overline{u_i}} = \overline{u_i}.$	$\overline{u_i'} \neq 0$, and $\overline{\overline{u_i}} \neq \overline{u_i}.$
Reynolds stress tensor	*SGS[4] stress tensor*
$\tau_{ij}^R = \overline{u_j' u_i'}$	$\tau_{ij}^S = -\left(\overline{u_i}u_j' + \overline{u_i'\overline{u_j}} + \overline{u_i'u_j'}\right) = \overline{u_i u_j} - \overline{u_i}\,\overline{u_j}$

Notes: [3]Spatial filter $G(x_0, x, \Delta)$ with filter size Δ
[4]SGS

3 Boundary conditions

In diesel engines, the fuel is injected into a cylinder by a high pressure atomiser with a nozzle hole diameter d_0 which creates the fuel spray. In terms of computational difficulty, the flow is not statistically stationary and has three directions of statistical inhomogeneity. Those conditions together with the two phase appearing in the fuel at high velocity sets the spray evolution as one of the most complicated turbulent flow to simulate (Pope, 2000; Chesnel et al., 2010). As depicted at the introduction, besides the simplifications brought by the experimental researches, CFD still presents limitations in term of the modelling of the atomisation process of the nearby zone which is not the goal of the present study. Consequently, the simplification of the computational domain presented by Vuorinen (2010) is also assumed. In this work, the inlet boundary condition is set far enough from the nozzle avoiding the problems of the void fraction limits which grid resolution required by LES makes it more restrictive. In addition, the present work can be seen as a previous approach to the inclusion of droplets (Lagrangian term) as a source of mass and momentum. These particle-laden gas jets are considered by the authors as the logical following step as it has been widely used to analyse dilute sprays (Faeth, 1987, 1996). As it can be inferred from the description of the computational

domain this is the region of the spray where the research is focused. Furthermore, by keeping the same computational domain will provide a better application of present conclusions to future L-E LES calculation and a more suitable framework for further comparison between them. As presented below, turbulent gas jet theory will be applied to set the fields in the inlet boundary conditions of the domain.

Studies show how under certain conditions, for any section perpendicular to the spray axis in the steady region of the gas jet or diesel spray, momentum flux is conservative, and thus equal to that existing at the nozzle exit (Desantes et al., 2003; Payri et al., 2005). Therefore, a proper implementation of the inlet boundary condition would perform the same spray development independent of where it would be placed. Hence, the inlet boundary condition must be perpendicular to the spray axis, contain the whole spray and the same momentum flux as at the nozzle exit and in order to ensure a more realistic development of the flow the boundary inlet has to reproduce the same profile of the fields as in a steady spray.

Since momentum flux can be obtained from experimental data, the unknown factors to setup the boundary condition can be identified by integrating momentum over the whole spray section:

$$\dot{M}_0 = \dot{M}(x) = \int_0^R 2\pi\rho(x,r)U(x,r)rU(x,r)dr, \tag{6}$$

where the *x*-coordinates coincides with the spray axis and the *r*-coordinate is the radial position (perpendicular to the spray axis), ρ is the local density in the diesel spray and U is the axial velocity. Writing the density at an internal point of the spray in terms of local concentration and assuming a Gaussian radial profile (Correas, 1998) for fuel concentration and axial velocity, Desantes et al. (2007) obtained the following expression for the spray momentum:

$$\dot{M}_0 = \frac{\pi}{2\alpha}\cdot\rho_a\cdot\tan^2\left(\frac{\theta_u}{2}\right)\cdot x^2\cdot U_{axis}^2 \cdot\sum_{i=0}^{\infty}\frac{1}{\left(1+i\frac{S_C}{2}\right)}\cdot\left[\left(\frac{U_{axis}}{U_0}\right)\left(\frac{1+S_C}{2}\right)\left(\frac{\rho_f-\rho_a}{\rho_f}\right)\right]^i. \tag{7}$$

Here, the Schmidt number (S_C) represents the relative rate of momentum and mass transport and θ_u is the spray cone angle. The point of interest for the present work can be seen in Figure 1 where the $U_{axis} = U_0$. The spray injected under the physical conditions shown in Table 3 has been simulated (Correas, 1998). In these conditions, the end of the non-perturbed zone for the isodense case is located at 4.073 mm, approximately $8d_{eq}$ from the nozzle exit (with $d_{eq} = d_0\sqrt{\rho_f/\rho_a}$) and the gas jet diameter is 2.07 mm which is set as the inlet boundary condition diameter. The velocity and concentration reference profiles are defined as:

$$U(x,r) = U_{axis}(x)\cdot\exp\left(-\alpha\left(\frac{r}{R}\right)^2\right), \tag{8}$$

$$C(x,r) = C_{axis}(x) \cdot \exp\left(-\alpha \cdot S_C \cdot \left(\frac{r}{R}\right)^2\right), \tag{9}$$

with (α = 4.6) the shape factor of the Gaussian distribution. Since LES calculation requires perturbed inlet boundary conditions, the reference signal is randomly perturbed a 10% as a first approximation. The discussion of the convenience of this hypothesis will be overcome in the followings sections.

Table 3 Definition of experimental and gas jet CFD simulation

	Exp. (Correas, 1998; Gimeno García, 2008) (M = 1.11 N)	*Simulation*
Fuel	$C_{13}H_{28}$ (l)	Fuel (N_2)
Air	N_2	N_2
P_{inj} (MPa)	73.995	-
$P_{a,\infty}$ (MPa)	3.5	3.55
$T_{f,0}$ (K)	307.58	307.58
$T_{a,\infty}$ (K)	307.58	307.58
$\rho_{f,0}$ /ρa,∞	21.26	1
U_0 (m/s)	373.27	373.27
d_{inlet} (μm)	112[a]	2,070[b]
d_{eq} (μm)	516	516

Notes: [a]Nozzle diameter
[b]Jet diameter at the end of the non-perturbed zone

Figure 1 Axis velocity (see online version for colours)

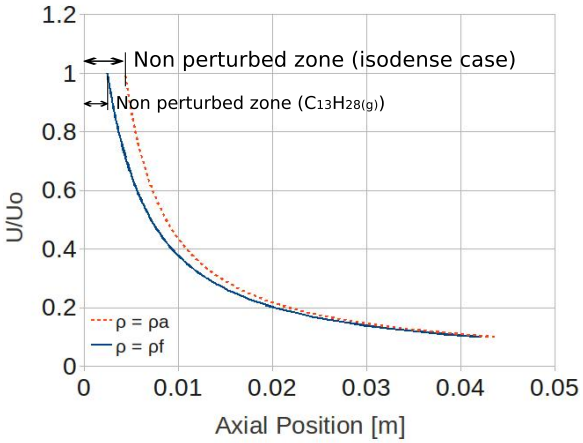

Notes: Red dot line: isodense case; Blue solid line: $C_{13}H_{28}$ (g) case

The computational domain is a cylindrical volume (d = 40 mm, L = 70 mm) that represents the shape of the injection test rig chamber. The meshing methodology is fairly the same for the RANS and LES calculations, with different grid densities depending on the turbulence formulation. Hexahedral cells have been preferred for the grid generation,

since they provide better accuracy and stability than tetrahedral cells. The computational domain has been decomposed into hexahedral subparts in order to get a semi-structured topology mesh, as shown in Figure 2(a). Cells are concentrated around the spray diameter (d = 2.07 mm) to get a cell size of 57.5 μm and 22.5 μm for the RANS and LES meshes respectively. Downstream the nozzle the mesh is progressively adapted to the shape of the computational domain in order to obtain a homogeneous cell size at sections located downstream the inlet boundary condition, see circular sections on the right of Figure 2. The numbers of cells are 4.05×10^5 and 4.9×10^6 for the RANS and LES formulation respectively.

In this mesh, the circular faces of the cylinder are splitted into four parts and then meshed with a non-structured hexahedral mesh using the same cell size than that described above. Previous studies performed on RANS Euler-Euler (Abraham, 1997) in similar spray conditions show that the structure of the mesh and cell size are enough to get a grid independent solution. Also, the meshes used for the LES formulation have comparable and also smaller cell sizes than recent LES studies (Vuorinen, 2010) for sprays characterisation where the grid independence is proved. Finally, three boundary conditions are assigned in the computational domain as depicted in Table 4.

Figure 2 Calculation domain and boundary conditions for the RANS case (see online version for colours)

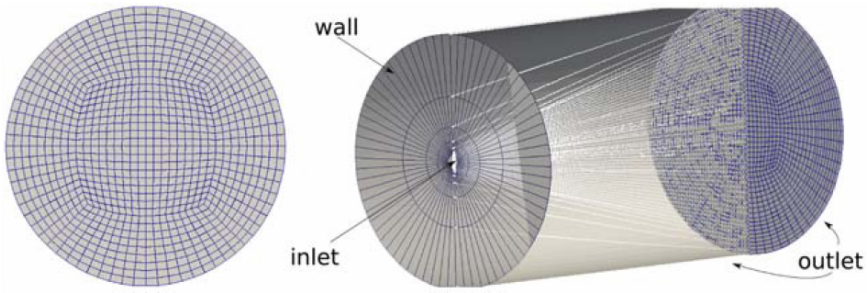

Note: LES grid is a finer version of this one.

Table 4 Definition of gas jet CFD boundary conditions

Surface	*Boundary type*	*Defining variables*
Inlet	Turbulent velocity inlet	U_0 (r) and $C(r)$, T_f
Wall	Rigid wall, non-slip cond.	-
Outlet	Constant pressure, wave transmissive	$P_{a,\infty}$ $T_{a,\infty}$

4 Numerical results

The obtained numerical results are contrasted with those predicted by classical RANS models and compared with experimental data. Experimental results have been obtained from previously published data from the authors' research group. Momentum flux data was achieved by measuring the impact force of the spray in a surface with a piezo-electric sensor (Payri et al., 2005). The droplet velocity measurements have been performed under non-vaporising conditions inside a SF6 (a dense gas) atmosphere at

room temperature (298 K). The environmental density at low pressure (0.5 MPa) was 40 Kg/m^3, close to the reference case (Araneo et al., 2006).

Temporal evolution of the axial velocity at 25 mm of the virtual nozzle has been used to justify the beginning for the statistical measurements. In Figure 3, the criteria of a constant spray angle was used to set the radial position of the probes. Thus, the first probe in the isodense calculation is located at the edge of the spray and the last at 4.25 mm from the edge. Since no significant velocity variation was detected by the most far-off probe, its measurements do not appear. It is also shown the velocity value imposed in the centre of the inlet boundary condition (4.073 mm from the virtual nozzle under the isodense conditions).

Differences in both the frequency content and the width of the velocity signals in the inlet boundary condition and the axis velocity at 25 mm show a lack of precision of the spray fields simulated at the inlet boundary condition. Its effect in LES in terms of the classical parameters to characterise the spray is decisive as shown in Figure 4.

Figure 3 Measurements of radial probes (x = 25 mm)

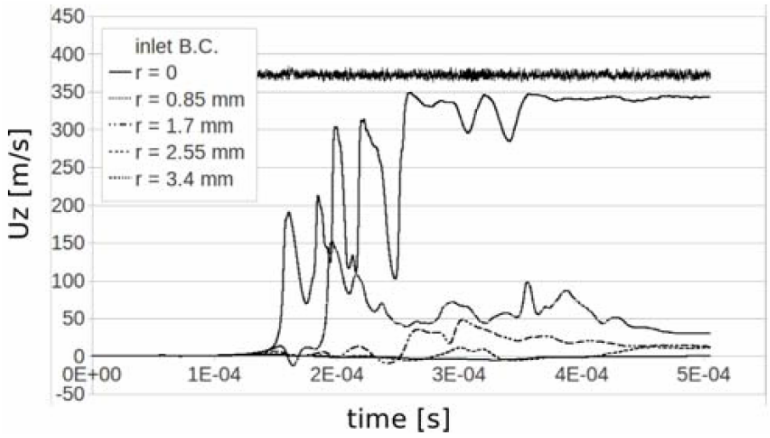

Figure 4 Measurements of axial velocity

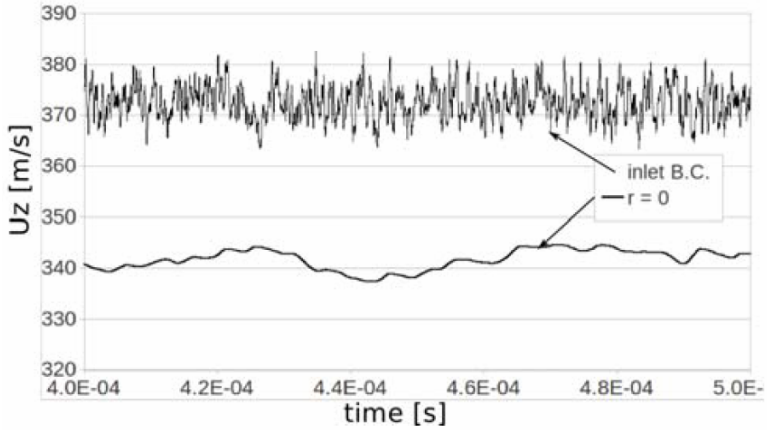

The maximum axial distance for a 1% fuel concentration is the criteria used to define the penetration. Notice that this distance is located at the edge of the spray for theoretical and RANS calculations but not necessarily for LES simulations as shown in Figure 5 (solid red line). RANS and LES (E-E) calculations correspond to isodense gas jets cases detailed in previous sections. A description of the L-E approach will be done in future works when comparing RANS with LES L-E calculations. This approach is outside of the scope of the present paper and has been shown as a reference of a good experimental estimation to compare with.

The over prediction of both the RANS and LES E-E penetration is highly affected by the different injection mass flow rate shape. The L-E injection follows the experimental progressive evolution while the E-E injection is a constant value, simplified in this way to avoid disguising the first stages of the jet with this variable.

The over prediction of both the RANS and LES E-E penetration at is also affected by the fact that spray is more effective in transferring injection momentum to the ambient than the gas jet (Abraham et al., 1994). In the L-E approach, the Lagrangian term carries the 45% of the momentum at $8d_{eq}$ of the nozzle.

Figure 5 Comparison between RANS and LES concentration iso-surfaces (t = 0.3 ms) (see online version for colours)

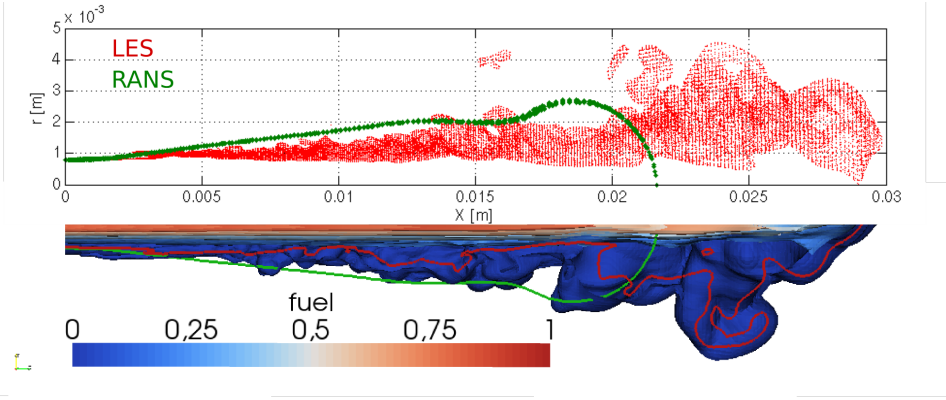

Notes: Lower part: longitudinal clip of fuel concentration contours. Upper part: Radial coordinates of stoichiometric iso-surfaces.

Furthermore, in this initial part of the spray the local density is far from the assumption of constant density of the gas jets. Therefore, the isodense hypothesis that allows to compare the gas jet with the diesel spray is so restrictive from the actual boundary condition placed at $8d_{eq}$. The assumption is acceptable beyond the developing region (x / d_{eq} > 30) where differences in axis velocity under turbulent gas jet theory are less than 3%.

Moreover, for the LES calculation, the first 5 mm can be seen as a length required developing turbulence Figure 5. Thus, the first assumption of a 10% of velocity fluctuation at the inlet boundary condition is not a good enough turbulent initialisation of the flow. Given that the inlet is placed at the end of a not well-known zone, authors think a more realistic turbulent condition can be achieved by applying measured or more accurate calculated profiles of velocity variation (Hussein et al., 1994; Levy and Lockwood, 1981). Figure 5 shows iso-surfaces of fuel concentration for the LES simulation at 0.3 ms. The red line and the green line mark the stoichiometric iso-surface

for LES and RANS (E-E) simulations respectively. These areas have a relevant importance in combustion processes. The upper part of the figure plots the radial distance of these surfaces where detached surfaces far from the jet can be found.

A comparison with the Gaussian radial profiles is shown in Figure 6 and Figure 7. In both the axial velocity has been normalised with the axis velocity. In Figure 6, the radial distance is normalised with the jet's half-width as defined by Pope (2000) where in Figure 7 is normalised with the axial distance. A spatial average at 25 mm of the nozzle of the axial velocity (t = 0.5 ms) shows a good agreement with the theoretical Gaussian profile from the edge to more than the half of the jet radius (up to 30% of the axis speed) Figure 6. Differences in simulated profiles at 20 and 25 mm in Figure 7 can be affected by the amount of statistics for each location (around 0.05 ms less data at 25 mm). Experimental data is close to LES simulated profile near the edge of the spray but moves to the Gaussian one as r increases.

Figure 6 Radial velocity profiles (t = 0.5 ms) (see online version for colours)

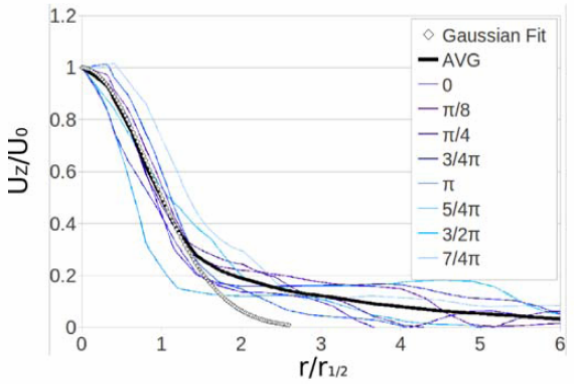

Note: Spatial average of eight different angles

Figure 7 Radial velocity profiles (t = 0.5 ms) (see online version for colours)

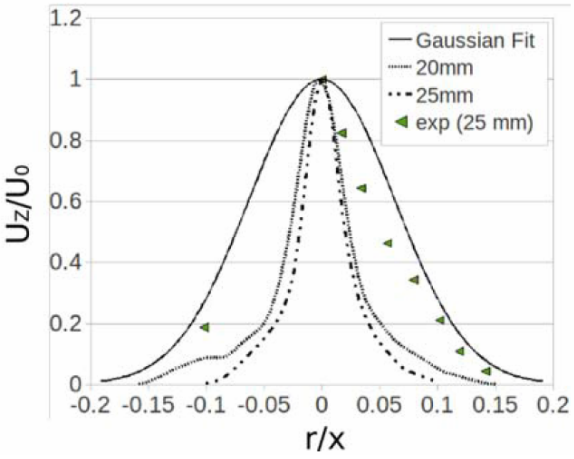

Note: Time-averaged

5 Conclusions

Using the OpenFOAM code, the authors have performed a completed simulation of diesel spray in LES. A comparison between the propose method and trusted (E-E) RANS sprays simulations has been performed, obtaining a very good agreement. Configuration and turbulent boundary conditions election have been justified and validated. Internal structure of the spray has been deeply studied, showing some characteristics of the spray. LES results have been also validated against experimental measurements of the velocity field. Some specific needs are presented in our paper as challenges to overcome. LES modelling can become the practical tool in both industry and academic in the design process of combustion system. The future research is now focusing on identifying the important parameters that affect the model and on improving the stability and accuracy of algorithms within OpenFOAM code. By so doing, the better spray simulation will be performed and a reliable tool will be used in modelling the spray simulation in the near future.

Acknowledgements

This research has been funded by the Spanish Government in the frame of the Project 'Métodos LES para la simulación de chorros multifásicos', Ref. ENE2010-18542. The authors also acknowledge the financial support of the Universidad Politécnica de Valencia under the contract Reference PAID-2759 and the Generalitat Valenciana, under the contract GV/2010/039. We are also grateful to Dr. Franciso Javier Salvador and Dr. José Manuel Pastor for providing experimental data and fruitful advices. In addition, we gratefully acknowledge helpful discussions with many researchers in CMT-Motóres Térmicos, especially Ms. Palma González and Ms. Mariany Chávez.

References

Abraham, J. (1997) 'What is adequate resolution in the numerical computations of transient jets?', SAE 970051, pp.81–95.

Abraham, J., Magi, V., Macinnes, J. and Bracco, F.V. (1994) 'Gas versus spray injection: which mixes faster?', SAE paper 940895, pp.163–177.

Araneo, L., Soare, V., Payri, R. and Shakal, J. (2006) 'Setting up PDPA system for measurement in a diesel spray', *Journal of Physics*, Vol. 45, pp.85–93.

Barton, I.E. (1998) 'Comparison of simple- and piso-type algorithms for transient flows', *International Journal for Numerical Methods in Fluids*, Vol. 26, No. 4, pp.459–483.

Befrui, B., Corbinelli, G., Robart, D. and Reckers, W. (2008) 'LES simulation of the internal flow and near-field spray structure of an outward-opening GDI injector and comparison with imaging data', SAE paper 2008-01-0137, pp.163–177.

Bharadwaj, N. and Rutland, C.J. (2010) 'A large-eddy simulation study of sub-grid two-phase interaction in particle-laden flows and diesel engine sprays', *Atomization and Spray*, Vol. 20, No. 8, pp.673–695.

Chesnel, J., Réveillon, J., Ménard, T., Berlemont, A. and Demoulin, F.X. (2010) 'Large eddy simulation of liquid atomization: from the resolved scales to subgrid spray', *International Conference on Multiphase Flow (ICMF)*.

Correas, D. (1998) 'Theoretical and experimental study of isothermal diesel free sprays', (in Spanish), PhD thesis, Universidad Politcénica de Valencia.

Deportes, A., Zellat, M., Desoutter, G., Liang, Y. and Ravet, F. (2010) 'Application of the Eulerian-Lagrangian spray atomization (ELSA) model for the diesel injection simulation', *THIESEL (2010)*.

Desantes, J.M., Payri, R., García-Oliver, J.M. and Salvador, F.J. (2007) 'A contribution to the understanding of isothermal diesel spray dynamics', *Fuel*, Vol. 86, Nos. 7–8, pp.1093–1101.

Desantes, J.M., Payri, R., Salvador, F.J. and de la Morena, J. (2010) 'Influence of cavitation phenomena on primary break-up and spray behaviour at stationary conditions', *Fuel*, Vol. 89, No. 10, pp.3033–3041.

Desantes, J.M., Payri, R., Salvador, F.J. and Gimeno, J. (2003) 'Measurements of spray momentum for the study of cavitation in diesel injection nozzles', SAE Paper 2003-01-0703.

Faeth, G.M. (1987) 'Mixing, transport and combustion in sprays', *Prog. Energy Combust. Sci*., Vol. 13, pp.293–345.

Faeth, G.M. (1996) 'Spray combustion phenomena', *26th International Symposium on Combustion*, pp.1596–1612.

Fevrier, P., Simonin, O. and Squires, K.D. (2005) 'Partitioning of particle velocities in gas-solid turbulent flows into a continuous field and a spatially uncorrelated random distribution: theoretical formalism and numerical study', *J. Fluid Mech*., Vol. 533, pp.1–46.

Germano, M. (1992) 'Turbulence: the filtering approach', *J. Fluid Mech*., Vol. 238, pp.325–336.

Gimeno García, D.J. (2008) Desarrollo y aplicación de la medida del flujo de cantidad de movimiento de un chorro diesel, PhD thesis, Universidad Politécnica de Valencia.

Horiuti, K. (1993) 'A proper velocity scale for modelling subgrid-scale eddy viscosities in large eddy simulation', *Physics of Fluids*, Vol. 5, No. 1, pp.146–157.

Hoyas, S. and Jiménez, J. (2006) 'Scaling of the velocity fluctuations in turbulent channels up to Re_tau = 2000', *Phys. Fluids*, Vol. 18, No. 1, pp.1–4.

Hussein, H.J., Capp, S.P. and George, W.K. (1994) 'Velocity measurements in a high-Reynolds-number, momentum-conserving, axisymetric, turbulent jet', *J. Fluid Mech*., Vol. 258, pp.31–75.

Jiménez, J. (2003) 'Computing high-Reynolds-number turbulence: will simulations ever replace experiments?', *Journal of Turbulence*, Vol. 4, Art no. 22.

Jones, W.P., Lyra, S. and Marquis, A.J. (2010) 'Large eddy simulation of evaporating kerosene and acetone sprays', *International Journal of Heat and Mass Transfer*, May, Vol. 53, Nos. 11–12, pp.2491–2505.

Launder, B.E. and Spalding, D.B. (1974) 'The numerical computation of turbulent flows', *Computer Methods in Applied Mechanics and Engineering*, March, Vol. 3, No. 2, pp.269–289.

Levy, Y. and Lockwood, F.C. (1981) 'Velocity-measurements in a particle laden turbulent free jet', *Combustion and Flame*, Vol. 40, No. 3, p.333–339.

Margot, X., Hoyas, S., Fajardo, P. and Patouna, S. (2010) 'A moving mesh generation strategy for solving an injector internal flow problem', *Mathematical and Computer Modelling*, Vol. 52, Nos. 7–8, pp.1143–1150.

Pastor, J.V., López, J.J., García, J.M. and Pastor, J.M. (2008) 'A 1D model for the description of mixing-controlled inert diesel sprays', *Fuel*, Vol. 87, No. 8, pp.2871–2885.

Payri, F., Margot, X., Patouna, S., Ravet, F. and Funk, M. (2009a) 'A CFD study of the effect of the needle movement on the cavitation pattern of diesel injectors', *Proceedings ICE2009*, SAE Naples Section 2009-24-0025.

Payri, R., Salvador, F.J., Gimeno, J. and de la Morena, J. (2009b) 'Effects of nozzle geometry on the direct injection diesel engine combustion process', *Appl. Therm. Eng*., Vol. 29, No. 10, pp.2051–2060.

Payri, R., García-Oliver, J.M., Salvador, F.J. and Gimeno, J. (2005) 'Using spray momentum flux measurements to understand the influence of diesel nozzle geometry on spray characteristics', *Fuel*, Vol. 84, No. 5, pp.551–561.

Payri, R., Tormos, B., Gimeno, J. and Bracho, G. (2010) 'The potential of large eddy simulation (LES) code for the modeling of flow in diesel injectors', *Mathematical and Computer Modelling*, Vol. 52, Nos. 7–8, pp.1151–1160.

Peng-Krrholm, F. (2008) 'Numerical modelling of diesel spray injection, turbulence and combustion', PhD thesis, Chalmers Uni. of Technology.

Piomelli, U. and Liu, J. (1995) 'Large-eddy simulation of rotating channel flows using a localized dynamic model', *Phys. Fluids*, Vol. 7, No. 4, pp.839–848.

Pitsch, H. (2006) 'Large-eddy simulation of turbulent combustion', *Annual Review of Fluid Mechanics*, Vol. 38, No. 1, pp.453–482.

Pope, S.B. (2000) *Turbulent Flows*, p.771, Cambridge University Press, UK.

Riley, J.J. (2006) 'Review of large-eddy simulation of non-premixed turbulent combustion', *J. Fluids Eng*., Vol. 128, No. 2, pp.209–215.

Scotti, A., Meneveau, C. and Lilly, D.K. (1993) 'Generalized Smagorinsky model for anisotropic grids', *Phys. Fluids A*, Vol. 5, No. 9, pp.2306–2308.

Smagorinsky, J.S. (1963) 'General circulation experiments with the primitive equations. I. The basic experiment', *Mon. Weather Rev*., Vol. 91, pp.99–164.

Vuorinen, V. (2010) 'LES of certain droplet size effects in fuel sprays', PhD Thesis, the Aalto University School of Science and Technology.

Yakhot, A., Orszag, S., Yakhot, V. and Israeli, M. (1989) 'Renormalization group formulation of large-eddy simulations', *J. Sci. Comput*., Vol. 4, No. 2, pp.139–158, USA.

2.2.3. Evaluation of the Eulerian-Lagrangian Spray Atomization (ELSA) in spray simulations. International Conference on Mechanical, Automotive and Aerospace Engineering 2011 (Published in International Journal of Vehicle Systems Modelling and Testing – IJVSMT)

Evaluation of the Eulerian-Lagrangian spray atomisation (ELSA) in spray simulations

Sergio Hoyas*, J.M. Pastor,
Dung Khuong-Anh and
Juan Manuel Mompó-Laborda

CMT – Motores Térmicos,
Universidad Politécnica de Valencia,
Camino de Vera S/N, 46022 Valencia, Spain
E-mail: serhocal@mot.upv.es
E-mail: jopasen@mot.upv.es
E-mail: ankh2@mot.upv.es
E-mail: juamomla@mot.upv.es
*Corresponding author

Frederic Ravet

Renault,
1 Avenue du Golf 78288, Guyancourt, France
E-mail: frederic.ravet@renault.com

Abstract: There are many approaches have been developing to simulate the spray structure especially in modelling fuel sprays, i.e., Eulerian, Lagrangian, Lagrangian-Eulerian, Eulerian-Eulerian and Eulerian-Lagrangian approaches. The present study uses an Eulerian-Lagrangian spray atomisation (ELSA) method which is an integrated model for capturing the whole spray evolution starting directly from injector nozzle still the end.

Our goal in this study is to evaluate the ELSA model which is implementing into the commercial software Star-CD, for numerically modelling of diesel sprays. There are two key studies in these validations, at first we examine the turbulent parameters through the three different scenarios and then we study mesh dependency. The results show in form of liquid penetrations, droplet velocity, and axial velocity profiles. All numerical results are compared with experimental data from our research institute, CMT-Motores Térmicos.

Keywords: spray penetration; droplet; injection; Eulerian-Lagrangian spray atomisation; ELSA; atomisation; turbulence.

Reference to this paper should be made as follows: Hoyas, S., Pastor, J.M., Khuong-Anh, D., Mompó-Laborda, J.M. and Ravet, F. (xxxx) 'Evaluation of the Eulerian-Lagrangian spray atomisation (ELSA) in spray simulations', *Int. J. Vehicle Systems Modelling and Testing*, Vol. X, No. Y, pp.000–000.

Biographical notes: Sergio Hoyas is an Associate Professor of Aerospace Engineering at the Universidad Politécnica de Valencia, where is also serving as a CFD Coordinator of CMT-Motores Térmicos Research Institute. He holds a PhD in Applied Mathematics, and his expertise includes supercomputation and wall turbulence.

J.M. Pastor obtained his PhD in Mechanical Engineering in 2003. He is currently a Senior Researcher at CMT-Motores Térmicos, Universidad Politécnica de Valencia. His research fields are analysis and modelling of engine combustion processes, and CFD applied to simulations of internal combustion engines and sprays.

Dung Khuong-Anh graduated with a degree in Mechanical Engineering (2005) and obtained his dual Master in Computational Mechanics from the Universitat Politècnica de Catalunya (2008) and École centrale de Nantes (2009), and his Master in Internal Combustion Engine from the Universidad Politécnica de Valencia (2011). His research interests are computational mechanics, FE, CFD and CAx. Currently, he works as a researcher for European Commission Marie Curie FP7 ITN 'VECOM' at UPV. His research activities include CFD simulation of direct injection diesel sprays within the framework of the Eulerian Lagrangian spray atomisation model in order to develop and validate a numerical tool for spray modelling in engine simulation and calculation.

Juan Manuel Mompó Laborda finished his degree in Mechanical Engineering (2009) with a six-month stay at the Yacht Research Unit (University of Auckland) with the first Promoe scholarship to New Zealand that has been managed by the Polytechnic University of Valencia (Spain). In November 2009, he joined the CMT-Motores Térmicos for his doctoral thesis on LES of diesel sprays with OpenFOAM. Previously, he participated in three R&D projects in his institute as a Research Fellow.

Frederic Ravet is an Engineer and a Specialist in combustion systems. He joined Renault in 2004 after working for ten years in aeronautics industry. He graduated from CORIA (Rouen University) as a Doctor in Energy. He is in charge of combustion designing.

1 Introduction

Everybody knows the auto world has shifted. New efficiency standards are requiring a fleet-wide fuel economy. Within this purpose, car manufacturers have paid more attention to enhance the improvement of R&D resources in automotive industry. There is a variety of research fields included noise, vibration and harshness (NVH), simulation of vehicle performance, dynamics, safety, durability, etc. Even though there have been big advances over the last decade in the efficiency of the diesel engine, automakers insist there is still much to improve about the humble combustion engines, especially in the diesel injection simulation.

In the 1980s, Lefebvre (1989) described the complexity of spray structure and its related theories. Fuel injection process and subsequent fuel-air mixing formation play a major role on combustion and pollutant emissions on internal combustion engines. As the development of a spray is dependent on many parameters and coefficients, simulation studies try to assess the impact of complex phenomena. It is characterised by orifice diameter, nozzle shape, pressure, density, temperature, physical chemistry components, contraction coefficient, discharge coefficient, vaporisation, etc.

Thus an accurate prediction of these processes is required in order to perform reliable engine combustion and pollutants formation simulations. Fuel spray injection is one of the most important phenomena in internal combustion engine which is still under

development and it has been attracted a high concerns from both academic and scientific researchers. Diesel fuel injection and spray formation modelling is still a challenging task due to the complex interrelated phenomena taking place. Still now some of them such as primary atomisation or nozzle cavitation are not fully understood.

Even though many models are mentioned in the abstract but each of them has both advantages and disadvantages in the various regions of spray consisting of the dense zone and the downstream dilute zone or atomisation.

In order to enhance CFD spray simulations, the Eulerian-Lagrangian spray atomisation (ELSA) model has been developing in recent years and integrated into the Star-CD CFD code by Renault. This model is based in an Eulerian approach for the description of the dense spray region, where standard discrete droplet model (DDM) method is not suited for. Hence, the ELSA is an integrated model for capturing the whole spray evolution. Within the diluted spray region the ELSA model could switch to the traditional Lagrangian description of the liquid phase, taking advantage from well established previously developed submodels.

The theoretical aspects of the model have been developing in the last decade, however we need to make it real and stable for engineering applications. The ELSA model has been implementing into Star-CD code. Through the toughest structuring period, we continued to validate and evaluate heavily to ensure the prompt correction in preliminary stage.

Targeting this general objective, it is included to evaluate and validate the different parameters, improve the simply model for computation and identify the well-described phenomena involved in diesel spray formation and development from nozzle outflow to complete fuel vaporisation. As a result, we form the set of correct models for producing a diesel engine simulation in real-life operation. This work is part of a more ambitious project, with the general objective of developing and validating a new spray model tool for practical applications on CFD engine calculations.

2 The ELSA model

In this section, the ELSA approach is described. The goal of the ELSA model is to realistically describe the dense zone of the spray. The ELSA model has been developed from 2001 ignited by Vallet et al. and during the time has been under development (Beau, 2006; Lebas, 2007; De Lucas, 2007; Ning, 2007; Blokkeel et al., 2003).

The ELSA model is used for situations when it assumes the following hypotheses:

- in the situation of high-speed turbulent sprays where Reynolds and Weber numbers are high
- and it exams a turbulent mixing process between the liquid and surrounding gaseous phases as a single-phase turbulent fluid flow with mean properties.

Basically, we can divide ELSA approach into three broad zones:

- *Eulerian mixture zone:* in the first part, single phase CFD code to describe the liquid/gas mixture in the dense part of the spray. In this region, liquid and gas phase are considered as a unique mixture flow. The classical Eulerian model is used to solve this single phase flow.

- *Transition zone:* switch from Eulerian to Lagrangian calculation.
- *Lagrangian zone:* classical Lagrangian tracking for droplets in the diluted spray zone.

Once the difference of velocity of a liquid jet with respect to the surrounding gas is very strong, atomisation of the jet occurs, and droplets are formed (atomisation regime).

In the two papers of Desportes et al. (2010a, 2010b), the author had summarised the key formulae as following, and we include here for completeness. Mean liquid mass fraction $\tilde{Y}_l$

$$\tilde{Y} = \frac{\overline{\rho Y}}{\overline{\rho}} \tag{1}$$

where $\overline{Y}$ is the mean liquid volume fraction,

The mean properties of this effective fluid or mixture (like mean density $\overline{\rho}$ or Favre averaged mean velocity $\tilde{U}_i$) are defined with the following relationships:

The state equation is obtained as

$$\overline{\rho} = \rho_l \overline{Y} + \rho_g \left(1 - \overline{Y}\right) \tag{2}$$

ρ_l is the liquid density and ρ_g is the gas density, which is expressed in terms of $\tilde{Y}_l$ as

$$\frac{1}{\overline{\rho}} = \frac{\tilde{Y}_l}{\rho_l} + \frac{1 - \tilde{Y}_l}{\rho_g} \tag{3}$$

$$\tilde{U}_i = \tilde{Y}_l U_{l,i} + \left(1 - \tilde{Y}_l\right) U_{g,i} \tag{4}$$

and the equation of state

$$\overline{P} = \frac{\left(1 - \tilde{Y}_l\right) \overline{\rho} R_g T_g}{1 - \tilde{Y}_l \cdot \overline{\rho} / \rho_l} \tag{5}$$

In the equation of state (5), we take into account the volume occupied by liquid.

Then, the classical transport equations are solved for these mean variables:

$$\frac{\partial \overline{\rho}}{\partial t} + \frac{\partial \overline{\rho} \tilde{U}_j}{\partial x_j} = S_{EL}^{\tilde{Y}_l} \tag{6}$$

$$\frac{\partial \overline{\rho} \tilde{U}_i}{\partial t} + \frac{\partial \overline{\rho} \tilde{U}_j \tilde{U}_i}{\partial x_j} = -\frac{\partial \overline{P}}{\partial x_i} - \frac{\partial \overline{\rho u_i'' u_j''}}{\partial x_j} + S_{EL}^{\tilde{U}_i} \tag{7}$$

It should be noticed that the last equation does not contain any momentum exchange terms between liquid and gaseous phases. In order to model the liquid dispersion, this set of equations is completed by the transport equation for the liquid mass fraction:

$$\frac{\partial \overline{\rho} \tilde{Y}_l}{\partial t} + \frac{\partial \overline{\rho} \tilde{U}_j \tilde{Y}_l}{\partial x_j} = -\frac{\partial \overline{\rho u_j'' y''}}{\partial x_j} + S_{EL}^{\tilde{Y}_l} \tag{8}$$

where $S_{EL}^{\tilde{Y}_l}$ and $S_{EL}^{\tilde{U}_i}$ are the sink or source terms due to the droplet generation or absorption when the transition from Eulerian to Lagrangian formulation is activated.

In equations (5) and (6), there are two turbulent fluxes to be closed. The turbulent stress tensor is modelled with a classical $k - \varepsilon$ model closure. Concerning the liquid turbulent diffusion flux, the gradient law approximation is applied:

$$\overline{\rho u_j'' y''} = -\overline{\rho}\frac{v_t}{Sc_t}\frac{\partial \tilde{Y}_l}{\partial x_j} \tag{9}$$

2.1 Liquid/gas interface density

In order to characterise the size of liquid fragments resulted from the jet atomisation, the notion of liquid surface density is introduced. This variable is defined as the quantity of liquid/gas interface per unit of volume $\overline{\Sigma}\left(m^{-1}\right)$. Using this new variable, we can obtain the Sauter mean diameter of droplet (Lebas et al., 2005):

$$\begin{aligned} D_{32} &= \frac{6\overline{\rho}\widetilde{Y}_l}{\rho_l \overline{\Sigma}} \\ n &= \frac{\rho_l^2 \overline{\Sigma}^3}{36\pi \overline{\rho Y_l}^2} \end{aligned} \tag{10}$$

A transport equation for liquid surface density is postulated by analogy with the flame surface density.

$$\begin{aligned} &\frac{\partial \overline{\rho}\widetilde{\Omega}}{\partial t} + \frac{\partial \overline{\rho}\widetilde{\Omega}\tilde{U}_j}{\partial x_j} = \frac{\partial}{\partial x_j}\left(\overline{\rho}\frac{v_t}{Sc_t}\frac{\partial \widetilde{\Omega}}{\partial x_j}\right) + S_{EL}^{\widetilde{\Omega}} \\ &\overline{\rho}\cdot\left(\dot{\widetilde{\Omega}}_{init} + \dot{\widetilde{\Omega}}_{mean} + \dot{\widetilde{\Omega}}_{turb} + \dot{\widetilde{\Omega}}_{coll} + \dot{\widetilde{\Omega}}_{coal}\right) \end{aligned} \tag{11}$$

Here, Beau (2006) introduced the other notion of liquid/gas interface per unity of mass that is defined as $\widetilde{\Omega} = \overline{\Sigma}/\overline{\rho}$ (m^2/kg).

The production and destruction of liquid surface are accounted for with source terms detailed below. The first term source $\dot{\widetilde{\Omega}}_{init}$ in equation (8) permits to initialise the calculations since all other terms source are proportional to $\widetilde{\Omega}$:

$$\dot{\widetilde{\Omega}}_{init} = \begin{cases} 2\dfrac{v_t}{Sc_t}\dfrac{6\overline{\rho}}{\rho_l \rho_g L_t}\dfrac{\partial \widetilde{Y}_l}{\partial x_i}\dfrac{\partial \widetilde{Y}_l}{\partial x_i} \; if \; \widetilde{Y}_l\left(1-\widetilde{Y}_l\right) \le 0.001 \\ 2\dfrac{v_t}{Sc_t}\dfrac{\widetilde{\Omega}}{\left(1-\widetilde{Y}_l\right)\widetilde{Y}_l}\dfrac{\partial \widetilde{Y}_l}{\partial x_i}\dfrac{\partial \widetilde{Y}_l}{\partial x_i}, \text{ otherwise} \end{cases} \tag{12}$$

The second term in the right hand side stands for a general definition that was obtained by the phenomenological considerations for the spray formed of the droplets with a

constant diameter. In the region closed to the injector $\widetilde{Y}_l \to 1$, the scale of the first liquid fragments is assumed to be proportional to the turbulent length scale, L_t.

The three next terms correspond to the production of liquid surface density due to the mean or turbulent stresses and due to the collisions:

$$\dot{\widetilde{\Omega}}_{mean} = \frac{\overline{\rho u_i'' u_j''}}{\overline{\rho}\tilde{k}} \frac{\partial \tilde{U}_i}{\partial x_j} \widetilde{\Omega}$$
$$\dot{\widetilde{\Omega}}_{turb} = \frac{\widetilde{\Omega}}{\tau_{turb}} \quad \text{and} \quad \dot{\widetilde{\Omega}}_{coll} = \frac{\widetilde{\Omega}}{\tau_{coll}} \tag{13}$$

The last term in the right hand of equation (8) deals with destruction of surface density due to coalescence:

$$\dot{\widetilde{\Omega}}_{coal} = -\frac{1}{\tau_{coll}} \frac{\widetilde{\Omega}^2}{\widetilde{\Omega}_{crit}} \tag{14}$$

with τ_{coll} and $\widetilde{\Omega}_{crit}$ are the characteristic time scale of collisions and the critical value of liquid/gas surface density.

3 Experiments for comparison

The obtained numerical results are compared with experimental data at CMT Motores Térmicos. Experimental results have been obtained from previously published data from the authors' research group (Payri et al., 2008; Gimeno García, 2008).

The injection velocity profile comes from measurements of mass and momentum fluxed performed in a pressurised test rig with nitrogen. The momentum flux measuring principle of this technique is explained in two references of Payri et al. (2005) and Gimeno Garcia (2008), and consists of measuring the impact force of the spray in a surface with a piezo-electric sensor. As long as the whole cross-section of the spray impacts on the sensor, the measured force equals to the momentum flux at that cross section. If the measurement position is close to the nozzle exit, the time evolution of the impact force is equal to the nozzle (hole) momentum flux, $\dot{M}_o$.

4 Geometry and boundary conditions

These cases have been simulated as axis-symmetric boundary-value problems. We study 2D axis-symmetric meshes (five-degree cylindrical segment along the axis). A 2D view, boundary conditions and coordinate system are shown in Figure 1.

Within this work, we used a data as similar as CMT diesel-type single-hole injector experiments for a diameter of 112 μm with variable velocity profile input at the injector as depicted in Figure 2 and some key parameters in Table 1.

Figure 1 Boundary conditions (see online version for colours)

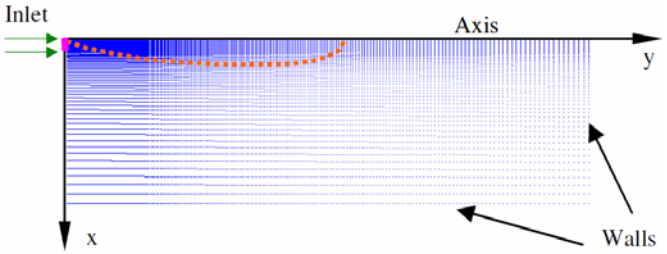

Figure 2 Starting velocity profile (see online version for colours)

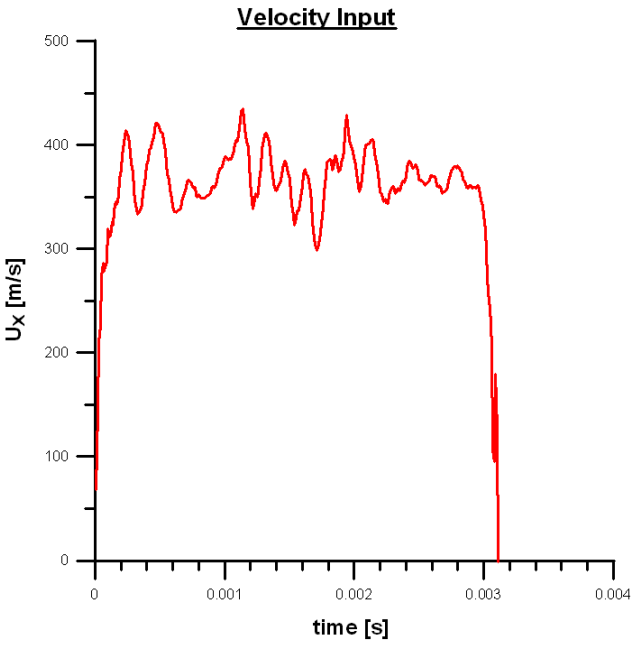

Table 1 Basis parameters

Ambient pressure	*Injection pressure*	*Temperature*	*Fuel density*
3.53 MPa	80 MPa	307.58 K	822.10 kg/m^3

Generally, the requirement for mesh structure is especially at the nozzle where the mesh size has to be small enough to capture the spray structure and the small droplets at the injector and surroundings. Our current mesh structure is based on the following criteria:

$$\Delta x \sim 0.05 - 0.1 D_{inj} \Rightarrow \quad \Delta t \approx 10^{-8} \text{ s}$$

Hence, two different configurations with 10, and 20 cells at the nozzle are used. The computational domains with the size of 80 × 25 mm are shown in Figure 3 according to the mesh structures in Table 2.

Figure 3 Geometry (see online version for colours)

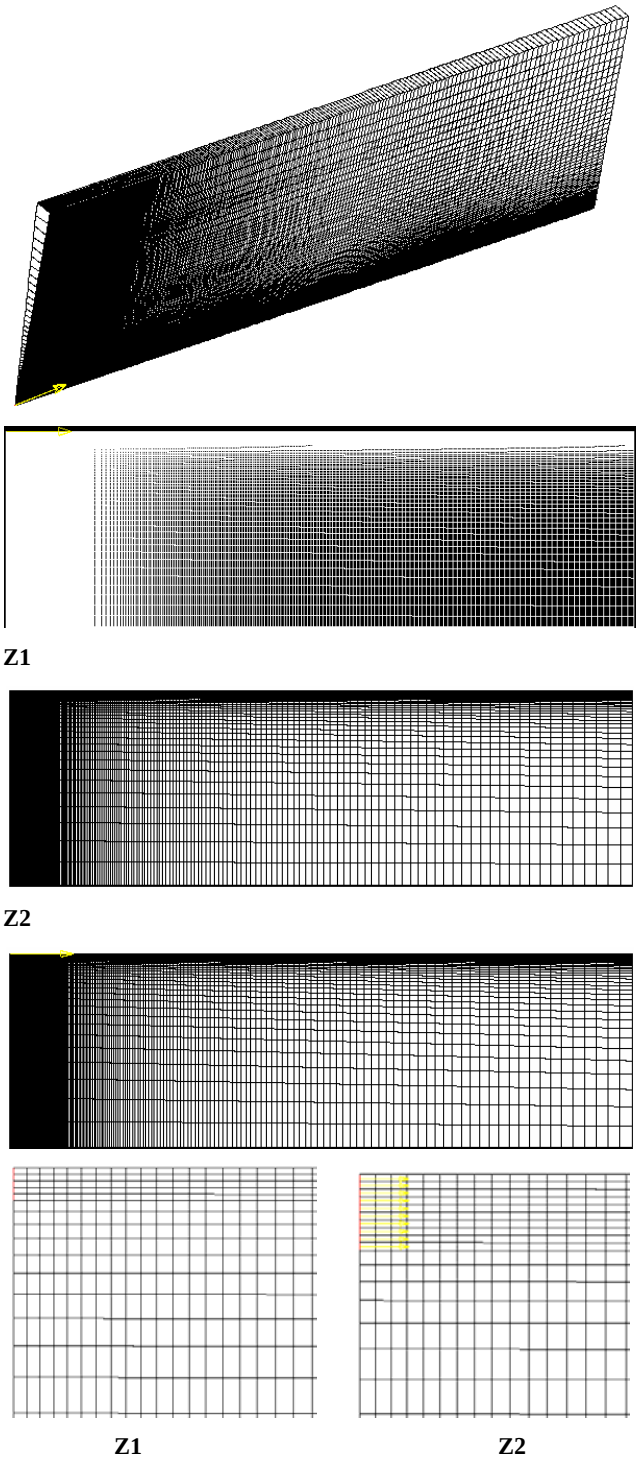

Table 2 Mesh structures

No cells at the nozzle	*No. axial cells*	*Axial ratio (first/last ratio)*	*No. radial cells*	*Radial ratio (last/first ratio)*
10	*435*	72	*90*	0.006
10	218	72	45	0.006
20	250	143	50	0.003

The first two graphs in Figure 3 are for the ten cells with fine meshes in isometric and side views respectively, the third one is for ten cells with coarse mesh. The forth figure from downward position is for the case with 20 cells at the nozzle. The detailed views of two types of meshes are also showed in pairs.

We used the $k - \varepsilon$/high Reynolds number turbulent model with the following constants in Table 3 that are usually accepted in most of the spray calculation where C-ε1 = 1.44 is the standard value, and we also use the suggested value C-ε1 = 1.60 in order to improve predictions on round jets modelling, moreover we examine the behaviour of the simulation with C-ε1 = 1.52. The turbulent Prandtl number has been set to 1 in order to produce similar solutions for the conservation equations of axial momentum, fuel mass and energy. We notice that the Prandtl (K.E.) in Table 3 is another Prandtl constant which is only used for solving the $k - \varepsilon$ equations.

Table 3 Turbulent parameters

	C-Mu	*C-ε1*	*C-ε2*	*C-ε3*	*Prandtl (K.E.)*	*Prandtl (Eps)*
Turb 1	0.09	*1.44*	1.92	1.44	1	1.219
Turb 2	0.09	*1.52*	1.92	1.44	1	1.219
Turb 3	0.09	*1.60*	1.92	1.44	1	1.219

Combining the above descriptions, we finalise six main cases in total:

Table 4 Computational cases

Case no.	*Cells at nozzle*	*Turbulent constant*	*Vertices*	*Cells*
Case 1	10	C = 1.60	78,916	39,150
Case 2	10	C = 1.44	19,929	9,810
Case 3		C = 1.52		
Case 4		C = 1.60		
Case 5	20	C = 1.44	25,351	12,500
Case 6		C = 1.60		

5 Numerical results

Figure 4 shows the comparison of the liquid penetrations using different meshes vs. time. At first, the plot for only 20 cells at nozzle diameter with the experimental result is depicted on top. With the constant equally to 1.44, the numerical result prone to the right hand side of the experimental results meanwhile with the value of 1.60, the spray

penetration tend to the other side of experimental results. This similar behaviour remains for the comparison with 10 cells. For the second plot, the critical changes are observed between the three turbulent constants. In the last plot, we could see the dramatically change in the fine mesh case where the penetration curve move far way in comparison with the coarse mesh. Thus, the choice of this parameter must be considered for each numerical simulation.

Figure 4 Liquid penetrations (see online version for colours)

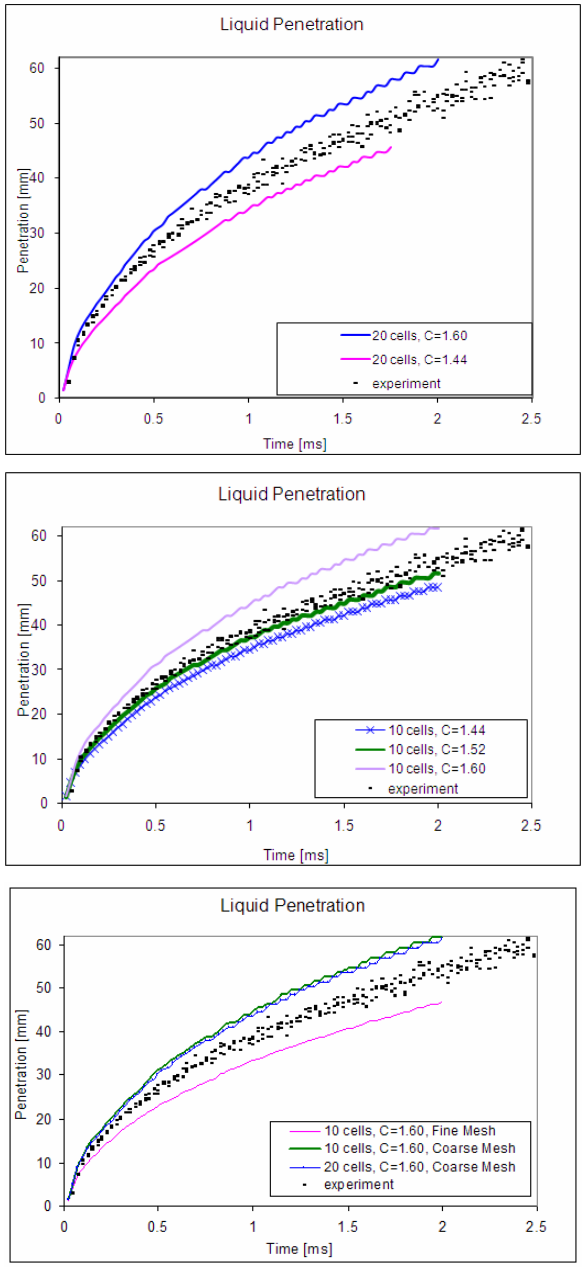

Figure 5 Spray structure and droplet formation (see online version for colours)

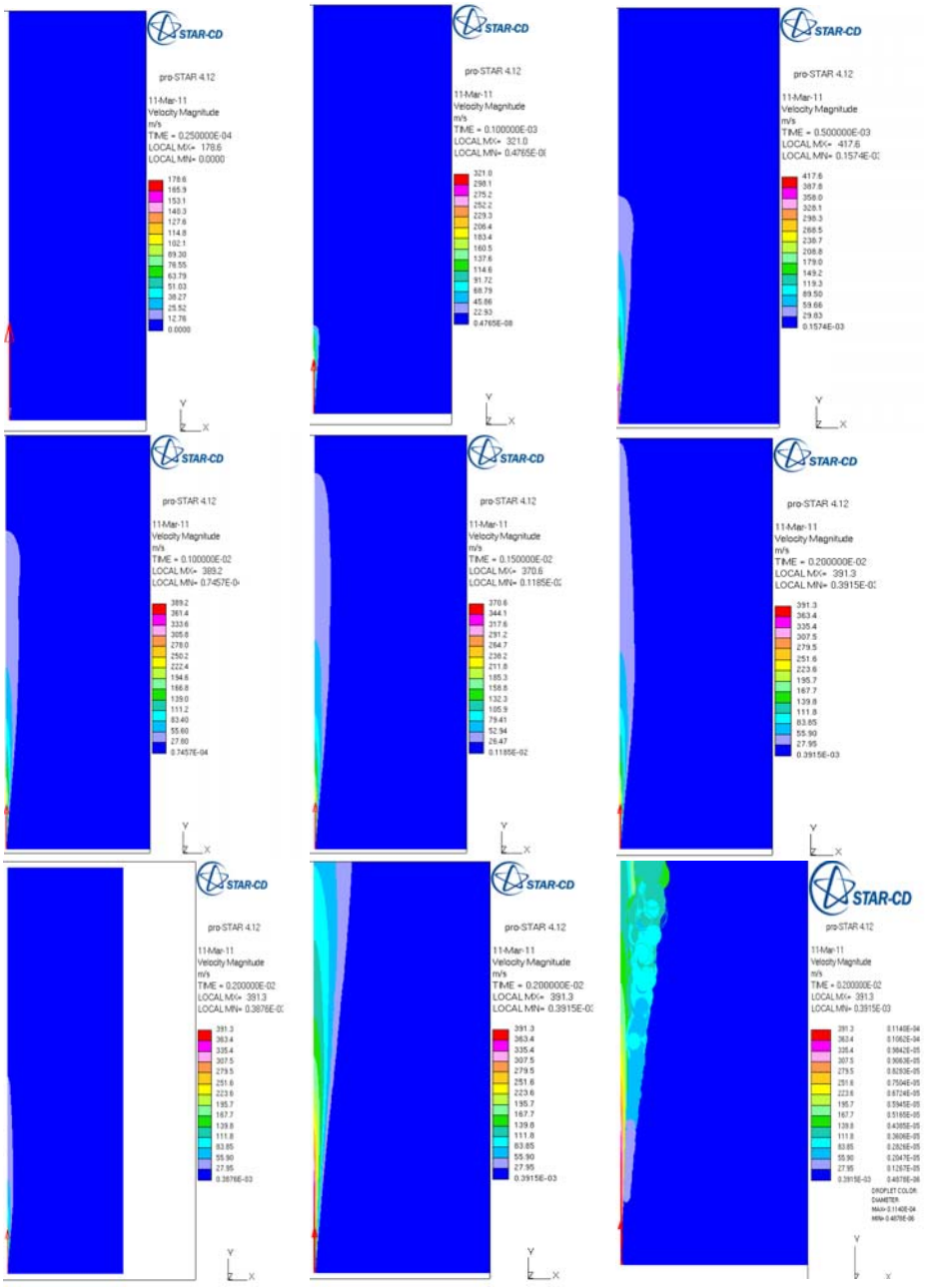

As visual presentation in Figure 5, it can be easily imagined the evolution of velocity profiles in various time steps of 0.025, 0.01, 0.5, 1, 1.5, 2 ms respectively, the structure of spray is represented for the number of cell size of 10 at the nozzle diameter and fine mesh case (case 1). It can be seen that velocity magnitude is highest in the zone surrounding the nozzle and in the liquid core zone where the Eulerian approach is used and lowest in

the droplet peak in the axial direction. The droplet figure describes the droplet formation is produced starting from the transition zone and continue to develop in the farther zone (Lagrangian zone) continuously. It is the combined plot where the contours profile represents for the velocity and the round circles show the droplet diameter but it shows in the same colour scale. Here, droplet diameter is in mm and the velocity unit as m/s. Definitely, there is no droplet in the Eulerian mixture zone. It confirms our initial setting and formulae for ELSA model. Mean velocities and droplet velocities in different radial and axial position are shown in Figure 5 and Figure 6. Generally, the velocity profiles in the numerical calculation are in line with the experiments.

Figure 6 Velocity profiles of spray (10 cells, C-ε1 = 1.60) (see online version for colours)

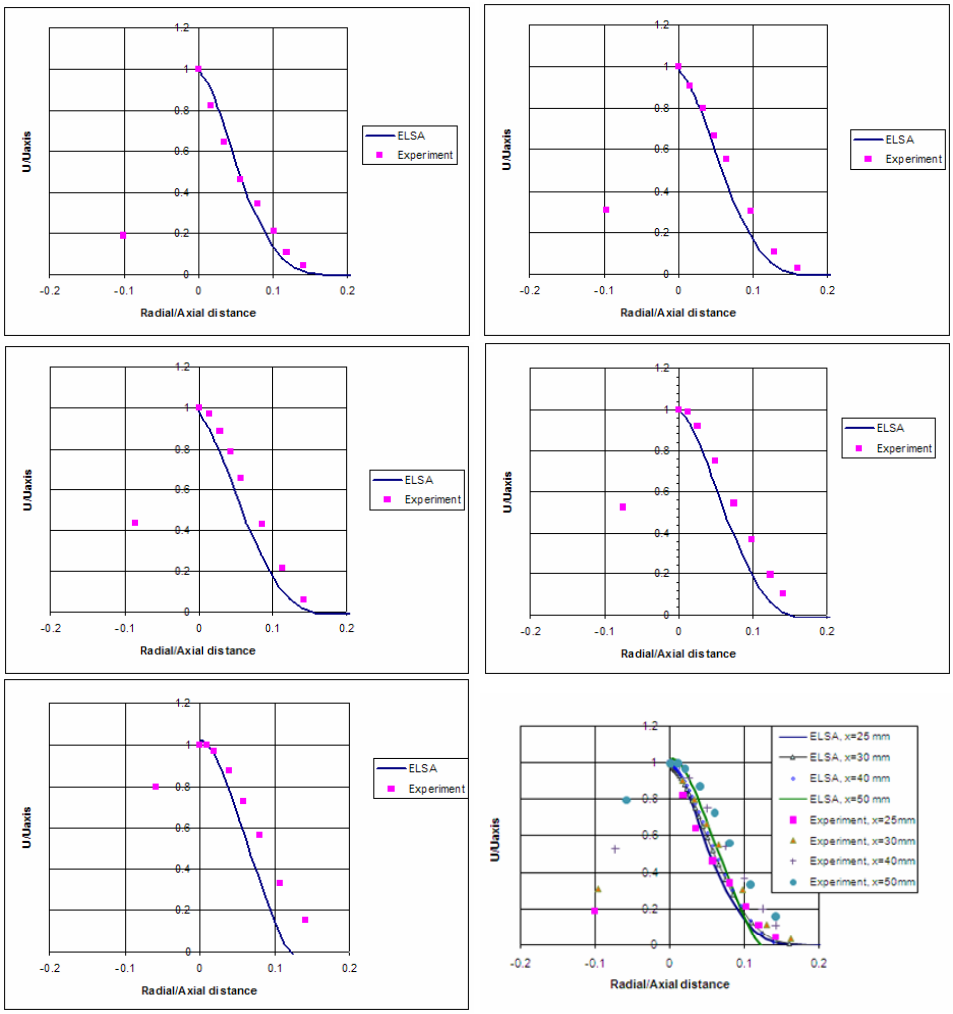

In Figure 6, we plot velocity profiles in different sections with five sections at round number of distance equal to 25 30, 35, 40, and 50 mm respectively in order to compare with the available experiments from R. Payri et al. (2008). It can be seen that the velocity profiles decrease according to the penetration distance.

Figure 7 Droplet velocity profiles (see online version for colours)

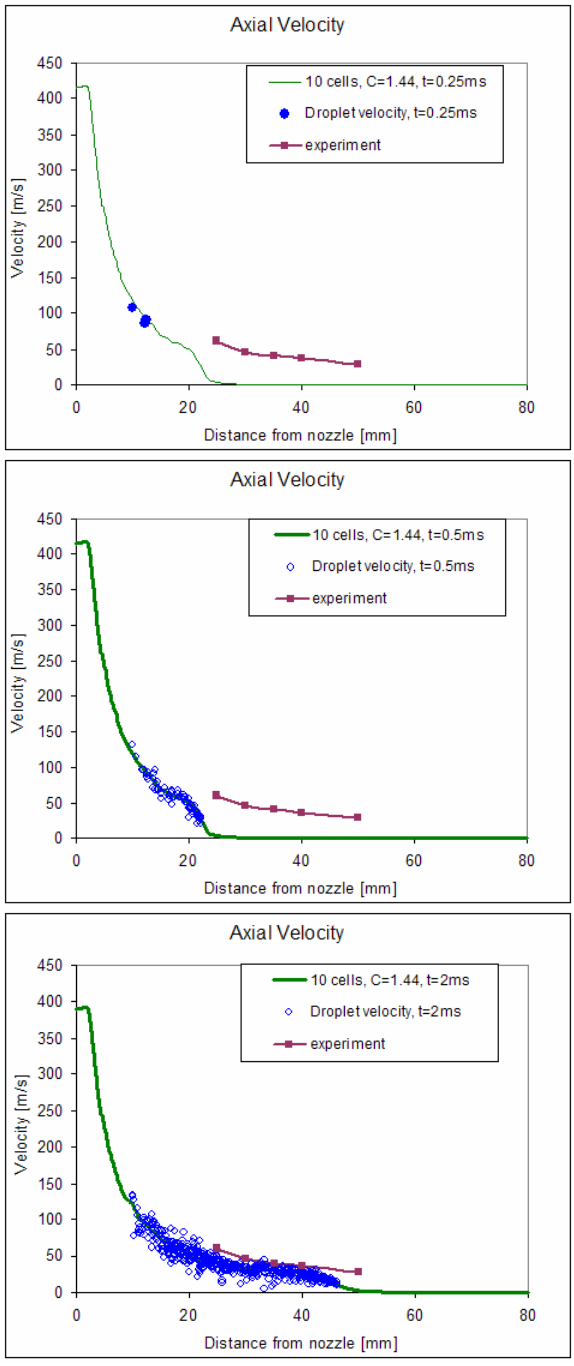

In Figure 7, the droplet velocity along axial direction and total number of droplets are sketched. To bear in mind that we only take into account total droplets which contain within the closest cells from the axial line.

We can see the number of droplets increase through each time steps and their velocity also change accordingly and long the mean velocity curve.

6 Conclusions

In this report we brought out some key different amongst those computational models and typical plots for certain cases. For the rest of figures which resulted similar behaviour, and do not add much value to the report are not showed here. As stated in our target, we showed the relationships or discrepancy among key elements of penetration, velocity, turbulent parameters and different in position or number of time step and mesh effects.

In sum, mean velocity profile and droplet velocity is staying very close with the experiment index especially in the highest time step. Liquid penetration is totally depend on the mesh size, topology and of course turbulent model and parameters which we used for our simulation. Grid sensitivity is shown in our calculations, thus for 2-D RANS (Reynolds-averaged Navier-Stokes) simulations, we can use meshes as much fine as possible if time simulation and computing power allowed in order to get nearly grid independent results. We have to do more test and computations to know exactly which value should be best fit to each case.

The diesel spray was performed with ELSA model produced a good accuracy even with the 2D axisymmetric meshes, the numerical results indicated the similar prediction in conjunction with the real experimental results conducted at CMT in 2008. Designers often focus on performance areas, thus our liquid sprays analysis and design using computational fluid dynamics (CFD) simulations were performed on the diesel spray and validated the ELSA model with the latest experimental results with almost the same configuration are very useful for them to refer to.

Acknowledgements

This work has been granted by Renault and vehicle concept modelling (VECOM) – EU FP7 Marie Curie Initial Training Network (ITN) Grant Agreement 213543 (from 1 October 2008 to 30 September 2012). The aim of the proposed training network is to provide dedicated research training in the emerging field of vehicle concept modelling for up-front pre-CAD functional performance engineering, bridging between industry and academia across Europe.

References

Beau, P.A. (2006) ‘Modelisation de l’atomisation d’un jet liquide – application aux sprays diesel’, PhD thesis, University of Rouen.

Blokkeel, G., Barbeau, B. and Borghi, R. (2006) ‘A 3D Eulerian model to improve the primary breakup of atomizing jet’, SAE Technical Paper 2003-01-0005.

De Lucas, M. (2007) ‘Contribution a la modelisation de la pulverisation d’un liquide phytosanitaire en vue de reduire les pollutions’, PhD thesis, University of Aix-Marseille II.

Desportes, A., Zellat, M., Desoutter, G., Abouri, D., Liang, Y. and Ravet, F. (2010) 'Validation and application of the Eulerian-Lagrangian spray atomization (ELSA) model for the diesel injection simulation', SAE.

Desportes, A., Zellat, M., Desoutter, G., Abouri, D., Liang, Y. and Ravet, F. (2010) 'Application of the Eulerian-Lagrangian spray atomization (ELSA) model for the diesel injection simulation', *THIESEL 2010 Conference*.

Gimeno García, D.J. (2008) 'Desarrollo y aplicación de la medida del flujo de cantidad de movimiento de un chorro diesel', PhD thesis, Universidad Politécnica de Valencia.

Lebas, R. (2007) 'Modelisation Eulerienne de l'atomisaton haute pression – influences sur la vaporisation et la combustion induite', PhD thesis, University of Rouen.

Lebas, R., Blokkeel, G., Beau, P-A. and Demoulin, F–X. (2005) 'Coupling vaporization model with the Eulerian-Lagrangian spray atomization (ELSA) model in diesel engine conditions', SAE100, 2005-01-0213.

Lefebvre, A.H. (1989) *Atomization and Sprays*, Taylor and Francis, USA.

Ning, W., Reitz, R.D., Lippert, A.M. and Diwakar, R. (2007) 'Development of a nextgeneration spray and atomization model using an Eulerian-Lagrangian methodology', *17th Int. Multidimensional Engine Modeling User's Group Meeting*, Detroit, MI.

Payri, R., García, J.M., Salvador, F.J. and Gimeno, J. (2005) 'Using spray momentum flux measurements to understand the influence of diesel nozzle geometry on spray characteristics', *Fuel*, Vol. 84, No. 5, pp.551–561.

Payri, R., Tormos, B., Salvador, F.J. and Araneo, L. (2008) 'Spray droplet velocity characterization for convergent nozzles with three different diameters', *Fuel*, Vol. 87, Nos. 15–16, pp.3176–3182.

Vallet, A., Burluka, A.A. and Borghi, R. (2001) 'Development of an Eulerian model for the atomization of a liquid jet', *Atomization and Sprays*, Vol. 11, No. 6, pp.619–642.

Definitions/abbreviations

CAD	computer-aided design
CMT	CMT Motores Térmicos
CFD	computational fluid dynamics
DDM	discrete droplet model
ELSA	Eulerian-Lagrangian spray atomisation
ITN	initial training network
PDPA	phase doppler particle analyser
RANS	Reynolds-averaged Navier-Stokes
SMD	Sauter mean diameter
VECOM	vehicle concept modelling
R&D	research and development
NVH	noise, vibration and harshness
FE	finite element
CAx	computer-aided x
UPV	Universidad Politécnica de Valencia

2.2.4. Application and evaluation of the Eulerian-Lagrangian Spray Atomization (ELSA) model on CFD Diesel spray simulations. SAE Paper 2011-37-0029

SAE International

Application and Evaluation of the Eulerian-Lagrangian Spray Atomization (ELSA) Model on CFD Diesel Spray Simulations

2011-37-0029
Published
06/09/2011

Sergio Hoyas, Jose M. Pastor, Dung Khuong-Anh and Juan Manuel Mompó-Laborda
CMT, Universidad Politécnica de Valencia

Frederic Ravet
Renault

doi:10.4271/2011-37-0029

ABSTRACT

During the last fifteen years Computational Fluid Dynamics (CFD) has become one of the most important tools to both understand and improve the Diesel spray development in Internal Combustion Engine (ICE). Most of the approaches and models used pure Eulerian or Lagrangian descriptions to simulate the spray behavior. However, each one of them has both advantages and disadvantages in different regions of the spray, it can be the dense zone or the downstream dilute zone. One of the most promising techniques, which has been in development since ten years ago, is the Eulerian-Lagrangian Spray Atomization (ELSA) model. This is an integrated model for capturing the whole spray evolution, including primary break-up and secondary atomization.

In this paper, the ELSA numerical modeling of Diesel sprays implementation in Star-CD (2010) is studied, and simulated in comparison with the Diesel spray which has been experimentally studied in our institute, CMT-Motores Térmicos. Since many of the most important characteristics of the spray development, as the penetration or the axial velocity, can be captured using 2D simulations, in this preliminary validation of ELSA model only two-dimensional simulations have been performed. Moreover, the main objective of the paper is to: firstly, obtain mesh independency for further analysis and secondly, improve the classic k - ε RANS model for ELSA model. Apart from this, several characteristics of the spray as can be the droplet formation of the liquid penetration are also showed.

INTRODUCTION

Fuel injection process and subsequent fuel-air mixing formation play a major role on combustion and pollutant emissions in internal combustion engines. It is one of the most important phenomena in internal combustion engines which is still under development and with high concerns from both academic and scientific researchers, due to the complex interrelated phenomena taking place (See for instance Lefebvre, 1989 [17]). Still now, some of them, such as primary atomization or nozzle cavitation, are not fully understood.

In order to enhance Computational Fluid Dynamics (CFD) spray simulations, the ELSA model (Vallet et al., 2001 [24]) has been developed in recent years. It has been integrated very recently into the Star-CD CFD code by RSA. ELSA model is based on an Eulerian approach for the description of the dense spray region, where standard Discrete Droplet Model (DDM) method is not able to describe the flow. Within the diluted spray region, the ELSA model could switch to the traditional Lagrangian description of the liquid phase, taking advantage from well established and previously developed submodels.

The goal of the ELSA model is to realistically describe the dense zone of the spray and the spray atomization. Since the seminal work of Vallet et al. [24] it has been under development by several authors, including Blokkeel et al., 2003 [6], Beau, 2006 [5], Lebas, 2007 [15], De Lucas M., 2007 [9] or Ning W., 2007 [19]. As we have said, the ELSA model takes advantages of the Eulerian description of the

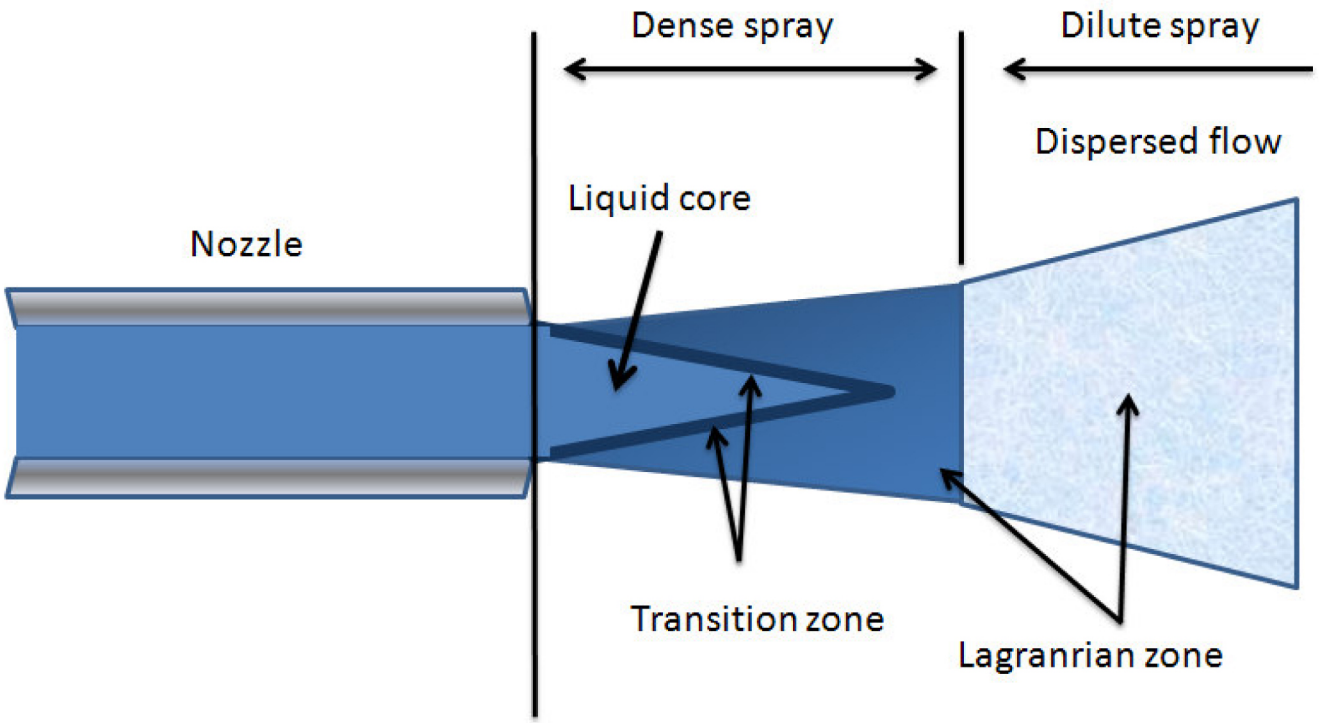

Figure 1. Illustration of the spray structure in the atomization regime (adapted from Faeth et al., 1995 [10]).

near nozzle flow where some assumptions of standard spray models based on discrete droplet method (DDM) shows strong limitations. This approach is valid only when the liquid volume fraction is small inside the computational cells and when the drops are homogeneously distributed in the computational space, neither of them is satisfied in the near field of the spray. In order to keep a low void fraction and assure numerical stability, it is necessary to use grid sizes larger than orifice diameter, which cannot adequately resolve the flow structures in this region. Additionally, it is also not required to assume any particular shape to represent drops and liquid ligaments on ELSA model, where the average area of the liquid-gas interface is introduced as a measure of the atomization extent. Moreover, the DDM method applies isolated drop based models in this region with strong interaction within the liquid phase, where its validity is hardly justified.

Basically, we have three separated zones in the ELSA model as shown in the following figure:

- **Eulerian mixture zone:** In this region (liquid core), liquid and gas phase are considered as a unique mixture flow. The classical Eulerian model is used to solve this single phase flow.
- **Transition zone:** switch from Eulerian to Lagrangian calculation.
- **Lagrangian zone:** classical Lagrangian tracking for droplets in the diluted spray zone and some regions of the Dense spray zone

The main hypothesis of ELSA, is that the flow must be a high-speed turbulent spray, where Reynolds bulk number and Weber number should be high (See Beau, 2006 [5] for a detailed study). In the case of Reynolds number, it must be at least $Re > 10^4$, (A. Doudou, 2005 [3]), whereas for Weber number, $We \sim 350$ (Lee and Reitz, 2001 [16] and Tanner, 2004 [23]). On the other hand, the main problem is that the turbulent mixing process between the liquid and surrounding gaseous phase is simulated as a single-phase turbulent fluid flow with mean properties, so it does not give a detailed information about both phases separately in the near nozzle region.

According to the previous statements, the purpose of the present study is to do a preliminary validation of the ELSA spray model implement in the Star-CD code. This work is part of a more ambitious project, with the general objective of developing and validating this spray model implementation for real-life applications on CFD engine calculations.

The structure of the paper is as follows. In the second section the model equations are written down. In the third section the geometry and the setup of the simulation are explained. Fourth section is devoted to the analysis of the results and conclusions are explained in the last section.

MODEL EQUATIONS

As we have said, the ELSA model was first described in an article of Vallet et al., 2001 [24]. Several other works as A.

Desportes et al., 2010 [2] Beau, 2006 [5], and Ning et al., 2007 [19] also discussed this set of equations, that we write down here in shake of completeness of the paper and a logical explanation of the ELSA model. These equations covered the several regions of the ELSA model, changing from one to another but, from now on and in all the regions, the subscript *l* stands for liquid and *g* stands for gas, whereas *i, j* are the direction in space. In order to facilitate the reading of the manuscript, we have added a symbol table at the end of the document.

a). Eulerian Mixture Zone

We define the mean liquid mass fraction, $\tilde{Y}_l$ as

$$\tilde{Y}_l = \frac{\overline{\rho Y_l}}{\overline{\rho}}, \tag{1}$$

where ρ is the density and Y_1 is the liquid mass fraction. Intuitively, mean density is defined as

$$\overline{\rho} = \rho_l \overline{Y_l} + \rho_g \left(1 - \overline{Y_l}\right), \tag{2}$$

which is expressed in terms of $\tilde{Y}_l$ as

$$\frac{1}{\overline{\rho}} = \frac{\tilde{Y}_l}{\rho_l} + \frac{1-\tilde{Y}_l}{\rho_g} \tag{3}$$

Favre averaged mean velocity is defined as

$$\tilde{U}_i = \tilde{Y}_l U_{l,i} + \left(1-\tilde{Y}_l\right) U_{g,i} \tag{4}$$

and mean pressure $\overline{P}$ is given by the equation of state

$$\overline{P} = \frac{\left(1-\tilde{Y}_l\right)\overline{\rho} R_g T_g}{1 - \tilde{Y}_l \cdot \overline{\rho}/\rho_l} \tag{5}$$

In this equation R_g is the gas constant and T_g is the mixture temperature.

Then, the classical transport equations are solved for these mean variables:

$$\frac{\partial \overline{\rho}}{\partial t} + \frac{\partial \overline{\rho} \tilde{U}_j}{\partial x_j} = S_{EL}^{\tilde{Y}_l} \tag{6}$$

$$\frac{\partial \overline{\rho} \tilde{U}_i}{\partial t} + \frac{\partial \overline{\rho} \tilde{U}_j \tilde{U}_i}{\partial x_j} = -\frac{\partial \overline{P}}{\partial x_i} - \frac{\partial \overline{\rho u_i'' u_j''}}{\partial x_j} \tag{7}$$

Her, $S_{EL}^{\tilde{Y}_l}$ are some source terms that are activated during the transition from Eulerian to Lagrangian when there exist droplet generation. It should be noticed that the last equation does not contain any momentum exchange terms between liquid and gaseous phases. In order to model the liquid dispersion, this set of equations is completed by the transport equation for the liquid mass fraction:

$$\frac{\partial \overline{\rho} \tilde{Y}_l}{\partial t} + \frac{\partial \overline{\rho} \tilde{U}_j \tilde{Y}_l}{\partial x_j} = -\frac{\partial \overline{\rho u_j'' y''}}{\partial x_j} \tag{8}$$

In equations (6) and (7), there are two turbulent fluxes unknown. The turbulent stress tensor is modeled with a classical k - ε model closure, which is discussed below. Concerning the liquid turbulent diffusion flux, a gradient law approximation is applied:

$$\overline{\rho u_j'' y''} = -\overline{\rho} \frac{v_t}{Sc_t} \frac{\partial \tilde{Y}_l}{\partial x_j} \tag{9}$$

In this equation v_t is the liquid viscosity and Sc_t is the turbulent Schmidt number.

b). Liquid/Gas Interface Density

In order to characterize the size of liquid fragments resulted from the jet atomization, the notion of liquid surface density is introduced. This variable is defined as the quantity of liquid/gas interface per unit of volume $\overline{\Sigma}\left(m^{-1}\right)$. Using this new variable, we can obtain the Sauter Mean Diameter of droplet, D_{32} and the drop number density (drop number per unit of volume), n (Lebas R., 2005 [14]):

$$D_{32} = \frac{6\overline{\rho}\widetilde{Y_l}}{\rho_l \overline{\Sigma}}$$

$$n = \frac{\rho_l^2 \overline{\Sigma}^3}{36\pi \overline{\rho Y_l}^2} \tag{10}$$

A transport equation for liquid surface density, $\widetilde{\Omega}$, is postulated by analogy with the flame surface density.

$$\frac{\partial \overline{\rho}\widetilde{\Omega}}{\partial t}+\frac{\partial \overline{\rho}\widetilde{\Omega}\tilde{U}_j}{\partial x_j}=\frac{\partial}{\partial x_j}\left(\overline{\rho}\frac{v_t}{Sc_t}\frac{\partial \widetilde{\Omega}}{\partial x_j}\right)+$$
$$\overline{\rho}\cdot\left(\dot{\widetilde{\Omega}}_{init}+\dot{\widetilde{\Omega}}_{mean}+\dot{\widetilde{\Omega}}_{turb}+\dot{\widetilde{\Omega}}_{coll}+\dot{\widetilde{\Omega}}_{coal}\right)+S_{EL}^{\widetilde{\Omega}} \qquad (11)$$

Where $\dot{\widetilde{\Omega}}_{init}$, $\dot{\widetilde{\Omega}}_{mean}$, $\dot{\widetilde{\Omega}}_{turb}$, $\dot{\widetilde{\Omega}}_{coll}$, and $\dot{\widetilde{\Omega}}_{coal}$, are the initial, mean, turbulence, collision and coalescence value of liquid/gas surface density respectively; $S_{EL}^{\widetilde{\Omega}}$ is the source term of the liquid/gas interface. Beau, 2006 [5] introduced other notion of liquid/gas interface per unity of mass that is defined as $\widetilde{\Omega}=\overline{\Sigma}/\overline{\rho}$ (m^2/kg).

The production and destruction of liquid surface are accounted for the five liquid/gas surface densities. The first term source $\dot{\widetilde{\Omega}}_{init}$ in Eq. (11) permits to initialize the calculations since all other terms source are proportional to $\widetilde{\Omega}$:

$$\dot{\widetilde{\Omega}}_{init}=\begin{cases}2\dfrac{v_t}{Sc_t}\dfrac{6\overline{\rho}}{\rho_l\rho_g L_t}\dfrac{\partial \widetilde{Y}_l}{\partial x_i}\dfrac{\partial \widetilde{Y}_l}{\partial x_i}, & if \quad \widetilde{Y}_l\left(1-\widetilde{Y}_l\right)\le 0.001\\ 2\dfrac{v_t}{Sc_t}\dfrac{\widetilde{\Omega}}{\left(1-\widetilde{Y}_l\right)\widetilde{Y}_l}\dfrac{\partial \widetilde{Y}_l}{\partial x_i}\dfrac{\partial \widetilde{Y}_l}{\partial x_i}, & otherwise\end{cases} \qquad (12)$$

L_t is the turbulent length scale.

Three next terms correspond to the production of liquid surface density due to the mean or turbulent stresses and due to the collisions:

$$\dot{\widetilde{\Omega}}_{mean}=\frac{\overline{\rho u_i'' u_j''}}{\overline{\rho}\tilde{k}}\frac{\partial \tilde{U}_i}{\partial x_j}\widetilde{\Omega};$$

$$\dot{\widetilde{\Omega}}_{turb}=\frac{\widetilde{\Omega}}{\tau_{turb}} \quad ; \quad \text{and}$$

$$\dot{\widetilde{\Omega}}_{coll}=\frac{\widetilde{\Omega}}{\tau_{coll}} \qquad (13)$$

τ_{turb} and τ_{coll} are the characteristic time scale of turbulence and collisions respectively and k is the turbulent kinetic energy.

The last term on the right hand side of Eq. (11) deals with destruction of surface density due to coalescence, $\dot{\widetilde{\Omega}}_{coal}$:

$$\dot{\widetilde{\Omega}}_{coal}=-\frac{1}{\tau_{coll}}\frac{\widetilde{\Omega}^2}{\widetilde{\Omega}_{crit}} \qquad (14)$$

c). Transition Zone

We rely on a critical value of the Eulerian liquid volume faction to decide whether it should turn from Eulerian to Lagrangian formulation (Beau, 2006 [5]). The Lagrangian droplets are formed where spray is assumed to be diluted enough. It follows the below equation.

$$\tilde{\Phi}_l=\widetilde{Y}_l\frac{\overline{\rho}}{\rho_l}\le\tilde{\Phi}_l^{crit} \qquad (15)$$

where $\tilde{\Phi}_l^{crit}$ is the critical value of the Eulerian liquid volume fraction.

The transitional criterion is based on the value of liquid volume fraction that is linked to the ratio of mean free path between two droplets and mean equivalent radius of the droplets in the cell. In our calculation, the transition is done when the liquid volume fraction becomes lower than 0.01 [2]. The transition zone is composed of the computational cells that form the border with the dense zone (i.e. zone where the liquid volume fraction is greater than 0.01) and only one parcel is generated per transition cell and per time step.

The velocity of the droplets is defined as

$$\overline{U}_{l,i}=\tilde{U}_i+\frac{\overline{\rho u_i'' y''}}{\overline{\rho}\tilde{Y}_l} \qquad (16)$$

The diameter of the droplet is equal to the Sauter Mean Diameter

$$D_{32}=\frac{6\widetilde{Y}_l}{\rho_l\tilde{\Omega}} \qquad (17)$$

The number of droplets per generated parcel n_{drop} is obtained from mass conservation

$$n_{drop}=\frac{\overline{\rho}\tilde{Y}_l V_{cell}}{\pi/6\,\rho_l D_{32}^3} \qquad (18)$$

where V_{cell} is the volume of one transitional cell

Table 1. Basis Parameters

Ambient pressure	Injection pressure	Ambient Temperature	Fuel Density
3.53 MPa	80 MPa	293 K	822.10 kg/m^3

MODEL VALIDATION SETUP

GEOMETRY AND BOUNDARY CONDITIONS

The geometry is to simulated an outflow of a non-cavitating single-hole injector (tapered nozzle), with an outlet diameter of 112 µm. The chamber has a size of 80×25mm. Some physical key parameters of chamber and spray are depicted in table 1.

This nozzle presents a variable velocity profile input at the nozzle exit that is showed in Figure 2. This is an average measure, not an instantaneous realization. The great irregularity showed in this picture seems to be an effect of wave reflections inside the nozzle (see R. Payri et al., 2008 [22] or J. Gimeno, 2008 [8] for more details about this issue).

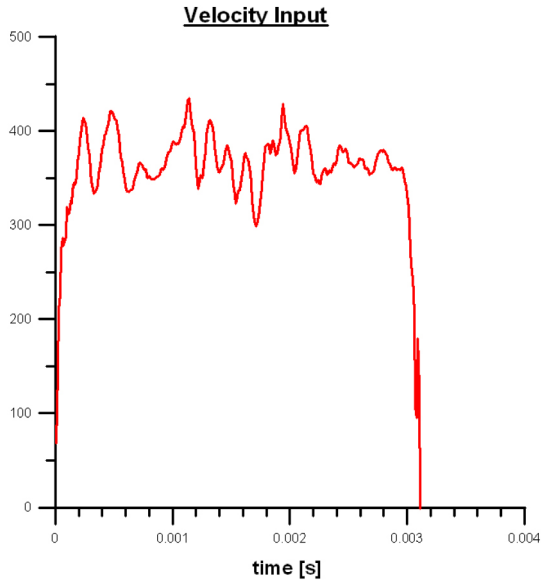

Figure 2. Velocity Profile (m/s).

In our computational cases we simulate the maximum time of 2ms, as the measurement obtained in CMT are matched well with our computational cases and velocity as explicitly shown in the later results. Moreover, the most important reason is the computational time is quite long especially once many droplets formed in ELSA modeling when time increased.

As this is axis-symmetric nozzle, a first approximation to this sort of problems is to perform 2D simulations. Of course, turbulence and engines are always 3D, but, as a first approximation to the real problem, 2D simulation can model reasonably the spray behavior. In our calculation, 2D simulations are actually a 3D simulation with only a cell in the azimuthal direction, modeling a 5° sector of the spray. This is showed in the rightmost part of Figure 4, where we also show the boundary conditions imposed on the spray and chamber. Figure 3 depicts the front view of two typical meshes.

Generally, the requirements for mesh structure are especially important at the nozzle, where the mesh size has to be small enough to capture the spray structure and droplets. The criterion used in this paper is to define the size of the first cell and then extrude the mesh, fixing the axial and radial ratio. The six cases studied in this paper are showed in table 2.

In table 3 we have the main formula based on the successive ratio used in constructing our meshes are showed. In these equations: l_1 is length of the first interval of the edge, l_n is length of the n interval of the edge, R is the interval length ratio, n is the number of intervals and L stands for the total edge length [11]. The sixth case is a little bit different. Instead of using first/last ratio of 72 on the axial direction, and the last/first ratio equal to 0.006 on the radial direction, we have taken the first segment of the mesh with $\Delta x_1 = \Delta z_1 = l_1 = 0.2R_{inj} = 0.1D_{inj} = 11.1\ (\mu m)$, and have used the same number of segments in the axial edge and radial edge, 218 and 25, respectively.

For the completeness, three different configurations with 3-, 5-, and 10-cell at the half of the nozzle are used (note that only half of the nozzle is simulated). In all of these cases we have fixed Δt in 10^{-8}, obtaining Courant numbers below 0.3. Mesh structures can be seen in Figure 3 with a zoom of the near nozzle region.

The RANS turbulent model chosen for our validation is the k - ε /High Reynolds Number, those equations are

$$\frac{\partial \tilde{k}}{\partial t}+\tilde{u}_j\frac{\partial \tilde{k}}{\partial x_j}=C_\mu\frac{\tilde{k}^2}{\tilde{\varepsilon}}\left(\frac{\partial \tilde{u}_i}{\partial x_j}+\frac{\partial \tilde{u}_j}{\partial x_i}\right)\frac{\partial \tilde{u}_i}{\partial x_j}+\frac{\partial}{\partial x_j}\left(\frac{C_\mu}{\sigma_k}\frac{\tilde{k}^2}{\tilde{\varepsilon}}\frac{\partial \tilde{k}}{\partial x_j}\right)-\tilde{\varepsilon} \quad (19)$$

and

$$\frac{\partial \tilde{\varepsilon}}{\partial t}+\tilde{u}_j\frac{\partial \tilde{\varepsilon}}{\partial x_j}=C_{\varepsilon_1}C_\mu\tilde{k}\left(\frac{\partial \tilde{u}_i}{\partial x_j}+\frac{\partial \tilde{u}_j}{\partial x_i}\right)\frac{\partial \tilde{u}_i}{\partial x_j}+\frac{\partial}{\partial x_j}\left(\frac{C_\mu}{\sigma_\varepsilon}\frac{\tilde{k}^2}{\tilde{\varepsilon}}\frac{\partial \tilde{\varepsilon}}{\partial x_j}\right)-C_{\varepsilon_2}\frac{\tilde{\varepsilon}^2}{\tilde{k}} \quad (20)$$

The constants of the model are listed in table 4. We are using the classical constants used in most of the spray calculation. However, as it is also known few decades back by Pope,

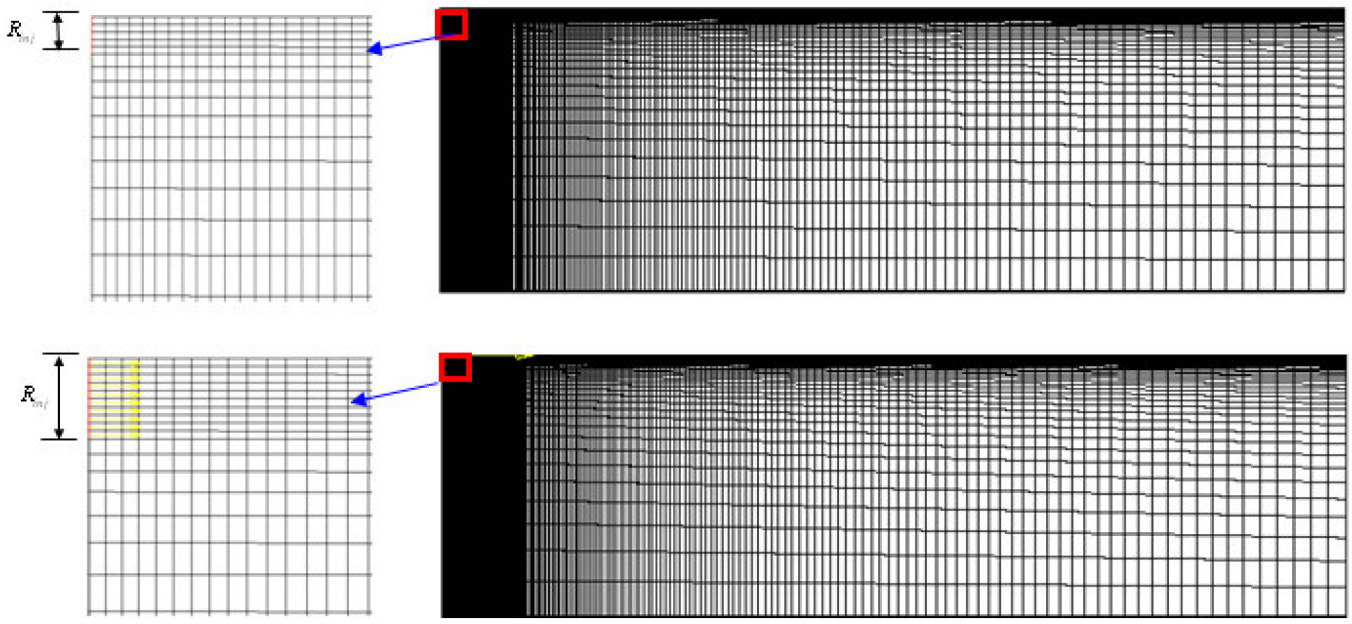

Figure 3. Computational meshes and detailed views (on the left side), for 5 cells and 10 cells at the same nozzle radius.

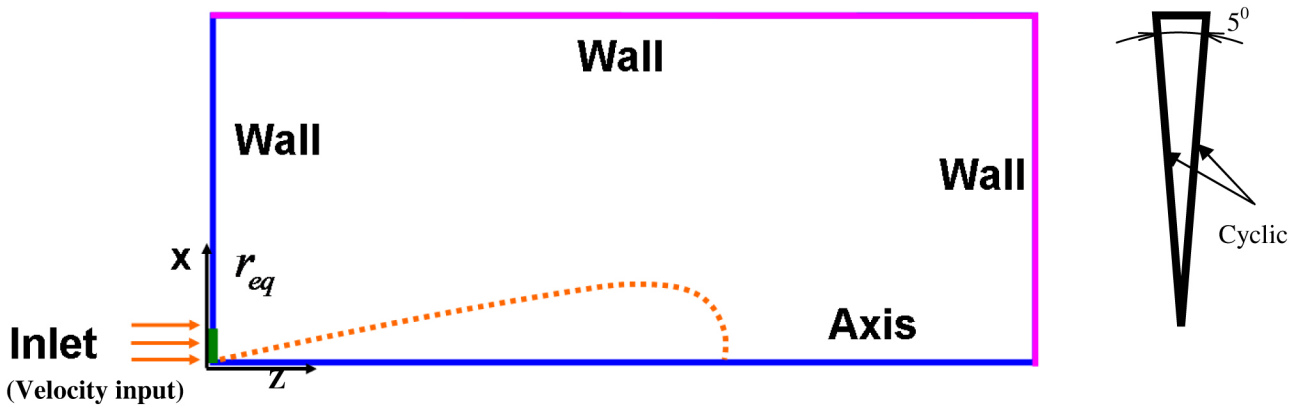

Figure 4. Geometry (front view and side view) & Boundary Condition.

1978 [20], the classical value of C_{ε_1} causes an overprediction of the spreading and decay of rate of a round jet flow.

The C_{ε_1} constant modifications are based on the suggestion of (J. Janicka et al., 1982 [13] and Dally B.B., 1998 [7]). Thus, we have used classical value $C_{\varepsilon_1}=1.44$ the suggested value $C_{\varepsilon_1}=1.60$ and an average value of 1.52 that in some cases give a better approximation. The turbulent Prandtl number has been set to 1 in order to produce similar solutions for the conservation equations of axial momentum, fuel mass and energy. Noting that the Prandtl (K.E.) in table 4 is another Prandtl constant which is only used for solving the k-ε equations which is well-known in CFD calculation and mentioned again in Diesel spray by Lebas and Blokkeel et al., 2005 [14].

Experimental Validation

The numerical results are compared with experimental data at CMT-Motores Térmicos. Experimental results have been obtained from quiescent vessel tests previously published in R. Payri et al., 2008 [22], and J. Gimeno, 2008 [8].

The injection velocity profile comes from measurements of mass and momentum fluxed performed in a pressurized test rig with nitrogen. Mass flow rate for the velocity inlet was measured by means of Bosch's method (Bosch, 1966 [4]) The momentum flux measuring principle of this technique is explained in two references of R. Payri et al., 2005 [21], and J. Gimeno, 2008 [8], and consists of measuring the impact

Table 2. Mesh parameters

Case No.	No cells at the half of nozzle	No. axial cells	Axial ratio (First/Last ratio)	No. radial cells	Radial ratio (Last/First ratio)	Total Vertices	Total Cells
1	**3**	218	72	**45**	0.006	19929	9810
2	5	218	72	**25**	0.006	11,169	5450
3	**5**	218	72	**45**	0.006	19,929	9,810
4	5	**435**	72	**90**	0.006	78,916	39,150
5	**10**	**250**	**143**	**50**	**0.003**	25,351	12,500
			First length		**First length**		
6	**5**	218	**11.1** μm	**25**	**11.1** μm	11,169	5450

Table 3. Successive Ratio of Mesh edges

Successive Ratio	Last/First ratio	First/Last ratio	First Length
Formula	$R=\left(\frac{l_n}{l_1}\right)^{1/(n-1)}$	$R=\left(\frac{l_1}{l_n}\right)^{-1/(n-1)}$	$\sum_{i=1}^{n} R^{i-1}=\frac{L}{l_1}$

Table 4. Turbulence Models

	C_μ	C_{ε_1}	C_{ε_2}	C_{ε_3}	C_{ε_4}	Prandtl (K.E.)	Prandtl (Eps)
Turb 1	0.09	**1.44**	1.92	1.44	-0.33	1	1.219
Turb 2	0.09	**1.52**	1.92	1.44	-0.33	1	1.219
Turb 2	0.09	**1.60**	1.92	1.44	-0.33	1	1.219

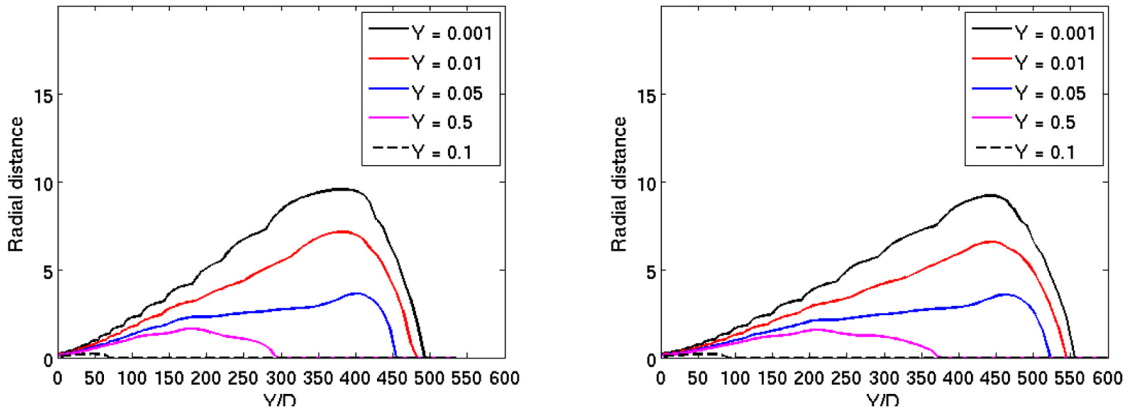

Figure 5. Comparison of iso-surfaces of 5-cell at 2ms, case 2 with C_{ε_1} =1.52 (left figure) and C_{ε_1} = 1.60 (right figure).

force of the spray in a surface with a piezo-electric sensor. As long as the whole cross-section of the spray impacts on the sensor, the measured force equals to the momentum flux at that cross section. If the measurement position is close to the nozzle exit, the time evolution of the impact force is equal to the nozzle (hole) momentum flux, Mo.

NUMERICAL RESULTS

The $C_{\varepsilon 1}$ effect of the penetration can be clearly seen in Figure 5, where several iso-surfaces of liquid mass fraction are showed. The longer axial distance of approximately 570 is obtained with C_{ε_1} =1.60, while it is only 490 with C_{ε_1} = 1.52. It is clear from the figures, the effect of C_{ε_1} reduces spray dispersion and consequently increases spray penetration.

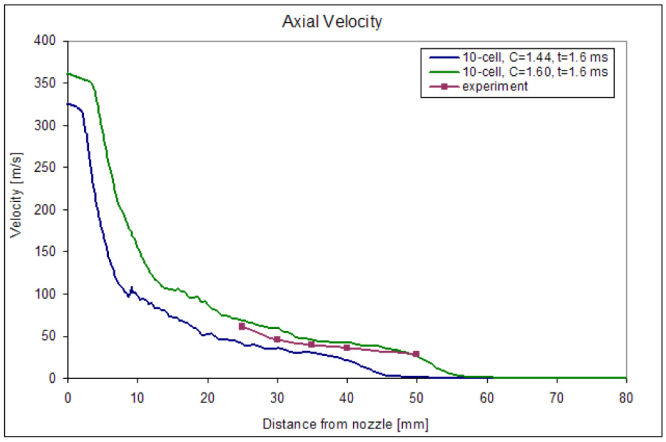

(a)

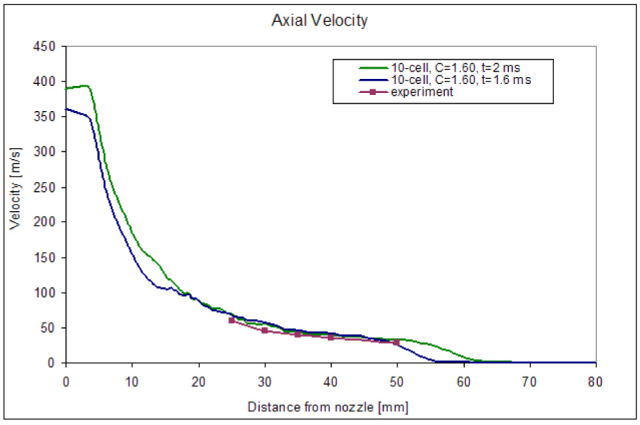

(b)

Figure 6. Axial velocity for 0.1 R_{inj} cases: (a) Changes in C_{ε_1}, (b) Changes in time.

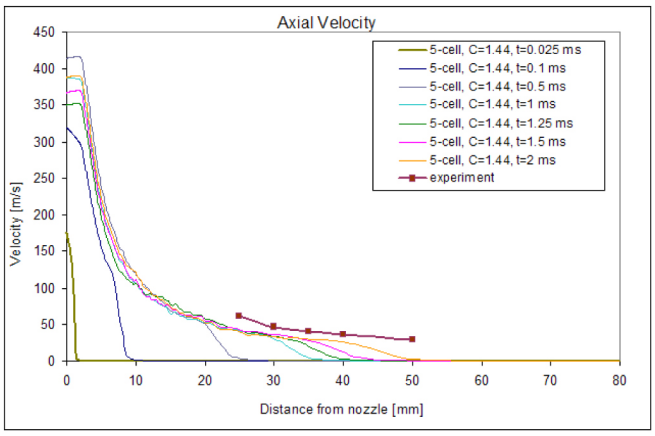

(a)

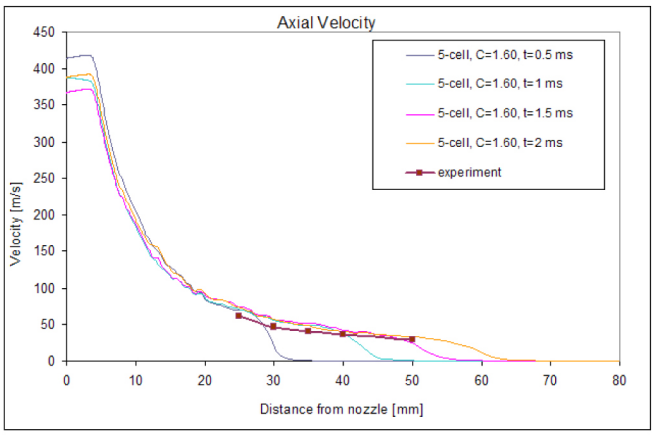

(b)

Figure 7. Comparisons of Axial velocity: (a) C_{ε_1} = 1.44; (b) C_{ε_1} = 1.60.

In the case of axial velocity, this effect is also very clear as can be seen in Figure 6, where the comparison of axial velocity for 10-cell case corresponding to two turbulent constants (1.44 and 1.60) at t=1.6 ms are illustrated. The matching of C_{ε_1} =1.60 is better than in the case of C_{ε_1} =1.44. Moreover, it seems to be clear from the figure that in the latter case, spray penetration is not enough to show an appreciable axial velocity at 50 mm from the nozzle. This result is also clear in the Figure 7, where we only have 5 cells at the nozzle. Clearly, C_{ε_1} =1.44 is underpredicting the axial velocity, whereas the 1.60 value gets more accurate results.

In Figure 8, a full view of droplet profile combined with the velocity in the same plot and a detailed view of the dense zone are depicted for 5-cell case (case no. 3), with turbulent constant equal to 1.60 at t = 2 ms. The first three figures on the left hand side are only depicted the velocity profile, and the last figure is illustrated both droplets and velocity. As it is expected, it confirms that velocity magnitude is highest in the zone next to the nozzle/inlet boundary and in the liquid core zone where the Eulerian approach is used. The farther distance from axial and radial edge, the less velocity we obtained. The last figure on the right hand side captures both velocity profile and the droplets, which are generated in regions where the velocity are approximately below 150 m/s.

The droplet formation is showed in Figure 9. According to the above description, the droplet formation starts at the transition zone and continue to develop in the farther zone (Lagrangian zone). As it was also expected, there is no droplet in the Eulerian mixture zone (regions contained the red color and its closed surroundings). These figures confirm that the initial setting and formulae for ELSA model are correctly captured in the final result. The Sauter Mean Diameters range from 8.88e- 9 µm to 4.896 µm in our computational cases, which is smaller than the smallest cell as stated in the previous part.

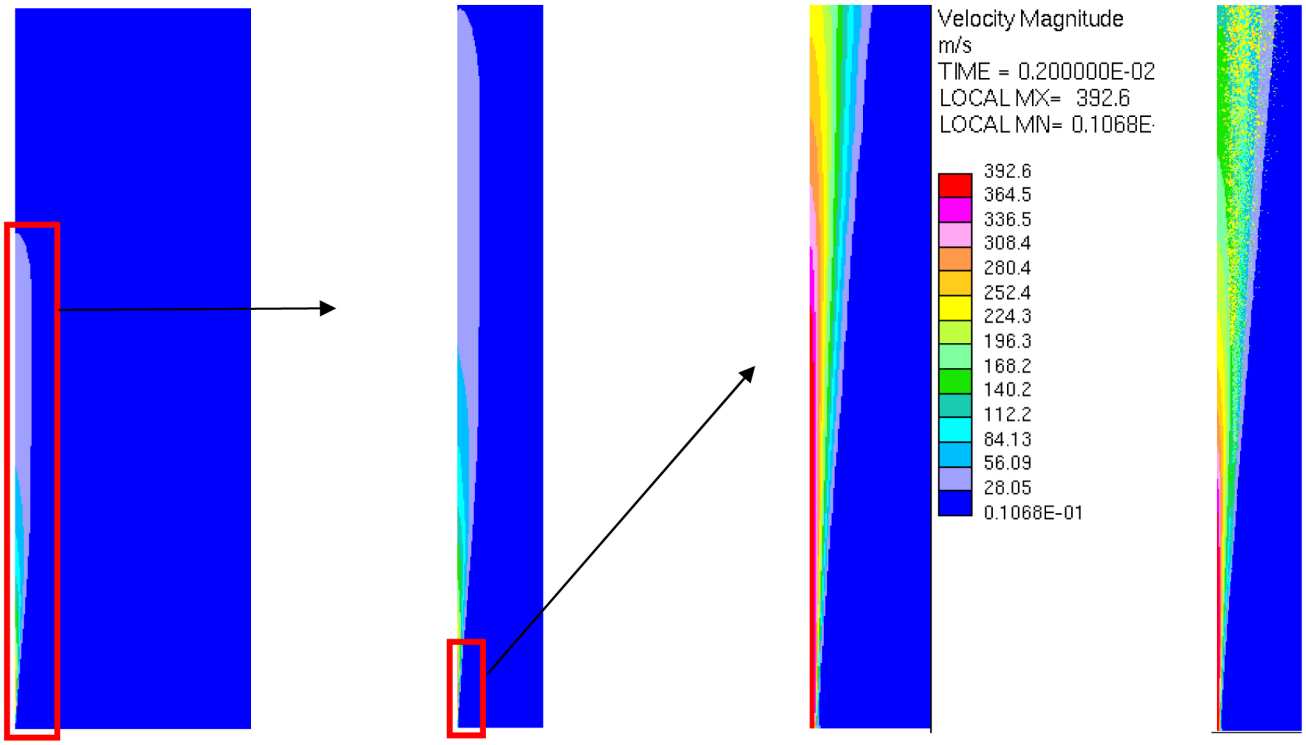

Figure 8. Velocity profile and droplet formation.

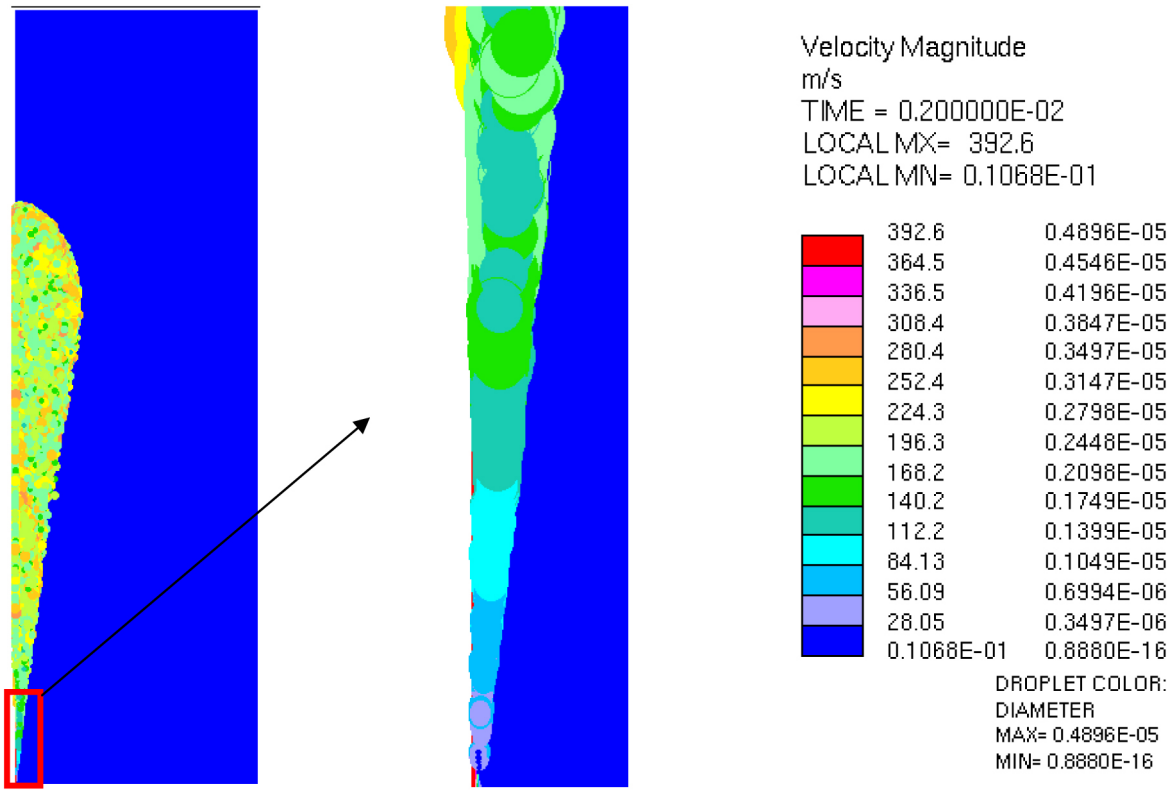

Figure 9. Droplet profile.

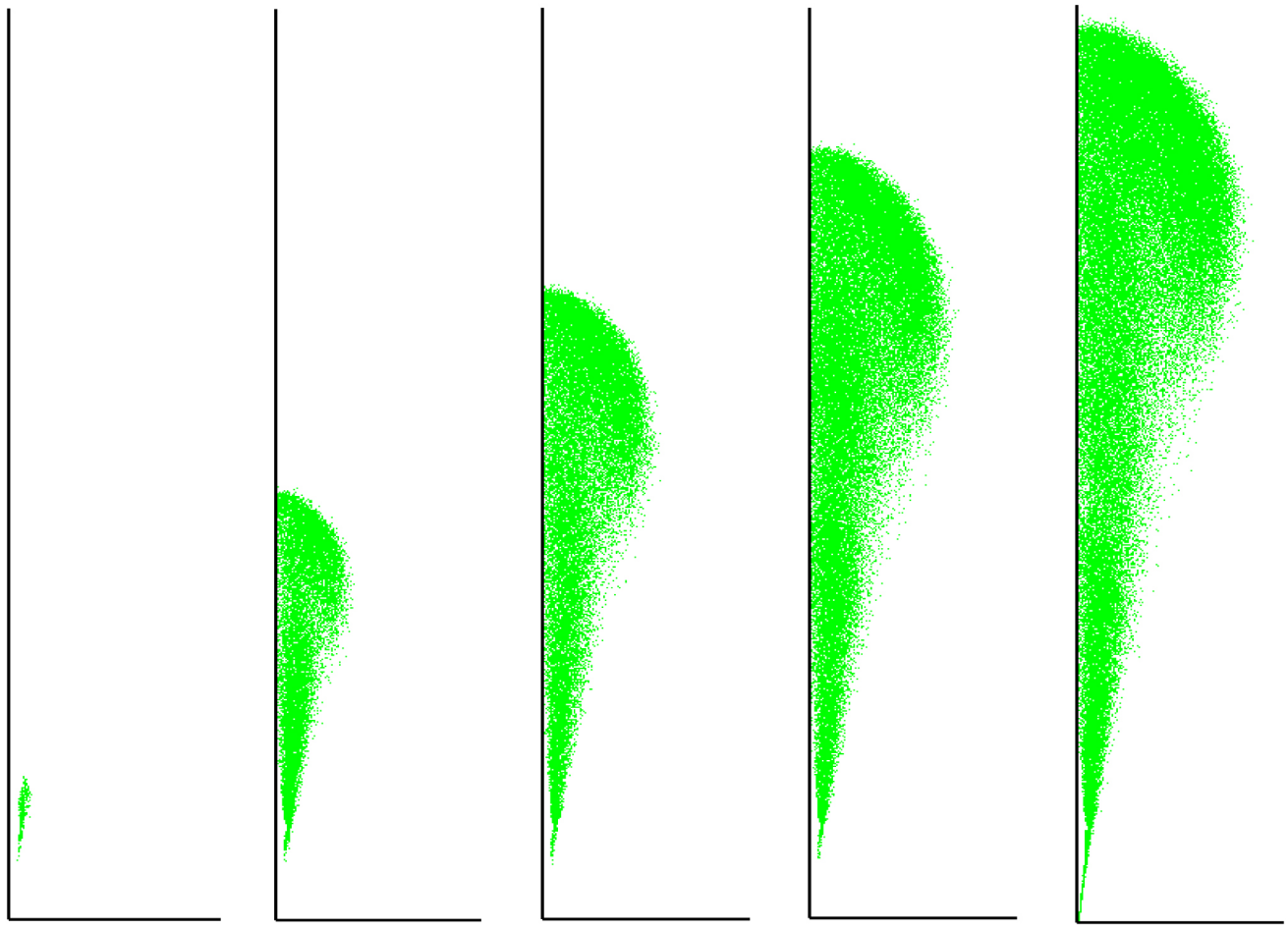

Figure 10. Droplet profiles at different time of 0.1, 0.5, 1, 1.5, and 2 ms (from left to right) for case 3, C_{ε_1} = 1.44.

Table 5. Droplet Information

	Time (ms)	Active Droplets	Evaporated / Disappeared / Absorption Droplets	Total Droplets
5-cell, C_{ε_1} **=1.44**	2	69101	422,994	492,095
5-cell, C_{ε_1} **=1.60**	2	125,739	529,320	655,059
10-cell, C_{ε_1} **=1.44**	1	706	3,734	4,440
10-cell, C_{ε_1} **=1.44**	1.5	78,894	398,061	476,955
10-cell, C_{ε_1} **=1.44**	1.75	87,969	440,249	528,218
10-cell, C_{ε_1} **=1.60**	2	107,549	630,334	737,883

Figure 10 shows the evolution of droplets in various time steps of 0.1, 0.5, 1, 1.5, 2 ms respectively for the case with 5 cells at nozzle radius. In those plots, all the droplets have the same size for the sake of visibility, independently of their actual diameter as already shown in Figure 9. A summary of the active and inactive droplets are shown in table 5. The total number of generated droplets increase rapidly after each time step for all the C_{ε_1} values. As an example, the case with 10-cell, C_{ε_1}=1.44, for t = 1, 1.5, and 1.75 in table 5 accumulated 4440, 476955, and 528218 droplets respectively. Several reasons could lead to the disappearance of droplets such as the evaporation due to the high temperature or their absoption into the Eulerian zone, where the flow is treated as a monophasic fluid.

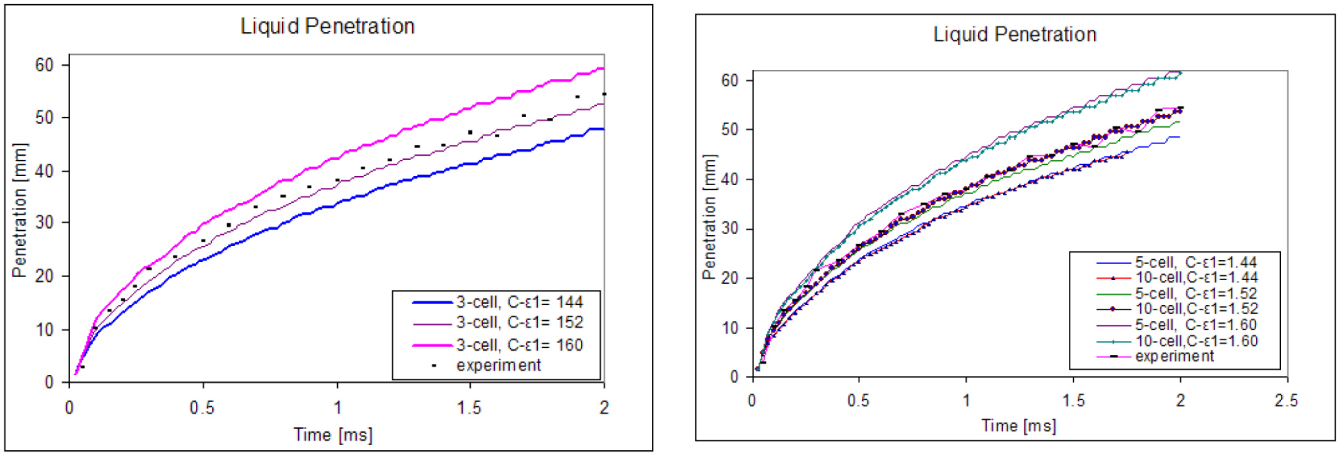

Figure 11. Spray penetration of the case with 3 cells and 5 cells.

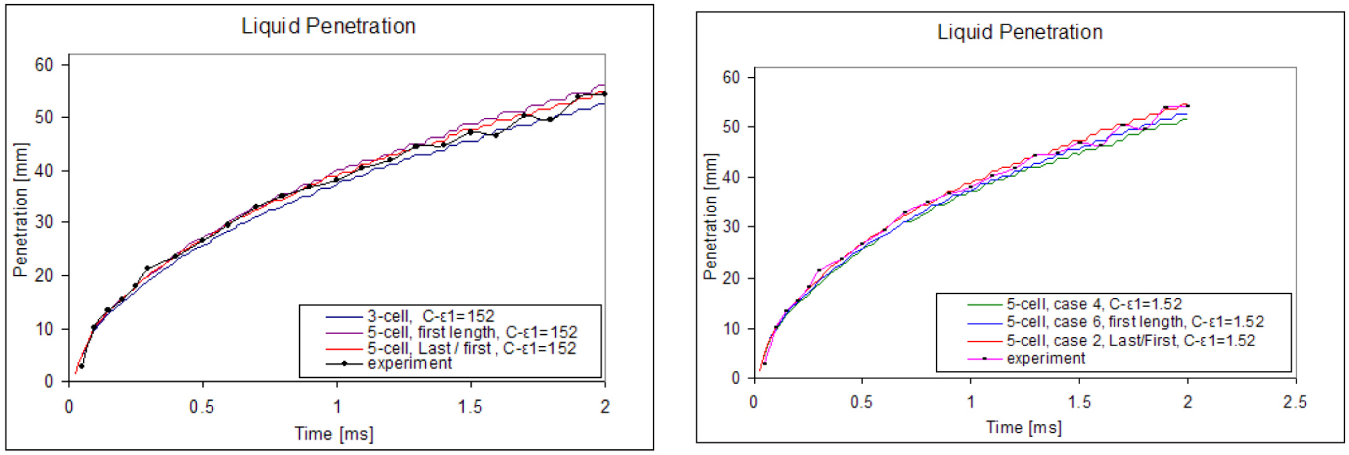

(a) (b)

Figure 12. Comparison of spray penetration.

Penetration rates also show a great dependency on the value of C_{ε_1}. Results on the penetration are showed in Figure 11 and 12. In this case, it is clear that the value of 1.60 is overprediting the penetration, while 1.44 is underpredicting in Figure 11, and for all the meshes has been tested so far. Hence, we have used a third value of 1.52 and we obtain the best fit with various meshes.

While the Figure 12 (a) illustrate the difference between 3- and 5-cell meshes, the averaged numerical errors of 3-cell case (case 1) is 0.9% whereas the 5-cell case with the first length equal to 11.1 µm (case 6) is 1%, and 5-cell case with last/first ratio (case 2) is only 0.42% as plotted in Figure 12 (b) and the detailed difference of representative errors are depicted in the Figure 13. The variance between 3-cell case and 5-cell case as in Figure 12 (a) is quite large in comparison with the discrepancy from 5-cell to 10-cell cases in Figure 11 (b). Using the same constant $C_{\varepsilon_1} = 1.52$, it only takes **138451** seconds (~39 hours) to complete one parallel calculation consisted of 6 processors for 5-cell case (case no. 3), while it must need **517741** seconds (~ 144 hours) to complete one parallel calculation consisted of 12 processors for 10-cell case (case no. 5). Hence, the 5-cell mesh with last/ first ratio consisted of 25 radial cells, and $C_{\varepsilon_1} = 1.52$ is the optimal setup, it should be enough for using the future RANS calculation of this nozzle diameter.

SUMMARY/CONCLUSIONS

In this study, several test cases are employed to have an initial validation of the ELSA model implemented in Star-CD. Mesh independency and the effect of changing C_{ε_1} constant are explored. All the simulations have been made in 2D meshes, considering axis-symmetric problems and have been validated against experimental data of a well characterized nozzle.

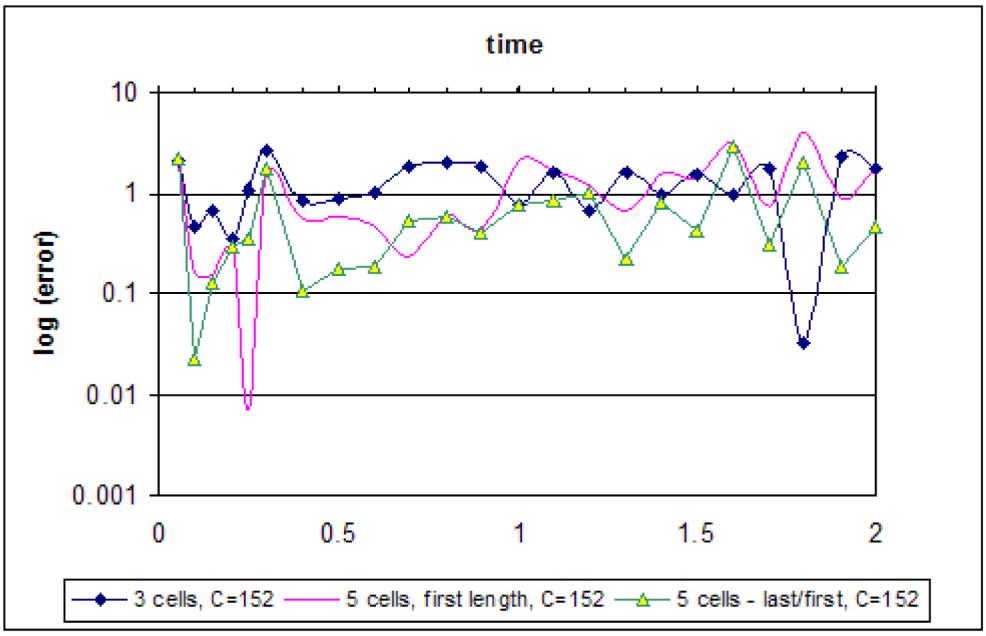

Figure 13. Numerical errors of 3-cell and 5-cell cases with turbulent constant = 1.52.

Two major conclusions are obtained from this work. Firstly, the classical value of C_{ε_1}, 1.44, leads to an overpredicting of the penetration, while the typical value used in sprays, 1.60, causes overprediticion. Secondly, mesh independency is obtained with only 5-cell at the nozzle radius, which satisfies the reasonable result, permits a considerable saving in computational time and storage space. The best fit in the penetration curve is obtained for $C_{\varepsilon_1} = 1.52$.

Obviously, a couple of 2D simulations are not a completed validation of the code. It is planned to continue with two other experimental cases analyzed in our institute, a full 3D simulation of the three nozzles, and last but not least, the effect of a cavitating nozzle.

REFERENCES

1. Araneo, L, Soare, V, Payri, R, Shakal, J (2006). Setting up a PDPA system for measurements in diesel spray. J Phys: Conf Ser 2006; 45:85-93.

2. Hoyas, S., Pastor, J., Khuong-Anh, D., Mompó-Laborda, J. et al., "Application and Evaluation of the Eulerian-Lagrangian Spray Atomization (ELSA) Model on CFD Diesel Spray Simulations," SAE Technical Paper 2011-37-0029, 2011.

3. Doudou, A., Turbulent flow study of an isothermal diesel spray injected by a common rail system, Fuel, Volume 84, Issues 2-3, January-February 2005, Pages 287-298.

4. Bosch, W., "The Fuel Rate Indicator: A New Measuring Instrument For Display of the Characteristics of Individual Injection," SAE Technical Paper 660749, 1966, doi: 10.4271/660749.

5. Beau, PA (2006). Modelisation de l'atomisation d'un jet liquide - Application aux sprays diesel. Ph.D. Thesis, University of Rouen.

6. Blokkeel, G., Barbeau, B., and Borghi, R., "A 3D Eulerian Model to Improve the Primary Breakup of Atomizing Jet," SAE Technical Paper 2003-01-0005, 2003, doi: 10.4271/2003-01-0005.

7. Dally, B.B.:'Flow and Mixing Fields of Turbulent Bluff-Body Jets and Flames, Combust.Theory Modelling, Band 2, S. 193-219 (1998).

8. García, D. Jaime Gimeno (2008). Desarrollo y aplicación de la medida del flujo de cantidad de movimiento de un chorro Diesel, PhD thesis, Universidad Politécnica de Valencia.

9. De Lucas, M (2007). Contribution a la modelisation de la pulverisation d'un liquide phytosanitaire en vue de reduire les pollutions. Ph.D. Thesis, University of Aix-Marseille II.

10. Faeth, G., Hsiang, L.-P., and Wu, P.-K. (1995). Sructure and breakup properties of sprays. Int. J. Multiphase Flow, 21:99-127.

11. Fluent, Gambit manual 13, Fluent, Inc. 05/03/00.

12. Faeth, G. M., Hsiang, L. -P., Wu, P. -K., Structure and breakup properties of sprays, International Journal of Multiphase Flow, Volume 21, Supplement 1, December 1995, Pages 99-127.

13. Janicka, J., Peters, N., Prediction of turbulent jet diffusion flame lift-off using a PDF transport equation, in: Symposium (International) on Combustion, vol. 19, 1, 1982, pp. 367-374.

14. Lebas, R., Blokkeel, G., Beau, P., and Demoulin, F., "Coupling Vaporization Model With the Eulerian-Lagrangian Spray Atomization (ELSA) Model in Diesel Engine Conditions," SAE Technical Paper 2005-01-0213, 2005, doi: 10.4271/2005-01-0213.

15. Lebas, R (2007). Modelisation Eulerienne de l'Atomisaton haute pression - Influences sur la vaporisation et la combustion induite. Ph.D. Thesis, University of Rouen.

16. Lee, S. and Reitz, R. (2001). Effect of liquid properties on the breakup mechanism of high-speed liquid drops. Atomization and Sprays, 11:1-19.

17. Lefebvre, A.H. (1989). Atomization and sprays, Taylor and Francis.

18. Naber, J. and Siebers, D., "Effects of Gas Density and Vaporization on Penetration and Dispersion of Diesel Sprays," SAE Technical Paper 960034, 1996, doi: 10.4271/960034.

19. Ning, W, Reitz, RD, Lippert, AM and Diwakar, R (2007). Development of a next generation spray and atomization model using an Eulerian-Lagrangian methodology. 17th Int. Multidimensional Engine Modeling User's Group Meeting, Detroit, MI.

20. Pope, S.: An explanation of the turbulent round-jet/plain-jet anomaly. AIAA J. 16, 279-281 (1978).

21. Payri, R., García, J.M., Salvador, F.J. and Gimeno, J. (2005). Using spray momentum flux measurements to understand the influence of Diesel nozzle geometry on spray characteristics, Fuel 84, pp. 551-561.

22. Payri, R., Tormos, B., Salvador a, F.J., Araneo, L. (2008). Spray droplet velocity characterization for convergent nozzles with three different diameters. Fuel 87, pp 3176-3182.

23. Tanner, F. (2004). Development and validation of a cascade atomization and drop breakup model for high-velocity dense sprays. Atomization and sprays, 14:20-32.

24. Vallet, A, Burluka, AA and Borghi, R (2001). Development of a Eulerian model for the atomization of a liquid jet. Atomization and sprays, vol. 11, pp. 619-642.

CONTACT INFORMATION

Sergio Hoyas, J.M. Pastor, Dung Khuong-Anh, Juan Manuel Mompó-Laborda
CMT - Motores Térmicos (Department of thermal engine)
Universidad Politécnica de Valencia.
Camino de Vera S/N, 46022
Valencia, Spain
E-mail: (serhocal, jopasen, ankh2, juamomla) @mot.upv.es

F. Ravet
Renault
1 Avenue du golf 78288
Guyancourt, France
frederic.ravet@renault.com

ACKNOWLEDGMENTS

The authors would like to thanks to the referee for his/her comments, which have greatly improved the article. This work has been granted by Renault and VECOM (Vehicle Concept Modeling) - EU FP7 Marie Curie Initial Training Network (ITN) Grant Agreement 213543 (from October 1st, 2008 to September 30, 2012). The aim of the proposed training network is to provide dedicated research training in the emerging field of vehicle concept modeling for up-front pre-CAD functional performance engineering, bridging between industry and academia across Europe. Authors also acknowledge the support of the Spanish Government in the frame of the Project "Métodos LES para la simulatión de chorros multifásicos", Ref.ENE2010-18542, the Universidad Politécnica de Valencia under the contract Reference PAID-2759 and the Generalitat Valenciana, under the contract GV/2010/039.

DEFINITIONS/ABBREVIATIONS

CAD
Computer-aided Design

CMT
CMT Motores Térmicos

CFD
Computational Fluid Dynamics

DDM
Discrete Droplet Model

ICE
Internal Combustion Engine

ELSA
Eulerian-Lagrangian Spray Atomization

ITN
Initial Training Network

PDPA
Phase Doppler Particle Analyzer

SMD
Sauter Mean Diameter

VECOM
Vehicle Concept Modeling

NOMENCLATURE

l
liquid

g
gas

i, j
direction in space

k
turbulent kinetic energy

$\overline{\Sigma}$
quantity of liquid/gas interface per unit of volume

D_{32}
Sauter Mean Diameter

n
drop number density (drop number per unit of volume)

n_{drop}
number of droplets per generated parcel

ρ
density

$\overline{\rho}$
mean density

Sc_t
turbulent Schmidt number

τ_{turb}
characteristic time scale of turbulence

τ_{coll}
characteristic time scale of collision

ν_t
liquid viscosity

$\overline{P}$
the mean pressure

L_t
turbulent length scale

R_g
the gas constant

$S_{EL}^{\tilde{Y}_l}$
source term when droplet generation during the transition from Eulerian to Lagrangian formulation

$S_{EL}^{\tilde{\Omega}}$
source term of the liquid/gas interface

T_g
the mixture temperature

$\tilde{\Phi}_l^{crit}$
critical value of the Eulerian liquid volume fraction

$\tilde{U}_i$
Favre averaged mean velocity

$\tilde{Y}_l$
mean liquid mass fraction

$\widetilde{\Omega}$
liquid/gas interface per unity of mass

$\dot{\widetilde{\Omega}}_{mean}$
mean value of liquid/gas surface density

$\dot{\widetilde{\Omega}}_{turb}$
turbulence value of liquid/gas surface density

$\dot{\widetilde{\Omega}}_{coll}$

collision value of liquid/gas surface density

$\dot{\widetilde{\Omega}}_{coal}$

coalescence value of liquid/gas surface density

$\widetilde{\Omega}_{init}$

first source term

V_{cell}

volume of one transitional cell

l_1

length of the first interval of the edge

l_n

length of the *n* interval of the edge

R

the interval length ratio

n

the number of intervals

L

the total edge length

ISSN 0148-7191

SAE Customer Service:
Tel: 877-606-7323 (inside USA and Canada)
Tel: 724-776-4970 (outside USA)
Fax: 724-776-0790
Email: CustomerService@sae.org
SAE Web Address: http://www.sae.org
Printed in USA

2.2.5. ELSA model of Diesel sprays. Mathematical Modelling in Engineering & Human Behaviour 2011 (oral presentation at IMM 2011, will submit final paper in Oct 2011)

2.3. INFORMES

2.3.1. D11: Intermediate report on Multi-attribute Balancing and Optimization in the Concept Design Phase, Balancing of injection/combustion efficiency and NVH: Optimal design approach for spray penetration of Diesel engine

EUROPEAN COMMISSION
DG RESEARCH

VECOM
Vehicle Concept Modelling

7th FRAMEWORK PROGRAMME
EU FP7 Marie Curie Initial Training Network (ITN)
Grant Agreement 213543
Duration: October 1st, 2008 - September 30, 2012
http://www.vecom.org

D11: Intermediate report on Multi-attribute Balancing and Optimization in the Concept Design Phase

Deliverable no.	D11
Dissemination level	VECOM partners
Authors	Marco Gubitosa, Giambattista Stigliano, Stijn Donders, Roberto d'Ippolito – **LMS International**
Co-authors	Khuong Anh Dung, Sergio Hoyas, Xandra Margot, CMT-Motores Térmicos - **Universidad Politécnica de Valencia**
Status (F: final, D: draft)	D

Partner	Task 5	Contributed already to this D11?	Multi-Attribute Balancing and Optimization Research
UPVLC	X	Yes	Balancing of injection/combustion efficiency and NVH
IDMEC	X	No	Balancing of body and chassis stiffness, crashworthiness and durability
PoliTo	X	No	Balancing of chassis ride and handling with body NVH
K.U.Leuven		/	
UNIFI	X	No	Balancing of vehicle structure crashworthiness and NVH
LAT		/	
CVUT		/	
FhG-LBF	X	No	Methodology research for efficient sensitivity analysis, robust design and uncertainty assessment
ARSENAL		/	
IFP	X	No	Optimization of energy and emission management for hybrid vehicles
LMS	Leader	Yes	Multi-objective, multi-disciplinary optimization methodology
AVL	X	No	Balancing of engine economy, energy management and powertrain NVH
CRF	X	No	Balancing of body and chassis concept modeling in industrial context
BMW	X	No	Integration of body concept modeling in industrial multi-disciplinary vehicle optimization process

1.1 Optimal design approach for spray penetration of Diesel engine

The aim of the work is the implementation of the adjustment of the built-in Star-CD spray models to predict the behaviour of Diesel spray more precise. This computational work, together with experimental data, will lead to a better understanding of the behaviour of Diesel sprays.

As far as the primary and secondary break up models are concerned, the default Huh-Gosman (Hu) – Hsiang-Faeth (HF) **[2]** allow a better prediction of experimental data (spray penetration and SMD **[1]**) than other models normally implemented into the Star-CD code.

The under-estimation of the spray penetration at the beginning of the experiments for example in this setup – before 0.2 ms – is independent of the atomization model used for the calculations. In order to improve the prediction, the most reasonable way to act on the spray penetration during this interval is through the injection velocity, and directly related to it, the injection rate. In this section, the experimental injection rate has been modified at the beginning of the signal, when the injection rate is very small and where there are more uncertainties in the measurements.

1.1.1 Test Cases

Within this study, the evaluation of the spray models has been carried out on the basis of the experiments, all of them in non-evaporating conditions. The injection pressure goes from 400 to 1800 bar and the back pressure lies in the interval from 20 to 50 bar. The detailed data and parameters are summarized in the tables below:

Test Cases

	P_{INJ} (bar)	P_{BACK} (bar)	Conditions
Test 1	800	50	Non-evaporating
Test 2	400	20	
Test 3	1800	50	

Table 1. Test cases.

Gas initial Conditions

	Po (bar)	To (ºC)	Ko (m2/s2)	Epso (m2/s3)	Y-N2o
Test 1	50	29	4.5	670	1
Test 2	20				
Test 3	50				

Table 2. Initial conditions.

Injector definition

	α_0 / 2 (deg)	T_{INJ} (ºC)	k_0 (m^2/s^2)	D_{eff} (µm)	Liquid	Mass Flow Rate (g/s)
Test 1	8.5	90	4.5	135	$C_{13}H_{28}$	Experiments (Figure 1)
Test 2	5.5					
Test 3	10					

Table 3. Injector definition.

The fuel injection rates for the three cases are represented in Figure 1:

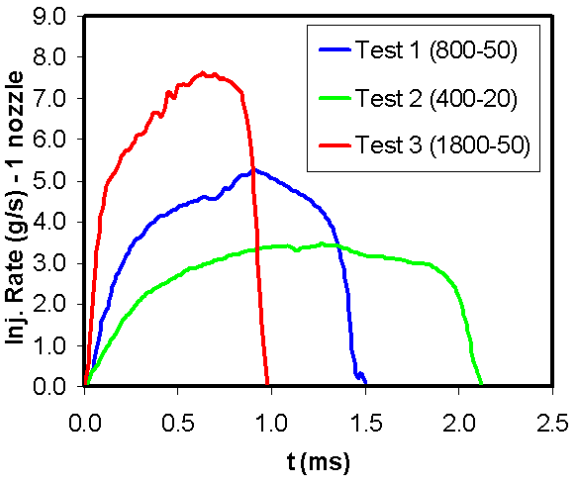

Figure 1 Injection rate (1 / 7 nozzle) for 3 test cases.

1.1.2 Spray penetration adjustment: Injection rate.

The main idea is based on the hypothesis that the measurements of the start of injection, when the injector opening is very small, are uncertain and at the same time that the velocities measured then are very small and do not significantly affect the mass flow rate measurement. By deleting the points with the lowest velocity at the beginning of injection, the slope of the initial part of the mass flow rate curve can be modified. Figure 2*left* shows a zoom of the injection rate of Test1 (*P_{inj}: 800 bar – P_{back}: 50 bar*) in logarithmic scale. Clearly, the first three points define a different curve slope than the rest of the points that define the linear behaviour of the injector opening, before the stabilisation of the mass flow rate. This observation allows considering that these points may be uncertain and could therefore be discarded. This means that the start of injection was considered to happen beyond these points. The final effect on the injection rate is a slight advance (t = 0 changes) in the corrected injection rate, as shown in Figure 2*right*.

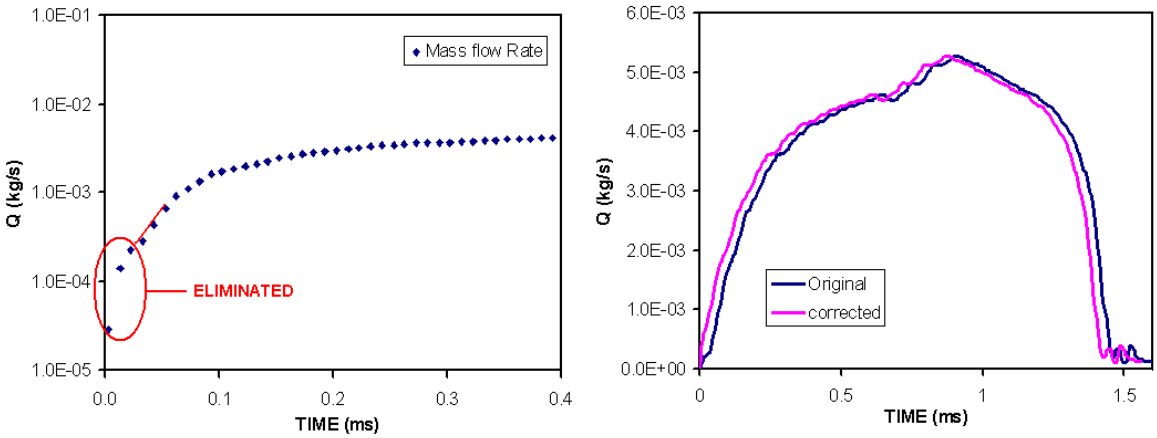

Figure 2 Injection rate. Left – Zoom and eliminated points, Right – Original and corrected injection rate. Test 1.

Figure 3 shows the spray penetration obtained for Test1 using the HG-HF model with the corrected injection rate and that obtained in the original calculation. It is clear that there is an improvement in the estimated primary spray penetration (before 0.2 ms), though it leads to a higher over-prediction in the later part of the spray.

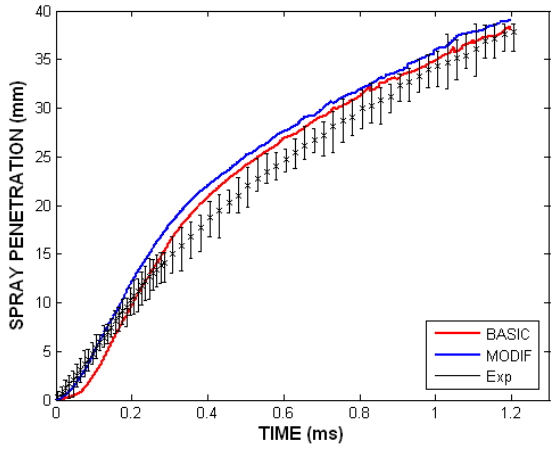

Figure 3 Spray penetration. Test1. Modification of the injection rate.

The same technique was applied to the other working points. In the case of Test 2 the results obtained at the beginning of the spray are in very good agreement with the original injection rate. The justification is that there are no points at the beginning of the signal (Figure 4*left*) that define a different slope (and very small injection rate), so it was not necessary to modify the signal of the injection rate (Figure 4*right*). Hence the results for this case would be the same as those presented in the previous section (Figure 5).

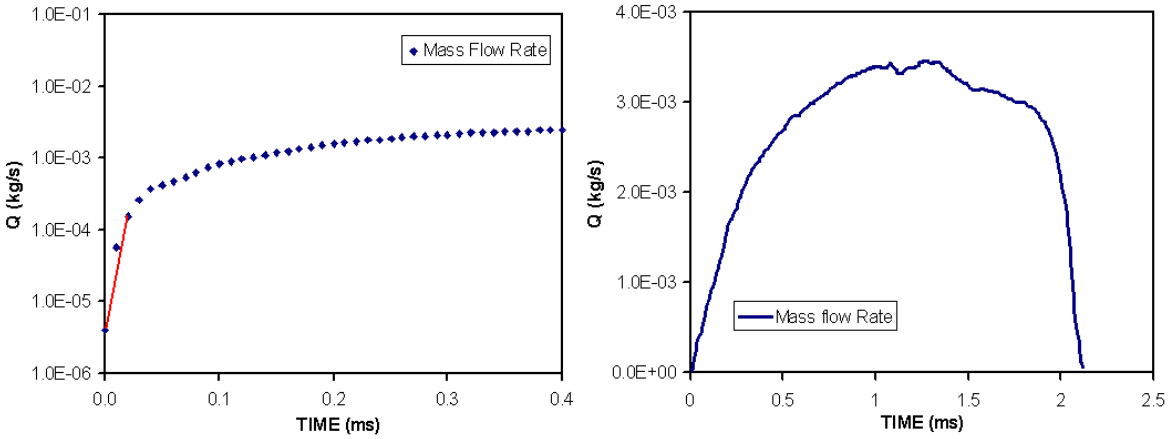

Figure 4 Injection rate. Left – Zoom and initial slope, Right – Original injection rate (Test 2).

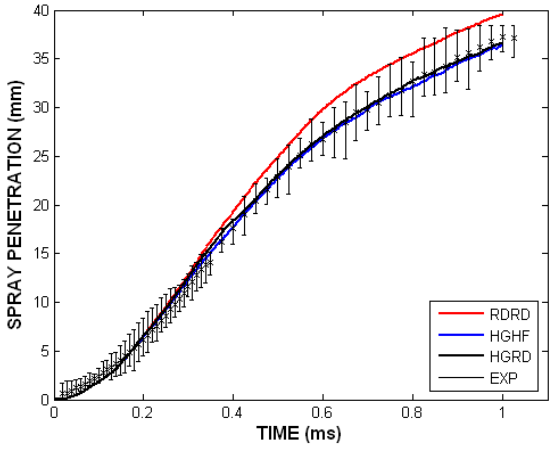

Figure 5 P_{inj}: 400 bar – P_{back}: 20 bar (Test 2). Spray Penetration.

In the case of Test3 only the first point of the original signal is removed (see Figure 6). The result of considering another temporal reference with this injection rate is that, as for Test1, the calculated spray penetration fits much better the spray during the beginning of the experiment (see Figure 7).

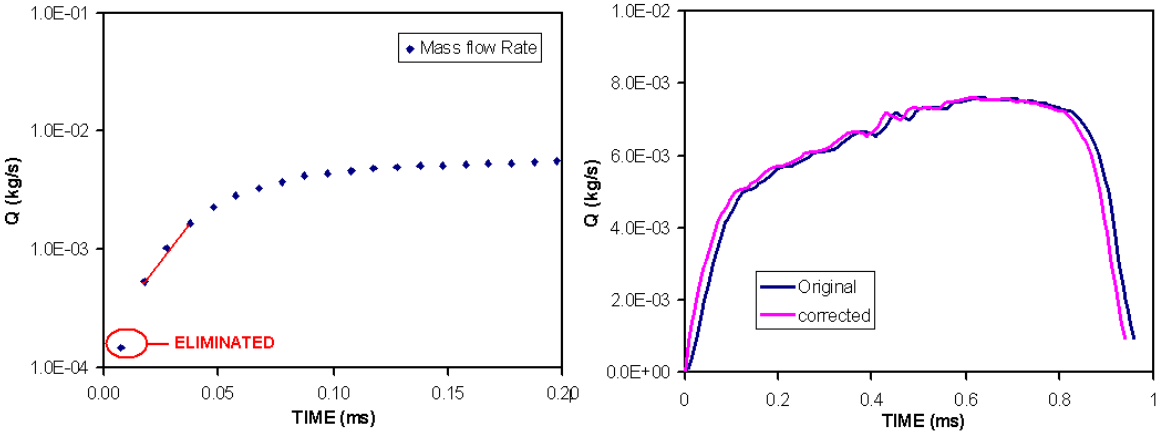

Figure 6 Injection rate. Left – Zoom and eliminated points, Right – Original and corrected injection rate in Test 3.

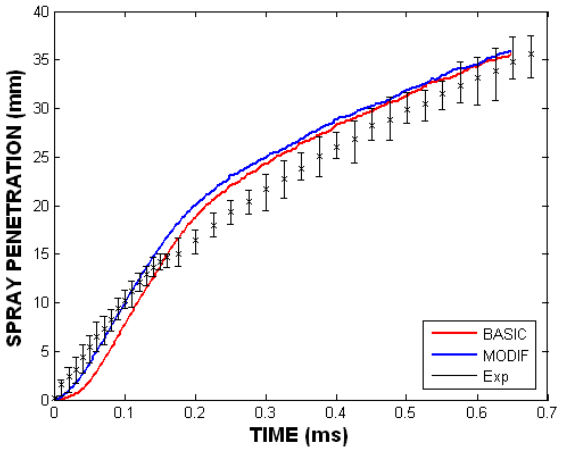

Figure 7 Spray penetration of Test3 with the modification of the injection rate.

1.1.3 Conclusion

Slight modifications in the start of injection (t = 0 s) of the mass flow rate leads to significant variations in the numerical spray penetration at the beginning of the spray. Better adjustment between the calculations and the experimental data can be observed for t < 0.2 ms with this modification.

1.1.4 Reference:

[1] T. Morel & S. Wahiduzzaman. *Modelling of Diesel Combustion and Emissions*. XXVI FISITA Congress, Praha, Czech Republic, June, 1996.

[2] STAR-CD User guide Version 4.10, CD-adapco, 2009.

2.3.2. Deliverable D8: Intermediate Report on Techniques for Powertrain Concept and Simulation. Representative approaches for powertrain concept modelling and simulation: Thermo-dynamic processes: injection/combustion, subjective noise, air management and turbo charging

Marie Curie Initial Training Network
"VECOM – Vehicle Concept Modelling"

7th FRAMEWORK PROGRAMME

Grant agreement no.: 213543

Deliverable D8: Intermediate Report on Techniques for Powertrain Concept and Simulation

Deliverable no.	D8
Dissemination level	VECOM partners
Work Package	WP2
Author(s)	Grigoris Koltsakis – LAT, Jan Macek, CVUT in Prague, Reinhard Tatschl - AVL, Sophie Bardubitzki – AVL, Helmut Kühnelt – AIT,
Status (final/draft)	Final
File Name	VECOM_D8_Interim_Report_Powertrain.doc
Project Start Date and Duration	October 1st, 2008 – September 30, 2012

Representative approaches for powertrain concept modelling and simulation

1.1 Thermo-dynamic processes: injection/combustion, subjective noise, air management and turbo charging

1.1.1 Introduction

Fuel injection process and subsequent fuel-air mixing formation play a major role on combustion and pollutant formation on internal combustion engines. Thus an accurate prediction of these processes is required in order to perform reliable engine combustion and pollutants formation simulations.

Diesel fuel injection and spray formation modeling is still a challenging task due to the complex interrelated phenomena taking place, some of them such as primary atomization or nozzle cavitation are not fully understood.

Standard CFD spray simulations are based on Discrete Droplet Method (DDM), which applied a Lagrangian approach for liquid spray modeling. This approach presents some drawbacks and thus usually requires extensive calibration in order to be employed in engine simulations. Main issues come from both physical and numerical limitations on the near nozzle dense spray region description.

1.1.2 Eulerian-Lagrangian Spray Atomization (ELSA) Method

In order to enhance CFD spray simulations, the ELSA (Eulerian Lagrangian Spray Atomization) model have been developed in recent years (Vallet et al., 2001; Lebas et al., 2005) and integrated into the StarCD CFD code by RSA. This model is based in an Eulerian approach for the description of the dense spray region, where standard DDM method is not suited for. Within the diluted spray region the ELSA model could switch to the traditional Lagrangian description of the liquid phase, taking advantage from well established previously developed submodels.

ELSA spray model allows nozzle resolved grid size and then could take benefit from internal nozzle flow simulations in terms of spatially resolved nozzle orifice exit conditions. Therefore it may also be possible to further investigate and enhance simulation concerning the linking between nozzle flow and spray formation.

Although the question whether intact cores exist or not (in high-speed liquid sprays) is open to debate, the ELSA method appears to be a promising and proper tool for atomization simulation, given the fact that the injection velocities are being increased significantly under current spray technology, and this leads to even smaller surface wavelengths that would need to be resolved using other methods. In this study, the ELSA method has been chosen for the next-generation spray and atomization modeling.

1.1.3 Objectives & methodology

According to the previous statements the overall topic of the thesis will be improved Diesel spray CFD simulation within the framework of the ELSA spray model and the StarCD code. The general objective of the thesis is to develop and validate a spray model tool for practical applications on CFD engine calculations. Within this general objective, it is included to evaluate and validate the different submodels representing the phenomena involved in Diesel spray formation and development from nozzle outflow to complete fuel vaporization.

The target is to focus on the coupling and consistency between different submodels instead of on isolated spray processes. It is proposed to emphasize on the transition from internal nozzle flow to initial spray development calculations. The work also will be focused on the proper integration of the submodels employed for the description of the dense and diluted spray region, in terms liquid break-up, coalescence, vaporization and droplet dynamics.

1.1.4 Numerical and physical model set-up

The CFD model based on StarCD code will be performed. Within this step both numerical and physical aspects are considered.

- Grid size and topology study for both internal nozzle flow and spray modeling.
- Influence of numerical discretization schemes.
- Turbulence model evaluation.
- Spray submodels for dense and diluted spray region.

1.1.5 References:

1. R. Lebas, P. A. Beau, F. X. Demoulin, Eulerian Lagrangian spray atomization (ELSA) model: slip velocity and vaporization modeling in Diesel engine conditions, Proceedings of the European Combustion Meeting 2005.
2. Vallet, A., Burluka, A.A. and Borghi, R., “Development of a Eulerian Model for the ‘Atomization’ of a Liquid Jet,” Atomization and Sprays, Vol. 11, pp. 619-642, 2001.

2.4. PRESENTACIONES Y CONFERENCIAS:

1. Presentación: "***ELSA model of Diesel sprays***", Mathematical Modelling in Engineering & Human Behaviour 2011, Valencia, Spain, 2011.

2. Presentación: "***Application and evaluation of the Eulerian-Lagrangian Spray Atomization (ELSA) model on CFD Diesel spray simulations***", SAE Torino symposium, Torino, Italy, June 2011.

3. Que asisten a la "The Automobile in the second decade: sharing all energy solutions, **13th EAEC European Automotive Congress"**, Valencia, 13 June – 16 June, 2011.

4. Presentación: ***"The mesh dependency of the Eulerian-Lagrangian Spray Atomization (ELSA) in spray simulations"***, VECOM-CLEPA suppliers workshop: Vehicle Concept Modeling in the Automotive sector, Brussel, Belgium, June 2011.

5. Presentación: ***"Evaluation of the Eulerian-Lagrangian Spray Atomization (ELSA) in spray simulations"***, International Conference on Mechanical, Automotive and Aerospace Engineering ICMAAE '11, Malaysia, May 2011.

6. Presentación: ***"A Large-Eddy Simulation of Diesel-like gas jets: Boundary conditions configuration"***, International Conference on Mechanical, Automotive and Aerospace Engineering ICMAAE '11, Malaysia, May 2011.

7. Presentación: ***"Evaluation of the gas phase turbulence in spray simulation"***, CRF (Centro Ricerche FIAT S.C.p.A.), Orbassano, Italy, March 2011.

8. Presentación: "***CFD simulation of direct injection Diesel sprays: ELSA approach***", AIT Austrian Institute of Technology GmbH, Vienna, Austria, Oct 2010.

9. Que asisten a la Thermo-and Fluid Dynamic processes in Diesel Engines (**THIESEL**) **conference**, Valencia, Sept 2010.

10. Presentación: "***Large Eddy Simulation of Diesel sprays***", Mathematical Models of Addictive Behaviour, Medicine & Engineering, Sept 2010.

11. Que asisten a la **Valencia Global 2010 conference**, April 2010. Plenary Address and Discussion:
    - "Computer aided design in transport engineering and its importance in higher education" and
    - "Green Car".

12. Presentación: "***Characteristics and generation of sprays***", Faculty of Engineering,University of Porto, Porto, Portugal, Mar 2010.

13. Presentación: "***Computational Fluid Dynamics (CFD) simulation of direct injection Diesel sprays***", LBF-Fraunhofer Institut, Darmstadt, Germany, Nov 2009.

* **Carteles**:

14. "***Mesh refinement studies for an iso-dense spray simulation in engine***", Vienna, Austria, Oct 2010.